

**CONVERSION OF SUGAR TO FUELS AND CHEMICALS VIA CATALYTIC
PHOTO-OXIDATION PROCESS**

**MS. OROUSA PANATTA
ID: 55300700519**

**A THESIS SUBMITTED AS A PART OF THE REQUIREMENTS
FOR THE DEGREE OF MASTER OF ENGINEERING
IN ENERGY TECHNOLOGY AND MANAGEMENT**

**THE JOINT GRADUATE SCHOOL OF ENERGY AND ENVIRONMENT
AT KING MONGKUT'S UNIVERSITY OF TECHNOLOGY THONBURI**

2ND SEMESTER 2013

COPYRIGHT OF THE JOINT GRADUATE SCHOOL OF ENERGY AND ENVIRONMENT

Conversion of Sugar to Fuels and Chemicals via Catalytic Photo-Oxidation Process

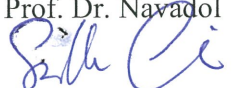
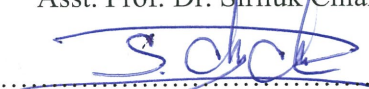
Ms. Orousa Panatta
ID: 55300700519

A Thesis Submitted as a Part of the Requirements
for the Degree of Master of Engineering
in Energy Technology and Management

The Joint Graduate School of Energy and Environment
at King Mongkut's University of Technology Thonburi

2nd Semester 2013

Thesis Committee

 (Assoc. Prof. Dr. Navadol Laosiripojana)	Advisor
 (Asst. Prof. Dr. Siriluk Chiarakorn)	Co-advisor
 (Dr. Surawut Chuangchote)	Member
 (Dr. Kunlanan Kiatkittipong)	Member
 (Assoc. Prof. Dr. Bunjerd Jongsomjit)	External Examiner

Thesis Title: Conversion of sugar to fuels and chemicals via catalytic photo-oxidation process

Student's name, organization and telephone/fax numbers/email

Ms. Orousa Panatta

The Joint Graduate School of Energy and Environment (JGSEE)

King Mongkut's University of Technology Thonburi (KMUTT)

126 Pracha Uthit Rd., Bangmod, Tungkru, Bangkok 10140 Thailand

Mobile: 083-990-6298

Email: nooah_1989@hotmail.com

Supervisor's name, organization and telephone/fax numbers/email

Assoc. Prof. Dr. Navadol Laosiripojana

The Joint Graduate School of Energy and Environment (JGSEE)

King Mongkut's University of Technology Thonburi (KMUTT)

126 Pracha Uthit Rd., Bangmod, Tungkru, Bangkok 10140 Thailand

Telephone: 02-872-6736 ext 4146

Email: navadol_1@jgsee.kmutt.ac.th

Topic: Conversion of sugar to fuels and chemicals via catalytic photo-oxidation process

Name of student: Ms. Orousa Panatta

Student ID: 55300700519

Name of supervisor: Assoc. Prof. Dr. Navadol Laosiripojana

Name of co-supervisor: Asst. Prof. Dr. Siriluk Chiarakorn

ABSTRACT

Glucose was successfully converted to high-value products, including xylitol, gluconic acid, and formic acid, via photocatalytic reaction with TiO₂, which is an alternative route for high-value chemical production. In detail, TiO₂ synthesized by the sol-microwave method resulted in small particles ($\varnothing=400$ nm), relatively high BET surface area (24.3 m²/g), and a mixed-crystalline structure of anatase and rutile phases (86:14) that enables to promote high photocatalytic activity. The effects of catalyst calcination temperature and calcination time were investigated, which the highest photocatalytic activity was obtained from TiO₂ calcined at 500 °C for 5 h. Moreover, it was observed that increasing of calcination temperature promoted phase transformation from anatase to rutile. The effect of several metal loadings over TiO₂ on its photocatalytic activity was later determined. In detail, Ag-TiO₂, Cu-TiO₂, and Ag-Cu-TiO₂ photocatalysts were synthesized by a sol-microwave method with a doping content of 1, 3, and 10 wt.%. It was found that 1wt.%Ag provided the highest photocatalytic activity due to small crystallite size, high BET surface area, small band gap, and suitable anatase-rutile ratio, which is efficiently promoted high photocatalytic activity. Lastly, the effect of microwave assisted wet impregnation was studied. It was found that microwave-assisted wet impregnation provided low BET surface area and resulted in low photocatalytic activity.

Keywords: Sugar, Titanium dioxide, Sol-gel synthesis, Photocatalytic oxidation, Ag, Cu.

ACKNOWLEDGEMENTS

I would like to acknowledge several people who kindly helped and supported my thesis.

Firstly, I would like to acknowledge my supervisors Assoc. Prof. Dr. Navadol Loasiripojana. He always answered my questions, and he put a lot of effort into my thesis. He gave me many ideas and knowledge, and he often encouraged me when I felt hopeless. I will remember his helpfulness. Thank you very much.

Secondly, I would like to acknowledge Asst. Prof. Dr. Siriluk Chiarakorn and Dr. Surawut Chuangchote. They always supported my thesis, guided me about the experiments, and helped me to discuss the results. Thank you very much.

Thirdly, I would like to thank Ms. Jiraporn Payormhorm. She always stood by me many times. She gave me wonderful ideas and guided the many steps of my experiments to success. She often advised me about thesis writing and thesis presentation, and made them better. Thanks for always being beside me.

Furthly, I would like to thank Ms. Nuch Puttiput. She was always beside me. We solved many problems together. She never let me fall. Thank you, my best friend.

Fifthly, I would like to thank my family. They supported me in everything and were always beside me whenever I had problems. Thank you very much, my lovely family.

Finally, I would like to acknowledge the financial support for this research by the Joint Graduate School of Energy and Environment, Rajamangla University of Technology Thanyaburi, and the National Center for Genetic Engineering and Biotechnology (BIOTEC).

CONTENTS

CHAPTER	TITLE	PAGE
	ABSTRACT	i
	ACKNOWLEDGEMENTS	ii
	CONTENTS	iii
	LIST OF FIGURES	v
	LIST OF TABLES	xi
	LIST OF ABBREVIATIONS	xviii
1	INTRODUCTION	1
	1.1. Rational/Problem Statement	1
	1.2. Literature Review	3
	1.3. Research Objective	23
	1.4. Scope of Research Work	23
2	THEORIES	24
	2.1. Definition of Photocatalysis	24
	2.2. Fundamental Theory of TiO ₂ Semiconductors	24
	2.3. TiO ₂ Photocatalyst	25
	2.4. Applications of TiO ₂	27
	2.5. Mechanism of Photocatalysis	28
	2.6. Photocatalytic of Sugar Conversion	29
	2.7. Preparation of Photocatalysts	30
	2.8. Metal Doped TiO ₂	32
	2.9. Glucose	33
3	METHODOLOGY	35
	3.1. Materials	35
	3.2. Titanium Dioxide Synthesis	35

CONTENTS (Cont')

CHAPTER	TITLE	PAGE
3	3.3. Photocatalytic Study	38
4	RESULTS AND DISSCUSSION	40
	4.1. Effect of TiO ₂ Preparation Methods on Its Photocatalytic Activity	40
	4.2. Effect of TiO ₂ Calcination Temperature	46
	4.3. Effect of TiO ₂ Calcination Time	51
	4.4. Effect of Metal Doped TiO ₂	54
5	CONCLUSION	80
	RECOMMENDATIONS	81
	REFERENCES	82
	APPENDIX	88
	A. Calculation of Crystallite Size and Phase Composition	89
	B. Calculation of Band Gap Energy	90
	C. Calculation of Conversion, Yield and Selectivity	91
	D. Domestic Microwave (Whirlpool AMW 585) for TiO ₂ (MW) Synthesis Manual	92
	E. Results Of HPLC Analysis	93

LIST OF FIGURES

FIGURE	TITLE	PAGE
1.1	XRD patterns of sol–gel-synthesized TiO ₂ (a) before and after thermal treatment at (b) 400 °C, (c) 500 °C, (d) 600 °C, and (e) 700 °C for 2 h	3
1.2	XRD patterns of TiO ₂ powders prepared under 28 kHz frequency US that were calcined at different temperature	7
1.3	Schlieren images of the luminescence pattern observed from top view of US bath while US irradiation with (a) 28 kHz, (b) 45 kHz, and (c) 100 kHz	8
1.4	XRD patterns of TiO ₂ prepared through the sol-microwave method: (a) pure TiO ₂ (MW), (b) un-calcined La-Zr-TiO ₂ , and (c) calcined La-Zr-TiO ₂	8
1.5	UV–vis absorption spectra of photocatalysts. (A) TiO ₂ , (B) Mn ²⁺ (0.06 wt.%)–TiO ₂ , (C) Ni ²⁺ (0.06 wt.%)–TiO ₂ , and (D) Zn ²⁺ (0.06 wt.%)–TiO ₂	10
1.6	XRD patterns of photocatalysts: (A) anatase, (R) rutile, and (*) Fe ₂ O ₃	11
1.7	UV–vis/DR spectra of different photocatalysts	12
1.8	X-ray diffraction patterns of 5% Fe:TiO ₂ annealed at (a) 400 °C, (b) 600 °C, and (c) 800 °C	13
1.9	XRD patterns of the samples: (a) P25; (b) TiO ₂ ; (c) 4.0% Fe/TiO ₂ ; (d) 4.5% Ni/TiO ₂ ; (e) 5.0% Fe–4.0% Ni/TiO ₂	14
1.10	The XRD photograph of the photocatalysts	16
1.11	XRD pattern of Ag doped TiO ₂ nanofibers	17

LIST OF FIGURES (Cont')

FIGURE	TITLE	PAGE
1.12	The effect of calcination temperature on crystallite size of photocatalysts	18
1.13	X-ray diffraction patterns of the TiO ₂ -Cu materials (a-d) annealed at 500 °C	18
1.14	pH changes during 3-hour illumination of 1.0 g dm ⁻³ glucose solution in the presence of TiO ₂	22
2.1	Representations of the TiO ₂ : anatase, rutile, and brookite forms	26
2.2	Mechanism of TiO ₂ photocatalysis	29
2.3	Mechanism of TiO ₂ photocatalysis $h\nu_1$: pure TiO ₂ ; $h\nu_2$: metal-doped TiO ₂	33
2.4	Structure of glucose	33
2.5	Structure of glucose (linear form)	34
3.1	The procedure of TiO ₂ synthesis with sol-gel method, ultrasonic assisted sol-gel method, sol-microwave method, wet impregnation method of metal-TiO ₂ and microwave assisted wet impregnation method of metal-TiO ₂	37
3.2	Photocatalytic reactor	39
4.1	X-ray diffraction patterns of TiO ₂ (SG), TiO ₂ (US), and TiO ₂ (MW)	41
4.2	SEM images (10000x) of (A) TiO ₂ (SG), (B) TiO ₂ (US), and (C) TiO ₂ (MW)	42

LIST OF FIGURES (Cont')

FIGURE	TITLE	PAGE
4.3	Effect of TiO ₂ synthesis methods on organic compounds in liquid phase after 120 min illumination: (a) TiO ₂ (SG), (b) TiO ₂ (US), and (c) TiO ₂ (MW)	45
4.4	Effect of TiO ₂ synthesis methods on maximum yields of xylitol, gluconic acid, and formic acid: TiO ₂ (SG), TiO ₂ (US), and TiO ₂ (MW)	46
4.5	X-ray diffraction patterns of TiO ₂ : 400 °C, 500 °C, and 600 °C	47
4.6	Effect of calcination temperature on organic compounds in liquid phase and glucose conversion after 120 min illumination: (a) 400 °C, (b) 500 °C, and (c) 600 °C	50
4.7	Effect of calcination temperature on maximum yields of xylitol, gluconic acid and formic acid: TiO ₂ calcined at 400 °C, TiO ₂ calcined at 500 °C, and TiO ₂ calcined at 600 °C	50
4.8	X-ray diffraction patterns of TiO ₂ : 2 and 5 h	51
4.9	Effect of calcination time on organic compounds in liquid phase and glucose conversion after 120 min illumination: (a) 2 h and (b) 5 h	53
4.10	Effect of calcination time on maximum yields of xylitol, gluconic acid and formic acid: TiO ₂ calcined for 2 h and TiO ₂ calcined for 5 h	54

LIST OF FIGURES (Cont')

FIGURE	TITLE	PAGE
4.11	X-ray diffraction patterns of pure TiO ₂ , 1wt.% Ag-TiO ₂ , 3wt.% Ag-TiO ₂ , and 10wt.% Ag-TiO ₂ .	55
4.12	UV-visible diffuse reflectance spectra of pure TiO ₂ , 1wt.% Ag-TiO ₂ , 3wt.% Ag-TiO ₂ , and 10wt.% Ag-TiO ₂	58
4.13	Effect of Ag doped TiO ₂ on glucose conversion and yields of xylitol, gluconic acid and formic acid after 120 min illumination: (a) pure TiO ₂ , (b) 1wt.% Ag-TiO ₂ , (c) 3wt.% Ag-TiO ₂ , and (d) 10wt.% Ag-TiO ₂	61
4.14	Effect of Ag doped TiO ₂ on maximum yields of xylitol, gluconic acid and formic acid: 0wt.% Ag, 1wt.% Ag, 3wt.% Ag, and 10wt.% Ag doped TiO ₂	62
4.15	X-ray diffraction patterns of pure TiO ₂ , 1wt.% Cu-TiO ₂ , 3wt.% Cu-TiO ₂ , and 10wt.% Cu-TiO ₂	63
4.16	UV-visible diffuse reflectance spectra of pure TiO ₂ , 1wt.% Cu-TiO ₂ , 3wt.% Cu-TiO ₂ , and 10wt.% Cu-TiO ₂	65
4.17	Effect of Cu doped TiO ₂ on glucose conversion and yields of xylitol, gluconic acid and formic acid after 120 min illumination: (a) pure TiO ₂ , (b) 1wt.% Cu-TiO ₂ , (c) 3wt.% Cu-TiO ₂ , and (d) 10wt.% Cu-TiO ₂	68
4.18	Effect of Cu doped TiO ₂ on maximum yields of xylitol, gluconic acid and formic acid: 0wt.% Cu, 1wt.% Cu, 3wt.% Cu, and 10wt.% Cu doped TiO ₂	68
4.19	X-ray diffraction patterns of TiO ₂ : 1wt.% Ag-TiO ₂ , 3wt.% Cu-TiO ₂ , and 1wt.% Ag-3wt.% Cu-TiO ₂	69

LIST OF FIGURES (Cont')

FIGURE	TITLE	PAGE
4.20	UV–visible diffuse reflectance spectra of 1wt.% Ag-TiO ₂ , 3wt.% Cu-TiO ₂ , and 1wt.% Ag-3wt.% Cu-TiO ₂	71
4.21	Effects of Ag, Cu and Ag-Cu doped TiO ₂ on glucose conversion and yields of xylitol, gluconic acid, and formic acid after 120 min illumination: (a) 1wt.% Ag-TiO ₂ , (b) 3wt.% Cu-TiO ₂ , and (c) 1wt.% Ag-3wt.% Cu-TiO ₂	73
4.22	Effects of Ag, Cu and Ag-Cu doped TiO ₂ on maximum yields of xylitol, gluconic acid, and formic acid: 1wt.% Ag-TiO ₂ , 3wt.% Cu-TiO ₂ , and 1wt.% Ag-3wt.% Cu-TiO ₂	74
4.23	X-ray diffraction patterns of TiO ₂ : 1wt.% Ag-TiO ₂ (wet impregnation) and 1wt.% Ag-TiO ₂ (microwave assisted wet impregnation)	75
4.24	UV–visible diffuse reflectance spectra of 1wt.% Ag-TiO ₂ (wet impregnation) and 1wt.% Ag-TiO ₂ (microwave assisted wet impregnation)	77
4.25	Effect of microwave assisted wet impregnation of Ag doped TiO ₂ on glucose conversion and yields of xylitol, gluconic acid and formic acid after 120 min illumination: (a) 1wt.% Ag-TiO ₂ (wet impregnation) and (b) 1wt.% Ag-TiO ₂ (microwave assisted wet impregnation)	79
4.26	Effect of microwave assisted wet impregnation of TiO ₂ on maximum yields of xylitol, gluconic acid and formic acid: 1wt.% Ag-TiO ₂ (wet impregnation) and 1wt.% Ag-TiO ₂ (microwave assisted wet impregnation)	79

LIST OF FIGURES (Cont')

FIGURE	TITLE	PAGE
D1	Domestic microwave (Whirlpool AMW 585)	92
E1	Results from HPLC of UV detector	108
E2	Results from HPLC of RI detector	109

LIST OF TABLES

TABLE	TITLE	PAGE
1.1	Results of XRD measurements for TiO ₂ samples.	4
1.2	Surface area of TiO ₂ samples	4
1.3	Weight percent (W%) and average crystallite size (d) of anatase and / or rutile phase(s) formed by calcination of dried sol-gel product at different temperatures (T)	5
1.4	Summary of characterization of photocatalytic systems	6
1.5	Properties of TiO ₂ prepared without and with US	7
1.6	Detailed characterization of doped titania	9
1.7	Physico-chemical properties of the photocatalysts (A: anatase; R: rutile)	12
1.8	Experimental particle size of 5%Fe:TiO ₂ annealed at 400, 600, and 800 °C	13
1.9	Specific surface area, band gaps and maximum absorption edges of doped TiO ₂	15
1.10	Physical properties of TiO ₂ and Ag-TiO ₂	16
1.11	Band gap E _g value of TiO ₂ and Ag-TiO ₂ values	17
1.12	Average crystallite size and E _g values for the Cu doping samples	19
1.13	Effect of photocatalysts and irradiation time on organic compounds distribution in the liquid phase (reaction conditions: C _{glucose} = 2.810 × 10 ⁻³ mol/L, 150 mL of H ₂ O:ACN = 10:90 v/v, catalyst 1 g/L, 30 °C, 1 atm)	20

LIST OF TABLES (Cont')

TABLE	TITLE	PAGE
1.14	Effect of solvent composition on glucose conversion and total selectivity for organic compounds (glucaric acid, gluconic acid and arabitol) in the liquid phase after 10 min of illumination	21
1.15	Derivatives of the compounds determined by GC-MS	22
2.1	Properties of anatase and rutile phase of TiO ₂	26
4.1	Summary of XRD, SEM and S _{BET} characterizations of the synthesized TiO ₂ : TiO ₂ (SG), TiO ₂ (US), TiO ₂ (MW), calcined at 500 °C for 5h, and P25	41
4.2	Summary of XRD characterizations of the synthesized TiO ₂ : catalysts synthesized by sol-microwave method, calcined at 400 °C, 500 °C, and 600 °C for 5 h	47
4.3	Summary of XRD characterizations of the synthesized TiO ₂ : catalysts synthesized by sol-microwave method, calcined at 500 °C for 2 and 5 h	52
4.4	Summary of XRD characterizations and S _{BET} of the catalysts synthesized by sol-microwave method, calcined at 500 °C for 5 h: pure TiO ₂ , 1wt.% Ag-TiO ₂ , 3wt.% Ag-TiO ₂ , and 10wt.% Ag-TiO ₂	55
4.5	Summary of UV-vis DR characterizations of the synthesized TiO ₂ : pure TiO ₂ , 1wt.% Ag-TiO ₂ , 3wt.% Ag-TiO ₂ , and 10wt.% Ag-TiO ₂	58

LIST OF TABLES (Cont')

TABLE	TITLE	PAGE
4.6	Summary of XRD characterizations and S_{BET} of the catalysts synthesized by the sol-microwave method, calcined at 500 °C for 5 h: pure TiO_2 , 1wt.% Cu- TiO_2 , 3wt.% Cu- TiO_2 , and 10wt.% Cu- TiO_2	63
4.7	Summary of UV-vis DR characterizations of the synthesized TiO_2 : pure TiO_2 , 1wt.% Cu- TiO_2 , 3wt.% Cu- TiO_2 , and 10wt.% Cu- TiO_2	65
4.8	Summary of XRD characterizations and S_{BET} of the catalysts synthesized by the sol-microwave method, calcined at 500 °C for 5 h: 1wt.% Ag- TiO_2 , 3wt.% Cu- TiO_2 , and 1wt.% Ag-3wt.% Cu- TiO_2	69
4.9	Summary of UV-vis DR characterizations of the synthesized TiO_2 : 1wt.% Ag- TiO_2 , 3wt.% Cu- TiO_2 , and 1wt.% Ag-3wt.% Cu- TiO_2	71
4.10	Summary of XRD characterizations and S_{BET} of the catalysts synthesized by sol-microwave method, calcined at 500 °C for 5 h: 1wt.% Ag- TiO_2 (wet impregnation), and 1wt.% Ag- TiO_2 (microwave assisted wet impregnation)	75
4.11	Summary of UV-vis DR characterizations of the synthesized TiO_2 : 1wt.% Ag- TiO_2 (wet impregnation) and 1wt.% Ag- TiO_2 (microwave assisted wet impregnation)	77

LIST OF TABLES (Cont')

TABLE	TITLE	PAGE
E1	Results obtained for photocatalytic reaction of glucose with TiO ₂ (synthesized by sol-gel method, calcined at 500 °C for 5 h) catalyst in terms of glucose conversion, yield and selectivity to organic compounds: gluconic acid and formic acid	93
E2	Results obtained for photocatalytic reaction of glucose with TiO ₂ (synthesized by ultrasonic assisted sol-gel method, calcined at 500 °C for 5 h) catalyst in terms of glucose conversion, yield and selectivity to organic compounds: gluconic acid and formic acid	94
E3	Results obtained for photocatalytic reaction of glucose with TiO ₂ (synthesized by sol-microwave method, calcined at 500 °C for 5 h) catalyst in terms of glucose conversion, yield and selectivity to organic compounds: xylitol, gluconic acid and formic acid	95
E4	Results obtained for photocatalytic reaction of glucose with TiO ₂ (synthesized by sol-microwave method, calcined at 400 °C for 5 h) catalyst in terms of glucose conversion, yield and selectivity to organic compounds: xylitol, gluconic acid and formic acid	96
E5	Results obtained for photocatalytic reaction of glucose with TiO ₂ (synthesized by sol-microwave method, calcined at 600 °C for 5 h) catalyst in terms of glucose conversion, yield and selectivity to organic compounds: xylitol, gluconic acid and formic acid	97

LIST OF TABLES (Cont')

TABLE	TITLE	PAGE
E6	Results obtained for photocatalytic reaction of glucose with TiO ₂ (synthesized by sol-microwave method, calcined at 500 °C for 2 h) catalyst in terms of glucose conversion, yield and selectivity to organic compounds: xylitol, gluconic acid and formic acid	98
E7	Results obtained for photocatalytic reaction of glucose with 1wt.% Ag-TiO ₂ (synthesized by sol-microwave method, calcined at 500 °C for 5 h and wet impregnation for Ag doping) catalyst in terms of glucose conversion, yield and selectivity to organic compounds: xylitol, gluconic acid and formic acid	99
E8	Results obtained for photocatalytic reaction of glucose with 3wt.% Ag-TiO ₂ (synthesized by sol-microwave method, calcined at 500 °C for 5 h and wet impregnation for Ag doping) catalyst in terms of glucose conversion, yield and selectivity to organic compounds: xylitol, gluconic acid and formic acid	100
E9	Results obtained for photocatalytic reaction of glucose with 10wt.% Ag-TiO ₂ (synthesized by sol-microwave method, calcined at 500 °C for 5 h and wet impregnation for Ag doping) catalyst in terms of glucose conversion, yield and selectivity to organic compounds: xylitol, gluconic acid and formic acid	101

LIST OF TABLES (Cont')

TABLE	TITLE	PAGE
E10	Results obtained for photocatalytic reaction of glucose with 1wt.%Cu-TiO ₂ (synthesized by sol-microwave method, calcined at 500 °C for 5 h and wet impregnation for Ag doping) catalyst in terms of glucose conversion, yield and selectivity to organic compounds: xylitol, gluconic acid and formic acid	102
E11	Results obtained for photocatalytic reaction of glucose with 3wt.% Cu-TiO ₂ (synthesized by sol-microwave method, calcined at 500 °C for 5 h and wet impregnation for Ag doping) catalyst in terms of glucose conversion, yield and selectivity to organic compounds: xylitol, gluconic acid and formic acid	103
E12	Results obtained for photocatalytic reaction of glucose with 10wt.% Cu-TiO ₂ (synthesized by sol-microwave method, calcined at 500 °C for 5 h and wet impregnation for Ag doping) catalyst in terms of glucose conversion, yield and selectivity to organic compounds: xylitol, gluconic acid and formic acid	104
E13	Results obtained for photocatalytic reaction of glucose with 1wt.% Ag-3wt.% Cu-TiO ₂ (synthesized by sol-microwave method, calcined at 500 °C for 5 h and wet impregnation for Ag doping) catalyst in terms of glucose conversion, yield and selectivity to organic compounds: xylitol, gluconic acid and formic acid	105

LIST OF TABLES (Cont')

TABLE	TITLE	PAGE
E14	Results obtained for photocatalytic reaction of glucose with 1wt.% Ag-TiO ₂ (synthesized by sol-microwave method, calcined at 500 °C for 5 h and microwave assisted wet impregnation for Ag doping) catalyst in terms of glucose conversion, yield and selectivity to organic compounds: xylitol, gluconic acid and formic acid	106
E15	Results obtained for photocatalytic reaction of glucose with P25 (commercial grade TiO ₂) catalyst in terms of glucose conversion, yield and selectivity to organic compounds: xylitol, gluconic acid and formic acid	107

LIST OF ABBREVIATIONS

XRD	=	X-ray diffraction
SEM	=	Scanning electron microscopy
UV-vis/DR	=	UV-vis diffuse reflectance spectrophotometry
HPLC	=	High-performance liquid chromatography
SG	=	Sol-gel
US	=	Ultrasonic
MW	=	Microwave
A	=	Anatase phase
R	=	Rutile phase

CHAPTER 1

INTRODUCTION

1.1. Rationale/Problem Statement

The conversion of biomass to renewable chemicals and fuels has received significant attention as one of the key technologies for a sustainable society (Kobayashi *et al.*, 2010). In recent years, many researchers attempt to find ways to utilize biomass as feedstocks for the production of chemicals and fuels because of its abundance, renewability, and worldwide distribution (Werpy *et al.*, 2004). On the basis of biomass, it consists of hydrocarbon compounds (carbon, hydrogen, and oxygen are mainly elementals) like fossil fuels, but its chemical compositions are different. Cellulose, hemicelluloses, and lignin are polymeric hydrocarbon, from which their structures are linear homopolysaccharide, branched heteropolysaccharide, and complex three-dimensional polymer of polyphenolic substance, respectively (Mohan *et al.*, 2006). To consider the glucose, it is abundant and is an important sugar monomer in the structure of cellulose. Recently, various processes have already been developed for biomass conversion including steam gasification (Erkiaga *et al.*, 2013), fast pyrolysis (Bridgwater *et al.*, 2012) and super critical conversion (Patel *et al.*, 2011). Nevertheless, these processes also require high temperature, high pressure, high energy consumption, and high system cost to produce chemicals and fuels. Photo-catalysis is one of promising process because it can be performed under solar irradiation at room temperature and mild condition (Chong *et al.*, 2010).

Titanium dioxide (TiO_2) has been considered to be the most attractive heterogeneous photocatalyst, because it possesses the excellent photocatalytic activity, low levels of toxicity, and strong oxidizing power (Chen *et al.*, 2007). It has been widely used for the degradation of organic species in waste water (Hwang *et al.*, 2012), H_2 production (Gomathisankar *et al.*, 2013), self-cleaning surfaces (Murugan *et al.*, 2013), and dye sensitized solar cells (Cheng *et al.*, 2013). TiO_2 can be fabricated by sol-gel method, which is easy to operate and inexpensive (Tseng *et al.*, 2010). In addition, the photocatalytic activity of TiO_2 depends mainly on morphological appearances and properties such as surface area, particle distribution, and crystallinity *etc.* It was reported that photoactivity of

TiO₂ particles could exhibit high crystallinity, high surface area, and consist mainly of anatase at low temperature preparation (Colmenares *et al.*, 2009). This has been mostly investigated because of its high activity in photocatalytic applications.

Furthermore, the use of ultrasonic irradiation during the synthetic procedure has been studied. Ultrasonic irradiation can help to obtain smaller homogeneous nanoparticles and lead to an increase in surface area (Colmenares *et al.*, 2011). Moreover, microwave irradiation requires very short reaction time, and can produce small particles with a narrow particle size distribution (Shojaie *et al.*, 2010). However, there are some disadvantages of TiO₂ such as: (i) TiO₂ has a wide band-gap and thus TiO₂ is only excited by UV-light but the excitation with visible light is not possible, and (ii) high recombination rate of the electron–hole pairs which can decrease the efficiency of the photocatalytic process.

Doping metal techniques have been applied in photocatalysis to overcome these limitations as well as the photocatalytic activity could be enhanced (Aramendia *et al.*, 2006). In recent years, metal ion-doped into TiO₂ has been widely studied. Inexpensive metals, e.g., Ag (Rengaraj *et al.*, 2006) and Cu (Lopez *et al.*, 2009) have been reported to be beneficial for photocatalytic reactions. Selective oxidation of glucose can be driven by photocatalytic reactions providing high-value chemicals, i.e. glucaric acid, gluconic acid, and arabitol (Colmenares *et al.*, 2011). Furthermore, Zmudzinski reported that the photo-oxidation of glucose leads to formation of acidic compounds–products, i.e. mannonic acid and gluconic acid (Zmudzinski *et al.*, 2010). The present investigation aims to study the photocatalytic oxidation of glucose to high-valued organic compounds (i.e. xylitol, gluconic acid, formic acid) and to improve photocatalytic activity of TiO₂ by doping Ag and Cu over TiO₂.

1.2. Literature Review

1.2.1. Sol-gel synthesis of TiO₂

Su *et al.* (2004) studied the micro-structure and properties of TiO₂ synthesized by a sol-gel method. TiO₂ sols were prepared by the hydrolysis and condensation of titanium (IV) *n*-butoxide in *iso*-propyl alcohol. The XRD patterns of the TiO₂ samples before and after heat treatment at 400, 500, 600, and 700 °C for 2 h are, respectively, shown in Fig. 1.1 (a–e).

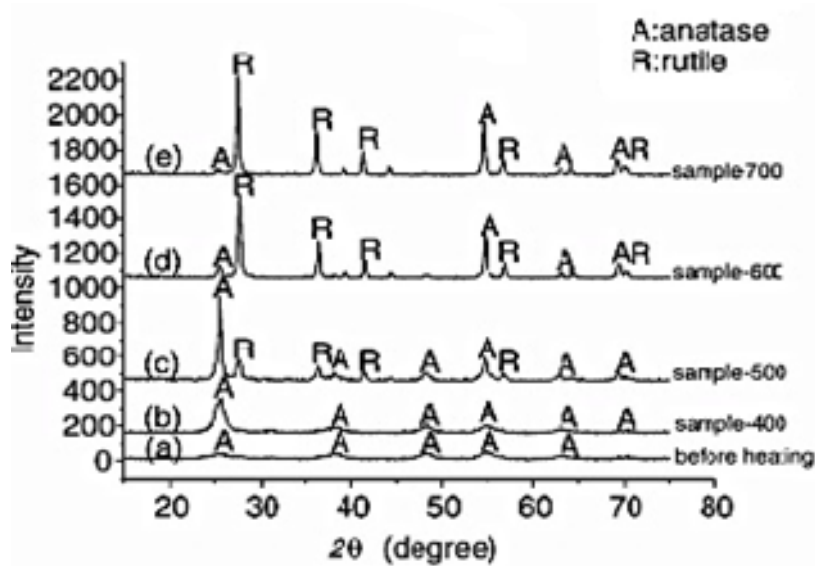


Fig. 1.1 XRD patterns of sol-gel-synthesized TiO₂ (a) before and after thermal treatment at (b) 400 °C, (c) 500 °C, (d) 600 °C, and (e) 700 °C for 2 h (Su *et al.*, 2004).

Obviously, the amorphous phase crystallizes into an anatase structure at the temperature of 400 °C. However, a phase transformation from anatase to rutile also occurred when increasing the calcination temperature. The high temperature facilitates bond breaking as well as atoms rearrangement and therefore the transformation of anatase to rutile occurs easily. The average crystal sizes of TiO₂ before and after annealing at various temperatures are listed in Table 1.1.

Table 1.1 Results of XRD measurements for TiO₂ samples (Su *et al.*, 2004).

Calcination Temperature (T _c) (°C)	Crystal size (nm)	A/R
Before annealing (A)	4.10	
400 (A)	13.96	9.8
500 (A)	17.60	3.23
500 (R)	18.78	
600 (A)	20.68	0.12
600 (R)	26.31	
700 (A)	26.44	0.03
700 (R)	35.07	

The crystal sizes for both anatase and rutile increased with increasing calcination temperature, indicating the aggregation of TiO₂ nanoparticles when annealing. During the heat treatment, the dehydration occurs and the crystals grow to a larger size than the original particles. Table 1.2 shows the dependence of the surface area on the temperature of calcination of the TiO₂ samples. Samples calcined at 400 °C possess high specific surface area (122 m²g⁻¹ according to BET, Table 1.2), which then decreased to 11.5 m²g⁻¹ with increasing the calcination temperature up to 800 °C. This observation indicates an increase in the crystal size of TiO₂ in increasing the calcination temperature.

Table 1.2 Surface area of TiO₂ samples (Su *et al.*, 2004).

Calcination temperature (°C)	Surface area (m ² g ⁻¹)
400	122.2
500	65.7
700	26.9
800	11.5
Degussa P-25	52.0

Chaudhary *et al.* (2011) studied the preparation of TiO₂ nanoparticles by the sol-gel process using titanium isopropoxide as a precursor with ethanol and water as the solvents. The synthesis involves gel formation, aging for 24 h, drying at 100 °C for 10 h, and calcination in air at 500-800 °C for 2 h. Table 1.3 shows resulting product at several

temperatures. With the increase of the calcination temperature to 800 °C, only the rutile phase occurs, which indicated that the anatase phase was suppressed, while that of rutile improved progressively with the rise in calcination temperature.

Table 1.3 Weight percent (W%) and average crystallite size (d) of anatase and/or rutile phase(s) formed by calcination of dried sol-gel product at different temperatures (Chaudhary *et al.*, 2011).

(T) °C	Anatase phase		Rutile phase	
	W%	d (nm)	W%	d (nm)
500	100	11	-	-
600	54.8	20	45.2	22
700	28.0	21	72.2	23
800	-	-	100.0	25

Colmenares *et al.* (2011) studied the powdered TiO₂ photocatalysts synthesized by an ultrasonic-promoted sol-gel method (US). A second catalyst, designated as TiO₂(R), was synthesized in the same manner, but under solvent reflux, instead of ultrasound. The characteristic of the photocatalysts is presented in Table 1.4. The TiO₂(US) and TiO₂(R) exhibited better features than Degussa P-25. The best features were observed from TiO₂(US), which was synthesized with ultrasonic (high specific surface area 65 m²/g, low band gap 3.03 eV and anatase phase 12.7 nm). Interestingly, TiO₂(US) absorbed light in the visible range (absorption threshold 409 nm) possibly due the presence of oxygen vacancies (electronic disturbance) on its surface promoted by cavitation during ultrasound-assisted synthesis.

Table 1.4 Summary of characterization of photocatalytic systems (Colmenares *et al.*, 2011).

Photocatalyst	N ₂ isotherms		UV-vis		XRD	
	S _{BET} ^a (m ² /g)	V _p ^a (mL/g)	Band gap (eV)	Absorption threshold (nm)	Crystal phase ^b (%)	Crystallite size (nm)
Degussa-P25	51	-	3.20	387	A(88)/R(12)	17.6/24.4
TiO ₂ (US)	65	0.14	3.03	409	A(100)	12.7
TiO ₂ (R)	54	0.12	3.17	391	A(100)	12.4

^a Specific surface area (S_{BET}), cumulative pore volume (V_p),

^b A and R denote anatase and rutile, respectively.

Latt *et al.* (2008) studied the anatase-TiO₂ powders prepared by the sol-gel process. The hydrolysis process was carried out with and without ultrasound (US) for 1 h at room temperature. The US reactor was able to be switch into three different frequencies, such as 28, 45, and 100 kHz with nominal output power 175–300 W. The TiO₂ powders were calcined at 300 °C and characterized its particle size and surface area as shown in Table 1.5. It is noted that US frequency strongly affects the particle size of TiO₂ powder. US-TiO₂ powder shows smaller size than non-US-TiO₂ powder. The average particle size of US-TiO₂ powder prepared under 28, 45 and 100 kHz frequency US were 0.11, 0.63, and 26 μm, respectively. The US irradiation influenced on particle size could be seen in 28 and 45 kHz frequencies and the smaller TiO₂ particles were prepared by the former case. As seen in Table 1.5, the BET surface area of the non-US TiO₂ is much lowered.

Latt *et al.* (2008) also reported that calcination treatment at different temperatures improved crystalline on TiO₂ powder. The sol-gel TiO₂ powders were prepared under 28 kHz US and calcined at 300, 400, 500, 600, and 700 °C. When TiO₂ powders were calcined, phase transformation from anatase to rutile occurred with increasing the calcination temperature. From XRD pattern in Fig. 1.2, the peak intensities of anatase at 25° increased in the range of calcined temperature from 300 to 600 °C. The appearance of the peak at 27° presented that rutile phase appeared at 600 °C and became the main phase when increased the temperature from 600 °C to 700 °C.

Table 1.5 Properties of TiO₂ prepared without and with US (Latt *et al.*, 2008).

Sample	US frequency (kHz)	Aggregated particle size ^a (μm)	Particle size ^b (nm)	BET surface area (m ² g ⁻¹)
Non-US-TiO ₂	-	24	12	133
US-TiO ₂ -28	28	0.11	7	188
US-TiO ₂ -45	45	0.63	9	166
US-TiO ₂ -100	100	26	10	141

^a LST was used to estimate aggregated particle size of each TiO₂ powder.

^b TEM images of each TiO₂ powder were measured and the particle size was estimated.

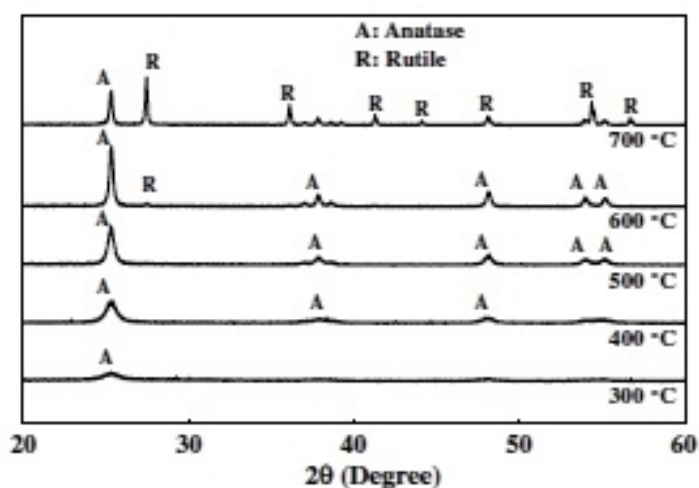


Fig. 1.2 XRD patterns of TiO₂ powders prepared under 28 kHz frequency US and calcined at different temperatures (Latt *et al.*, 2008).

The image in Fig. 1.3(a) also suggested that the large luminescence intensity and strong luminal pattern stripes could be observed. Dissimilarly in Fig. 1.3(b), slimmed luminol pattern stripes are occurred. In Fig. 1.3(c), 100 kHz US irradiation produced weak luminol sonochemical reaction. It was suggested that the generated cavity bubbles increased the mechanical shearing stress to form fine nano-sized particles in sol-gel TiO₂ process.

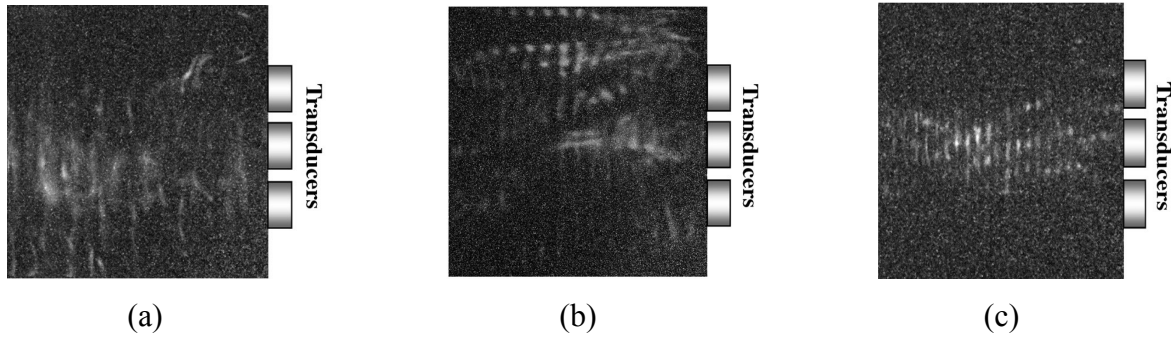


Fig. 1.3 Schlieren images of the luminescence pattern observed from top view of US bath while US irradiation with (a) 28 kHz, (b) 45 kHz, and (c) 100 kHz (Latt *et al.*, 2008).

Shojaie *et al.* (2010) studied the preparation of anatase nano-TiO₂ powders by the sol-microwave method (800W, 40% power). The anatase TiO₂ was formed in a short time (<4 min). The XRD patterns of microwave-assisted samples are shown in Fig. 1.4. Almost the sharp peaks could be indexed as anatase phase except rutile phase appeared in XRD pattern before calcination, it appears around $2\theta = 36.27^\circ$. The sharp diffraction peaks show that the obtained TiO₂ have high crystallinity of the nano TiO₂ increased after calcination. The microwave irradiation induced high crystallinity in a short time.

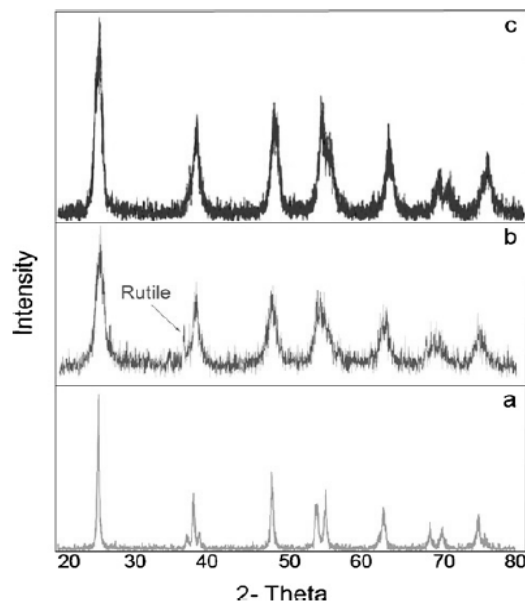


Fig. 1.4 XRD patterns of TiO₂ prepared through the sol-microwave method: (a) pure TiO₂ (MW), (b) un-calcined La-Zr-TiO₂, and (c) calcined La-Zr-TiO₂ (Shojaie *et al.*, 2010).

1.2.2. Photocatalyst modification

Devi *et al.* (2010) prepared metal ions doped TiO₂ such as Mn²⁺, Ni²⁺, and Zn²⁺ and characterized the materials by various analytical techniques. Ni²⁺ doped TiO₂ and Zn²⁺ doped TiO₂ catalysts showed anatase phase, while Mn²⁺ doped TiO₂ samples exhibited mixture phase of anatase and rutile (Table 1.6). The catalyst with dopant concentration of 0.02, 0.06, and 0.1 wt.% was labeled as M-1, M-2, and M-3 respectively (where M=Mn, Ni and Zn). The rutile fraction increased with increase in Mn²⁺ content. Due to the larger ionic radius of Mn²⁺ (0.80 Å) compared to Ti⁴⁺, Mn²⁺ ions can replace Ti⁴⁺ substitutionally in the lattice sites. The substitution of Mn²⁺ induces oxygen vacancies at the surface of anatase grains and rearrangement for the formation of rutile phase. The anatase crystallite size of Mn²⁺ was found to be 26.3, 23.6, 20.3, and 16.6 nm for a dopant concentration of 0, 0.02, 0.06, and 0.1 wt.% respectively while the rutile crystallite size in the samples Mn-2 and Mn-3 were similar to that of anatase. These results suggest that Mn²⁺ doping into the TiO₂ matrix effectively inhibit the grain growth of both the phases. Moreover, the decrease in the grain size also increases the specific surface areas.

Table 1.6 Detailed characterization of doped titania (Devi *et al.*, 2010).

Photocatalyst	A:R	C ^a (nm)	Lattice parameter (Å)	λ ^b (nm)	E _g ^c (eV)	SA ^d
TiO ₂	100:0	26.3	a = b = 3.7828, c = 9.5023	380	3.2	18
Mn-1	100:0	23.6	a = b = 3.7832, c = 9.5103	426	2.9	21
Mn-2	90:10	20.3:20.3 ^R	a = b = 3.7824, c = 9.5211	454	2.7	26
Mn-3	52:48	16.6:16.6 ^R	a = b = 3.7800, c = 9.5002	420	2.9	24
Ni-1	100:0	23.8	a = b = 3.7832, c = 9.5069	426	2.9	25
Ni-2	100:0	18.9	a = b = 3.7800, c = 9.5189	468	2.6	30
Ni-3	100:0	15.1	a = b = 3.7800, c = 9.5228	450	2.7	31
Zn-1	100:0	23.6	a = b = 3.7832, c = 9.5123	420	2.9	25
Zn-2	100:0	19.8	a = b = 3.7824, c = 9.5311	456	2.7	32
Zn-3	100:0	15.6	a = b = 3.7820, c = 9.5009	442	2.8	37

A:R anatase:rutile ratio, ^a Crystallite size calculated from Scherrer's Equation, ^b Band gap absorption, ^c Band gap, ^d Specific surface area.

The wavelength at which TiO_2 absorbed light are shown in Fig. 1.5. The doped samples showed a significant shift in the band gap absorption to the longer wavelength, due to the introduction of electronic level in the band gap induces red shift in the absorption. The light absorption ability increased with increase in the dopant concentration. The similarity in the band gap absorption values for Mn^{2+} and Zn^{2+} doped samples and a slight higher band gap absorption value for Ni^{2+} - TiO_2 sample can be explained by the electronegativity of doped metal atoms, large shift in the band gap absorption for Ni^{2+} doped TiO_2 in comparison with Mn^{2+} and Zn^{2+} doped TiO_2 was accounted to the higher electronegativity of Ni^{2+} .

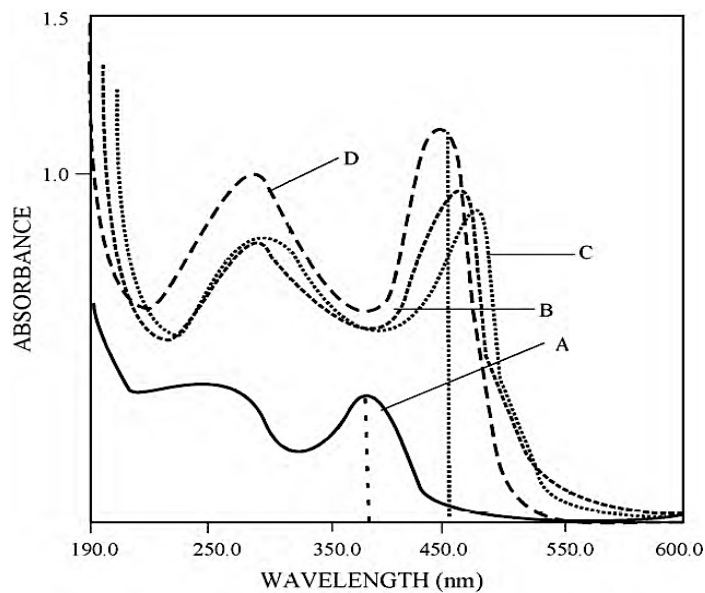


Fig. 1.5 UV-vis absorption spectra of photocatalysts. (A) TiO_2 , (B) Mn^{2+} (0.06 wt.%)– TiO_2 , (C) Ni^{2+} (0.06 wt.%)– TiO_2 , (D) Zn^{2+} (0.06 wt.%)– TiO_2 (Devi *et al.*, 2010).

MoZIA *et al.* (2011) studied the preparation of a TiO_2 modified with $\text{Fe}(\text{NO}_3)_3$ and calcinated at the temperatures of 400–600 °C in an argon atmosphere. The XRD patterns of the TiO_2 and Fe/TiO_2 photocatalysts are shown in Fig. 1.6. The phase composition of the photocatalysts is presented in Table 1.7. It can be observed that crude TiO_2 contained anatase and rutile phases in the ratio of 85:15. The diffraction lines were weak and broad suggesting poor crystallinity of the sample. The heat treatment of A-500 resulted in an improvement of TiO_2 crystallinity associated with anatase crystals growth (12nm vs. 7 nm). The crystallite size of anatase in the Fe/TiO_2 sample represents that the thermal

treatment did not significantly affect the crystallite size of anatase. Samples A-Fe10N500, A-Fe20N500 and A-Fe30N500 annealed at 500 °C exhibited crystallinity similar to that of crude TiO₂. Moreover, anatase crystals of these powders were a little smaller than in the case of A-500 (9 nm vs. 12 nm). These results indicate that Fe introduced in the form of Fe(NO₃)₃ did not catalyze anatase crystallite growth upon annealing as well as the fine dispersion of iron-restricting crystallite growth. In case of the samples containing 20 and 30 wt.% of Fe, iron oxide (Fe₂O₃) was identified. It can be seen that either an increase of annealing temperature in case of the catalysts containing 20 wt.% of Fe or introduction of a higher amount of Fe was responsible for growth of crystallite size of Fe₂O₃ (narrowing of diffraction lines) as presented in Fig. 1.6.

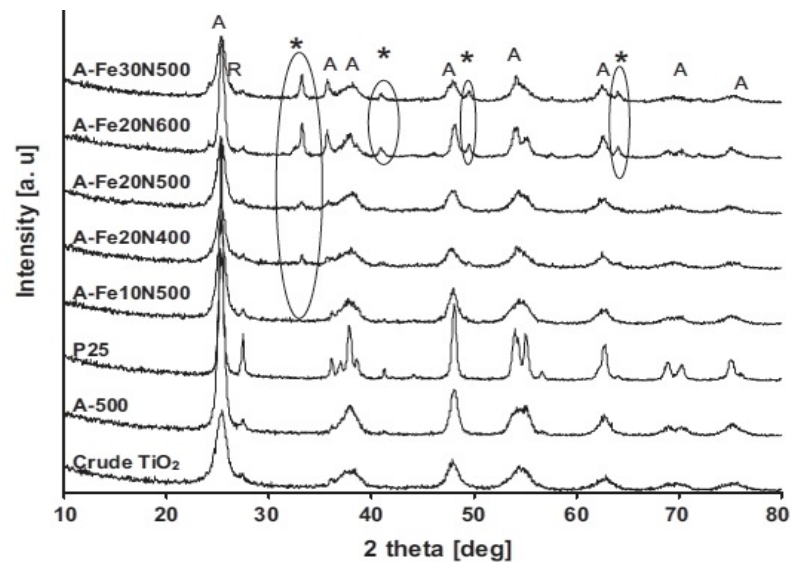


Fig. 1.6 XRD patterns of photocatalysts: (A) anatase, (R) rutile, and (*) Fe₂O₃ (Mozia *et al.*, 2011).

Additionally, the specific BET surface area (S_{BET}) of the pure titania samples decreased with increasing calcination temperature as shown in Table 1.7. In the case of Fe/TiO₂, the S_{BET} decreased with the annealing temperature. A decrease of S_{BET} with increasing annealing temperature in case of catalysts containing 20 wt.% of Fe might be attributed to growing crystallite size of anatase and Fe₂O₃.

Table 1.7 Physico-chemical properties of the photocatalysts (A: anatase; R: rutile) (Mozia *et al.*, 2011).

Sample	S_{BET} (m^2/g)	Phase composition by XRD	Crystallite of anatase (nm)	Anatase over rutile ratio (A:R)
Crude TiO_2	215	A, R	7	85 : 15
A500	103	A, R	12	92 : 8
P25	50	A, R	22	82 : 18
A-Fe10N500	109	A, R	9	89 : 11
A-Fe20N400	109	A, R, Fe_2O_3	8	85 : 15
A-Fe20N500	82	A, R, Fe_2O_3	9	87 : 13
A-Fe20N600	44	A, R, Fe_2O_3	15	93 : 7
A-Fe30N500	83	A, R, Fe_2O_3	9	87 : 13

The UV–vis/DR spectra (in Fig. 1.7) of the Fe/TiO_2 powders indicate that a significant increase in the absorption at $\lambda > 400nm$ was observed for the Fe/TiO_2 samples. The absorption in the visible range was stronger at higher Fe concentrations. The red shift could be attributed to a charge transfer transition between Fe and TiO_2 conduction or valence bands.

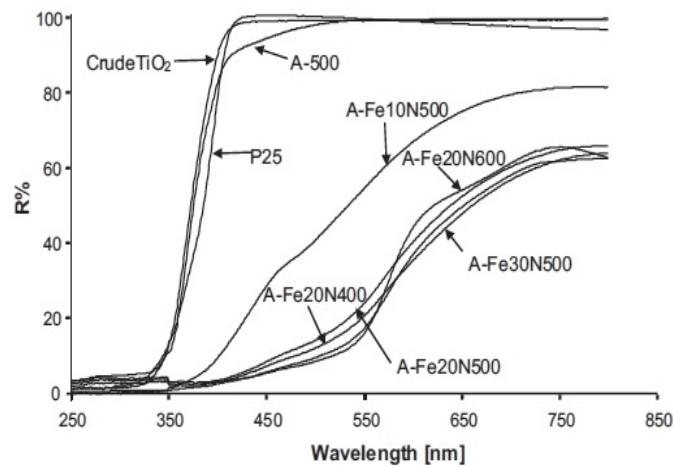


Fig. 1.7 UV–vis/DR spectra of different photocatalysts (Mozia *et al.*, 2011).

Nasralla *et al.* (2013) studied 5% (molar ratio) Fe doped TiO₂ nanoparticles were prepared by a sol gel method and the post annealing of the samples was carried out at 400 °C, 600 °C, and 800 °C in air. The XRD patterns of Fe-doped TiO₂ at different different annealing temperatures, as shown in Fig. 1.8, show that the samples annealing at T of 400 °C had both anatase and rutile structures with the dominance of the former. At T of 800 °C, the anatase structure disappears and the samples show monostructure. The samples did not show any diffraction peaks of iron or iron compounds, which suggest the formation of an iron-titanium solid solution, where the iron ion has been incorporated into the TiO₂ crystal structure substitutionally, due to similar ionic radii (Ti (0.68) and Fe (0.64)). From Table 1.8, it can also be seen that the particle size of TiO₂ increases with increasing calcination temperature.

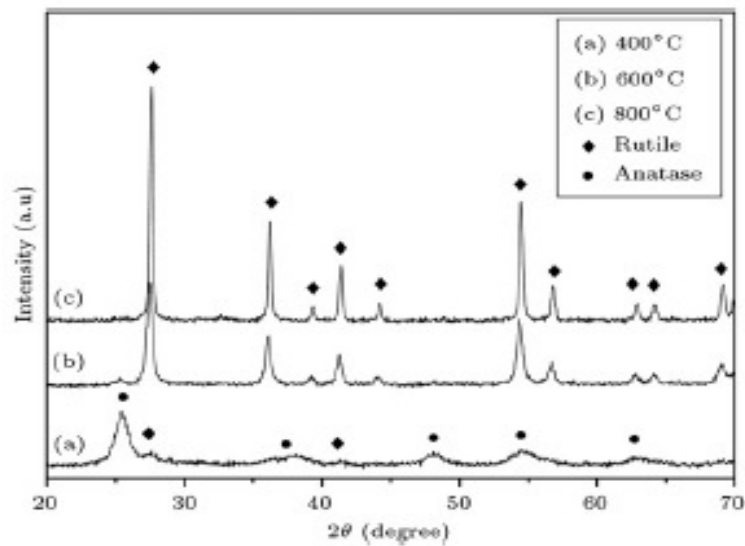


Fig. 1.8 X-ray diffraction patterns of 5% Fe:TiO₂ annealed at (a) 400 °C, (b) 600 °C, and (c) 800 °C (Nasralla *et al.*, 2013).

Table 1.8 Experimental particle size of 5%Fe:TiO₂ annealed at 400, 600, and 800 °C (Nasralla *et al.*, 2013).

Sample	Particle size (nm)	Phase
5%Fe, 400 °C	6-10	Anatase
5%Fe, 600 °C	22-30	Anatase, Rutile
5%Fe, 800 °C	50-100	Rutile

Sun *et al.* (2012) successfully prepared pure TiO₂, single-doped and (Fe, Ni) co-doped TiO₂ nanoparticles. The XRD patterns of TiO₂ nanoparticles prepared by the alcohol thermal method are shown in Fig. 1.9. Except for P25 (Degussa AG, Germany), all samples exhibit the diffraction peaks of the anatase phase, demonstrating that the samples are pure anatase. Crystallite sizes of TiO₂, 4.0% Fe/TiO₂, 4.5% Ni/TiO₂, and 5.0% Fe–4.0% Ni/TiO₂ are 20.6, 15.2, 15.3, and 13.8 nm, respectively. The TiO₂ crystallites exhibit smaller sizes compared with those of pure TiO₂ particles, since Fe and Ni doping can suppress its crystal growth.

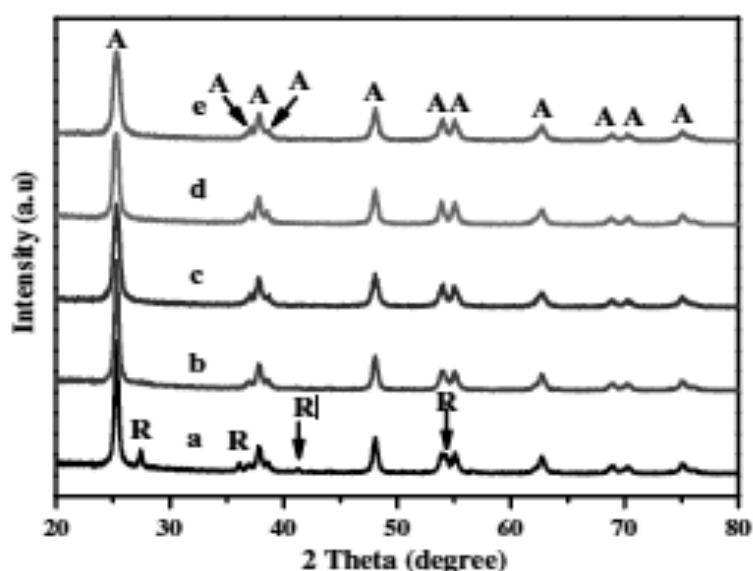


Fig. 1.9 XRD patterns of the samples: (a) P25; (b) TiO₂; (c) 4.0% Fe/TiO₂; (d) 4.5% Ni/TiO₂; (e) 5.0% Fe–4.0% Ni/TiO₂ (Sun *et al.*, 2012).

Table 1.9 indicates the physicochemical properties of pure TiO₂, Fe/TiO₂, Ni/TiO₂, and Fe–Ni/TiO₂. The 5.0%Fe–4.0%Ni/TiO₂ sample has the largest surface area of 98.35 m²/g. The surface area of 4.0% Fe–4.5% Ni/TiO₂ is 95.23 m²/g while that of 4.0% Fe/TiO₂ and 4.5% Ni/TiO₂ are 74.09 and 73.18 m²/g, respectively. The surface area of pure TiO₂ is 43.13 m²/g. TiO₂ doped with Fe and Ni owns a larger specific surface area, and it is consistent with the fact that smaller particle sizes should have a larger S_{BET}. A large surface area of a prepared catalyst will benefit its photocatalytic reactions. In this work, the optimal levels for Fe/Ti and Ni/Ti are 4.0% and 4.5%, respectively. The Fe and Ni co-doping displays a higher optical absorption of visible light than that of single doping

when the dopants are in a relatively high concentration. Fe and Ni doping can generate an impurity band in the crystal lattice of TiO₂, and that band is located in the middle of the optical band gap of TiO₂. Electrons in the valence band absorb longer wavelengths. The optimal co-doping ratio of Fe/Ti and Ni/Ti is 5.0% and 4.0%, respectively, and its absorption edge is 514 nm (Table 1.9). Because of Fe and Ni co-doping, the visible light absorption intensity of TiO₂ increases. The energy gap of the 5.0%Fe–4.0%Ni/TiO₂ sample is estimated to be 2.41 eV.

Table 1.9 Specific surface area, band gaps and maximum absorption edges of doped TiO₂ (Sun *et al.*, 2012).

Sample	Specific surface area	Maximum absorption edge	Band gap (eV)
TiO ₂	43.13	387	3.20
2.5%Fe	64.28	447	2.77
4.0%Fe	74.09	476	2.60
2.5%Ni/TiO ₂	66.22	404	3.07
4.5%Ni/TiO ₂	73.18	429	2.89
5.0%Fe-4.0%Ni/TiO ₂	98.35	514	2.41
4.0%Fe-4.5%Ni/TiO ₂	95.23	485	2.56

Rengaraj *et al.* (2006) studied Ag-TiO₂ nanocatalysts synthesized by the ultrasonic-assisted sol–gel method with a doping content up to 1.5 wt%-Ag. The TiO₂ and Ag-TiO₂ samples were examined by XRD and their phase conditions are shown in Fig. 1.10. The XRD results indicate that the catalysts have been predominantly crystallized into an anatase phase under this experimental condition. In this investigation, the intensity of the anatase peak at $2\theta = 25.4 \pm 0.1^\circ$ was considered (101), and the intensity of rutile peak at $2\theta = 27.5 \pm 0.1^\circ$ was considered (110).

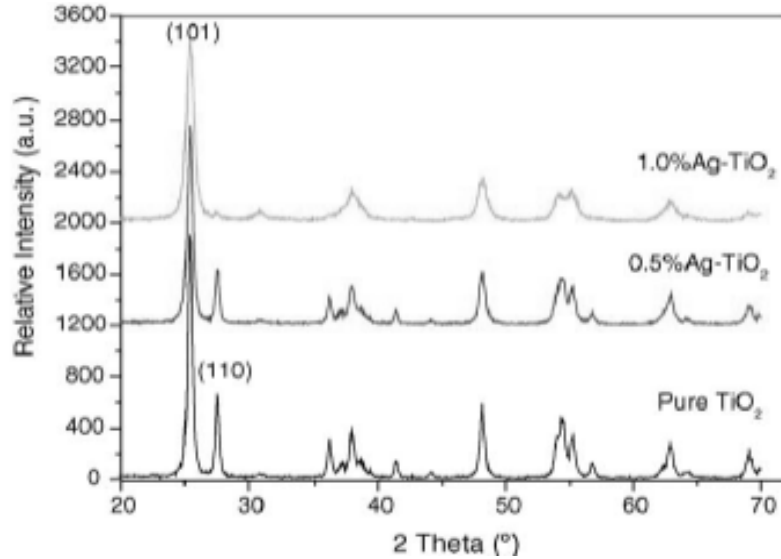


Fig. 1.10 The XRD photograph of the photocatalysts (Rengaraj *et al.*, 2006).

W_A for all samples is presented in Table 1.10, which indicates that the 0.5% Ag-TiO₂ and 1% Ag-TiO₂ had W_A values of 73.80 and 92.39%, higher than that of pure TiO₂ (69.90%). It might be concluded that the content of rutile decreased owing to Ag doping. Ag might be adsorbed on the more active face of rutile preventing thus its further growth. Hence, the anatase phase dominates over rutile. And the crystallite sizes of the TiO₂ and Ag-TiO₂ powders were found to be between 27 and 43 nm.

Table 1.10 Physical properties of TiO₂ and Ag-TiO₂ (Rengaraj *et al.*, 2006).

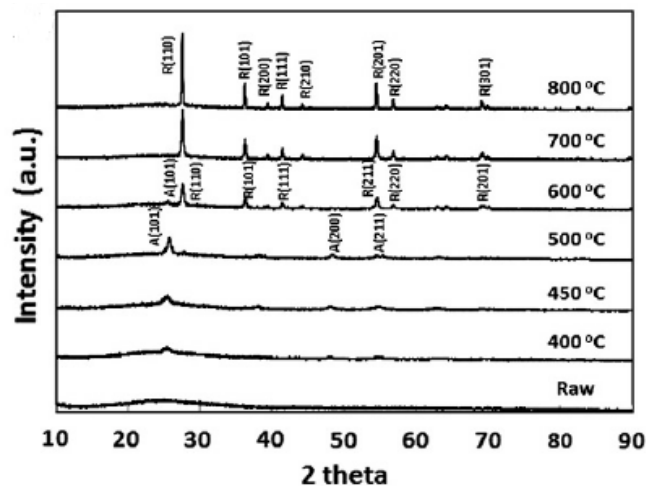
Catalysts	Crystal size, D (nm)	Weight percentage of anatase, W_A (%)
TiO ₂	43.36	69.90
0.5% Ag-TiO ₂	33.73	73.80
1% Ag-TiO ₂	27.57	92.39

Table 1.11 indicates the decrease of the band gap. The narrow band gap makes this material more attractive for photocatalytic applications, because the electron-hole pair separation efficiency was induced by enhancing the charge pair separation and inhibiting their recombination by the Ag dopant.

Table 1.11 Band gap E_g value of TiO_2 and Ag-TiO_2 values (Rengaraj et al., 2006).

No.	Percentage of Ag deposited on TiO_2	Band gap E_g (eV)
1	0	3.19
2	0.1	3.21
3	0.5	3.10
4	1.0	3.07
5	1.5	2.96

Park *et al.* (2010) studied the effects of silver and calcination temperature on the preparation of electrospun TiO_2 nanofibers. The XRD patterns of Ag-TiO_2 calcined at various temperatures, as shown in Fig. 1.11. It was found that the phase transformation from anatase to rutile increased, and crystallinity of anatase was hindered as Ag was doped. The rutile phase began to appear while the Ag-TiO_2 was calcined at 600 °C. It could be explained by the increasing Ag doping promoted the density of surface defects that facilitated the phase transformation. Moreover, the oxygen vacancy concentration of anatase grains is increased as Ag doped, which promoted the structure reorganization to rutile phase. The effect of calcination temperature on crystallite size of TiO_2 is shown in Fig. 1.12. The high calcination temperature induced larger crystallite size of TiO_2 . The crystallite size of Ag doped TiO_2 nanofiber is smaller than that of the pure TiO_2 nanofiber because silver inhibited the growth of anatase crystallite.

**Fig. 1.11** XRD pattern of Ag doped TiO_2 nanofibers (Park *et al.*, 2010).

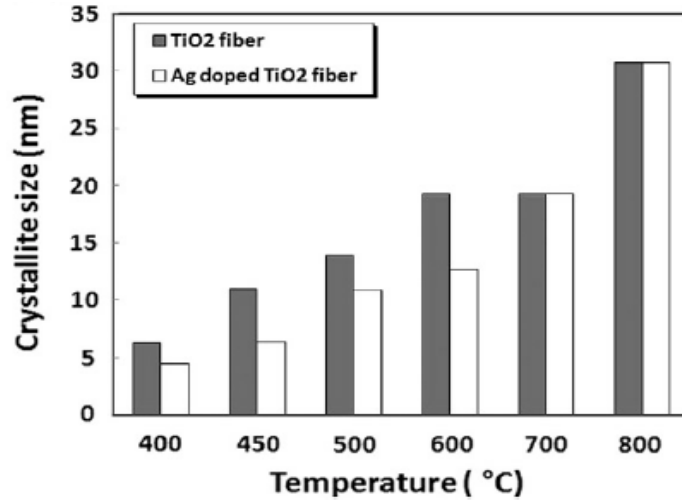


Fig. 1.12 The effect of calcination temperature on crystallite size of photocatalysts (Park *et al.*, 2010).

Lopez *et al.* (2009) studied the effect of doping TiO₂ with copper. TiO₂-Cu semiconductors (0.1, 0.5, 1.0, and 5.0 Cu wt.%) were synthesized by the sol-gel method. The X-ray diffraction patterns of the copper-doped titania samples annealed at 500 °C are shown in Fig. 1.13.

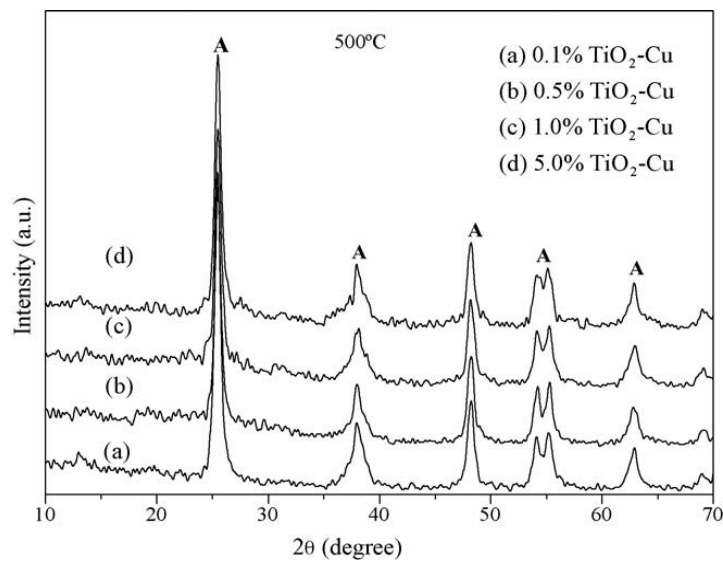


Fig. 1.13 X-ray diffraction patterns of the TiO₂-Cu materials (a-d) annealed at 500 °C (Lopez *et al.*, 2009).

In all samples (Fig. 1.13), the peaks corresponding to the formation of the anatase phase can be observed, showing that the incorporation of Cu preserves the anatase structure at temperatures around 500 °C. It must be noted that the presence of copper oxide cannot be observed even in the sample with the highest copper content. The similarity in the Cu and Ti ionic radii (0.72 Å for Cu and 0.68 Å for Ti) allows the interstitial incorporation of the dopant into the titania network. Cu could be placed in the interstitial sites due to $r_{\text{Ti}} < r_{\text{Cu}}$ producing the strain of the titania lattice. On the other hand, the crystallite size calculated by Scherrer's formula is listed in Table 1.12, where it can be seen that the solids are nanostructured with crystallite sizes comprising between 30.4 and 26.7 nm. The absorption edge energy (E_g) was obtained, where a shift in the visible region from 3.28 to 2.81 eV for the TiO₂ and TiO₂-Cu 5 wt.% semiconductors can respectively be seen. These results suggest that at low doping copper content (0.1, 0.5, and 1.0 Cu wt.%), the narrowing of the band gap could be due to the cationic substitution of titanium by copper. On the other hand, at a high doping content (5.0 Cu wt.%), the cationic substitution on the titania surface that play the role of electron traps could reduce electron-hole recombination.

Table 1.12 Average crystallite size and E_g values for the Cu doping samples (Lopez *et al.*, 2009).

TiO ₂ -Cu (wt.%)	Crystallite size (nm)	E_g (eV)
TiO ₂	40.5	3.28
0.1	30.4	3.19
0.5	29.3	3.13
1	26.7	3.05
5	29.0	2.81

1.2.3. Photocatalytic activity

Colmenares *et al.* (2011) studied the oxidization of glucose in the presence of powdered TiO₂ photocatalysts. The catalysts were more selective towards glucaric acid, gluconic acid, and arabitol (total selectivity approx. 70%) than the most popular photocatalyst, Degussa P-25. In the gas phase, mostly CO₂ and traces of light hydrocarbons, were detected. The best selectivity of 31.7% and 71.3% of total organic compounds for 10%H₂O/90%ACN and 50%H₂O/50%ACN used as solvents, respectively towards organic compounds in liquid phase was obtained with TiO₂(US) (Tables 1.13 and 1.14). It is noteworthy that good selectivity with appreciable conversion, especially with TiO₂(US), was achieved within 5 min. The photocatalyst with the lowest selectivity was P-25.

Their study hypothesized that more selective oxidations would occur in a mixture of water and acetonitrile (ACN) as a lower amount of water might give rise to a lower concentration of highly oxidative •OH radicals. Photo-conversion can be stopped when particular products have accumulated and before complete mineralization has occurred. A mixture of 50:50 H₂O:ACN (v/v) was the best solvent composition (Table 1.14).

Table 1.13 Effect of photocatalysts and irradiation time on organic compounds distribution in the liquid phase (reaction conditions: $C_{\text{glucose}} = 2.810 \times 10^{-3}$ mol/L, 150 mL of H₂O:ACN = 10:90 v/v, catalyst 1 g/L, 30 °C, 1 atm) (Colmenares *et al.*, 2011).

Photocatalyst	Selectivity to organic compounds [%]								
	Glucaric acid			Gluconic acid			Arabitol		
	Irradiation time			Irradiation time			Irradiation time		
	5 min	10 min	15 min	5 min	10 min	15 min	5 min	10 min	15 min
TiO ₂ (US)	16.6	14.0	11.0	14.9	13.4	10.2	7.8	4.3	4.2
TiO ₂ (R)	14.4	13.0	11.4	13.7	14.0	11.9	5.6	5.0	3.2
P-25	6.7	7.7	6.1	6.7	7.1	6.1	1.6	2.0	1.5

Table 1.14 Effect of solvent composition on glucose conversion and total selectivity for organic compounds (glucaric acid, gluconic acid, and arabitol) in the liquid phase after 10 min of illumination (Colmenares *et al.*, 2011).

Photocatalyst	Solvent composition					
	10%H ₂ O/90%ACN		50%H ₂ O/50%ACN		100%H ₂ O	
	Conversion [%]	Selectivity [%]	Conversion [%]	Selectivity [%]	Conversion [%]	Selectivity [%]
TiO ₂ (US)	28.8	31.7	11.0	71.3	41.2	0
TiO ₂ (R)	35.0	32.0	41.5	17.2	50.3	0
P-25	60.4	16.8	67.3	8.5	78.8	0

The relatively high carboxylic acid selectivity could be due to the lower affinities of these acids for the TiO₂(US) surface in the presence of acetonitrile. In the case of the Degussa P-25 photocatalyst, •OH radicals react efficiently with the well-adsorbed substrate (glucose), giving mainly carbon dioxide and water (products of complete oxidation), whereas less-adsorbed glucose on TiO₂(US) yielded more selective products which desorbed easily from the catalyst's surface and diffused into the environment created by ACN.

Zmudzinski *et al.* (2010) studied the preliminary results of glucose oxidation on titania. It was mentioned that during the photocatalytic reactions, the pH of the slurry was measured at 30 minute intervals. The lowering of pH was observed during three-hour reaction, from initial pH 6.5 to 4.8. As an example Fig. 1.14 shows the changes of 1.0 g·dm⁻³ glucose solution in the presence of TiO₂.

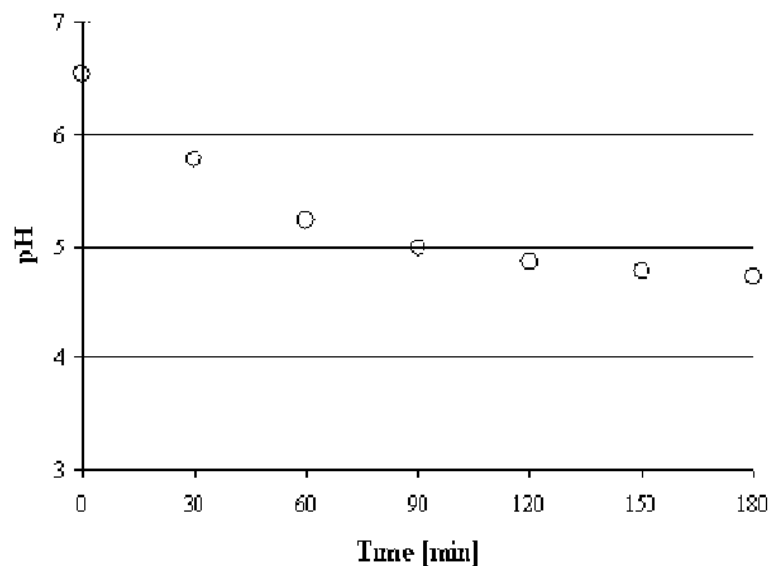


Fig. 1.14 pH changes during 3-hour illumination of 1.0 g dm^{-3} glucose solution in the presence of TiO_2 (Zmudzinski *et al.*, 2010).

The formation of acidic intermediates was detected by GC-MS. Many intermediate products are formed in the processes caused by $\text{OH}\cdot$ radicals (Table 1.15).

Table 1.15 Derivatives of the compounds determined by GC-MS (Zmudzinski *et al.*, 2010).

D-Glucose	Glucopyranose
Alpha-D-Glucopyranose	Mannose
Alpha-D-Xylopyranose	D-Xylopyranose
D-Arabinose	Beta-L-Arabinopyranose
D-Ribofuranose	D-Glucuronic acid
Gluconic acid	Allonic acid
Erythro-Pentonic acid	Mannonic acid
2-Furanacetaldehyde	Inosose-2
Glucuronolactone	D-Erythrotetrofuranose

The GC-MS analysis shows that the highest peak corresponded to the next compounds in the order: glucopyranose > glucose > gluconic acid > 2-furanacetaldehyde > allonic acid. Note that acidic derivatives had indeed formed during the photocatalytic reaction confirming the results of the pH measurements.

1.3. Research Objectives

- To study the modification techniques (microwave and ultrasonic) of TiO₂ synthesis and study their activity toward the photocatalytic oxidation of glucose into high-valued organic compounds.
- To optimize the operating conditions where the conversion and product yield could be maximized.
- To improve the photocatalytic activity of TiO₂ by doping Ag and Cu for 1, 3, 10 wt.% of metal loading content and test their photocatalytic oxidation activity.
- To improve the photocatalytic activity of TiO₂ by Ag-Cu co-doping and test its photocatalytic oxidation activity.
- To study the effect of microwave-assisted wet impregnation of metal doping and test its photocatalytic oxidation activity.

1.4. Scope of Research Work

TiO₂ was synthesized by the sol-gel, ultrasonic assisted sol-gel and sol-microwave methods. The effects of ultrasound and microwave during TiO₂ synthesis, calcination temperature and calcination time on the catalyst properties were determined. In this study, photocatalyst was characterized by XRD, SEM and UV-vis DR spectrophotometer. Then, its activity toward photocatalytic conversion of glucose was studied. As the next step, the effects of Ag and Cu doped TiO₂ (1, 3, and 10 wt% of metal loading) on the improvement of photocatalytic activity of TiO₂ were investigated. Lastly, the effects of Ag-Cu co-doping and microwave assisted wet impregnation of metal doping were also tested.

CHAPTER 2

THEORIES

2.1. Definition of Photocatalysis

The word "photocatalysis" is composed of the words "photo" and "catalysis", and therefore, means catalysis in the presence of light. It implies that the process of a photocatalytic reaction must involve light and a catalyst. "Catalysis" is defined as "an action process of a catalyst on a chemical reaction". "Catalyst" is defined as "a substance which increases the rate at which a chemical reaction approaches equilibrium, without being consumed in the process". The definition of "catalyst" has two important implications: Firstly, it implies that the position of equilibrium attained in the presence of a catalyst is the same as that ultimately attained when no catalyst is present, *i.e.*, a catalyst cannot change the equilibrium of a reaction, it can only reduce the time it takes to reach equilibrium. Secondly, it implies that a catalyst can only increase the rate of reactions. In this work, photocatalysis is defined as "an action process of a photocatalyst on a chemical reaction", from which Photocatalyst is a substance activates a chemical reaction and/or to accelerate the rate in the presence of light, without being consumed in the process (Chen *et al.*, 1997).

2.2. Fundamental Theory of TiO₂ Semiconductors

The electronic state of a single atom or a single molecule can be described by means of electron orbitals with a definite energy. According to the band theory of solid state physics on the formation of a crystal from a large number of atoms or molecules, electron orbitals of similar energy levels combine to form a so-called energy band. It may be assumed that the energy levels of the electron orbitals in a band are continuous, and that electrons can move easily within a band if it is not fully occupied. Atomic or molecular orbitals with different energy levels form different energy bands. The orbitals of the valence electrons (the highest filled orbits) form the valence band (VB), and the lowest unoccupied orbitals of atoms form the conduction band (CB). The highest energy level in the valence band is called the valence band edge (E_{vb}), which is presented as the energy of the valence band. The lowest energy level in the conduction band is called the conduction band edge (E_{cb}), which is presented as the energy of the conduction band. The energy

difference between the valence band edge and the conduction band edge is called the band gap or energy gap (E_g) (Chen *et al.*, 1997).

2.3. TiO₂ Photocatalyst

Common photocatalysts are semiconductors such as ZnO, GaP, TiO₂, SiC, CdS, and Fe₂O₃ (Tseng *et al.*, 2010). Among various common photocatalysts, TiO₂ has always been the subject of work for application in environmental purification due to its low cost, non-toxicity, high oxidizing power, chemical stability, and environmentally friendly characteristics (Cao *et al.*, 2000). The anatase form of titania is reported to give the best combination of photoactivity and photostability. Nearly all studies have focused on the crystalline forms of titania, namely anatase and rutile. The minimum band gap energy required for photons to cause the photogeneration of charge carriers over TiO₂ semiconductor (anatase form) is 3.2 eV corresponding to a wavelength of 388 nm. Practically, TiO₂ photoactivation takes place in the range of 300–388 nm. The photo induced transfer of electrons occurring with adsorbed species on semiconductor photocatalysts depends on the band-edge position of the semiconductor and the redox potentials of the adsorbates (Dvoranova *et al.*, 2002). Titanium dioxide has three types of crystalline phases, namely, anatase (tetragonal), rutile (tetragonal), and brookite (orthorhombic) found in nature (Figure 2.1). Even though their structures are similarly based on octahedrals (TiO₆), they still differ from one another by the distortion of each octahedral and by the assembly patterns of the octahedral chains. Anatase is built up from octahedrals which are mainly connected by their vertices. Octahedral structures in rutile are mostly connected by the edges. Both vertical and edge connections are found in the octahedral structure of the brookite form. Although both anatase and rutile are the same tetragonal system, anatase has longer its vertical axis of the crystals than rutile. Meanwhile, brookite crystallizes in the orthorhombic system (Hanaor *et al.*, 2011).

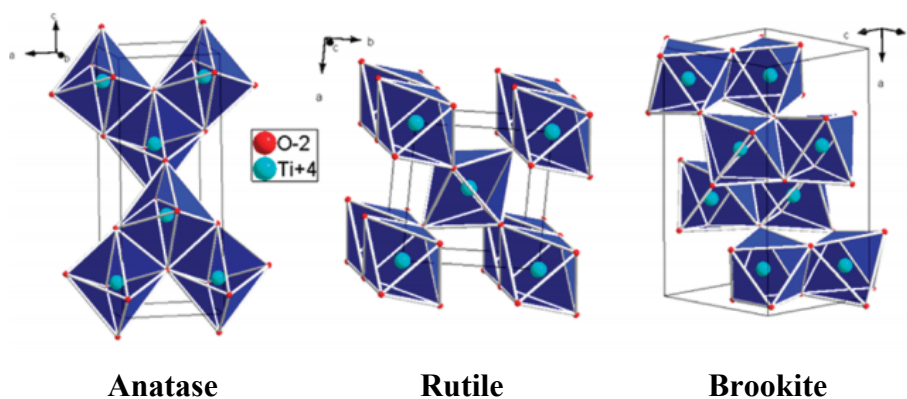


Fig. 2.1 Representations of the TiO_2 : anatase, rutile, and brookite forms (Hanaor *et al.*, 2011).

Anatase and rutile are commonly used in photocatalysis. However, anatase shows a higher photocatalytic activity than dose rutile (Fua *et al.*, 2008). The band gap energy required for photon to cause photogeneration of charge carriers over TiO_2 semiconductor (anatase form) is 3.2 eV corresponding to a wavelength of 388 nm (Colmenares *et al.*, 2009).

Table 2.1 Properties of anatase and rutile phases of TiO_2 .

Properties	Anatase	Rutile
Crystalline form	Tetragonal system	Tetragonal system
Band gab energy (eV)	3.200	3.030
Hardness (Mohs)	5.5-6.0	6.0-7.0
Density (g/cm ³)	3.894	4.250
Gibbs free energy, ΔG_f° (kcal/mole)	-211.4	-212.6
Lattice constant, a (Å)	3.784	4.593
Lattice constant, c (Å)	9.515	2.959
Refractive index	2.52	2.71
Permittivity	31	114
Melting point (°C)	1835	2500-3000

2.4. Applications of TiO₂

2.4.1. Photocatalytic splitting of water

Since Fujishima and Honda (1972) carried out the photocatalytic splitting of water using TiO₂, great effort has gone into maximizing the potential of the process as it can provide clean renewable energy from sustainable sources. If energy from the light greater than the band gap, an electron will be excited from the valence band to the conduction band. The photo generated e⁻/h⁺ pair causes redox reactions. Water molecules are reduced by excited electrons to form H₂ and oxidized by holes to form O₂ leading to water splitting (Sun *et al.*, 2012).

2.4.2. Photocatalytic degradation of pollutants

Titanium dioxide has attracted great interest in the past decade due to its environmental applications, such as air purification and water remediation. The photocatalytic mechanism is activated by light of energy greater than that of the semiconductor band gap. Upon photo-activation, an electron-hole pair is produced that reacts with adsorbed species to produce radical species. These radicals are powerful oxidizing agents and will oxidize organic contaminants to CO₂ and H₂O (Pelaeza *et al.*, 2012).

2.4.3. Self-cleaning surfaces

Self-cleaning glass clearly displays the benefits of titanium dioxide's self-cleaning and super hydrophilic properties. Titanium dioxide can be incorporated into concrete to produce photocatalyst-modified cement. It can be used to coat hospital surfaces and provide anti-bacterial protection against harmful bacteria, such as E. coli. By applying TiO₂ to road side partitions and lights, the surfaces can be kept clean while having the added advantage of reducing harmful exhaust gases such as NO_x and VOCs (Pelaeza *et al.*, 2012).

2.4.4. The dye sensitized solar cell

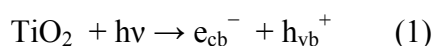
The dye sensitized solar cell (DSSC) has shown great potential as the next generation of solar cells. The DSSC has several advantages over current photovoltaic cells, such as low production costs, more consistent energy production from diffuse and direct

sunlight, color choice, and transparency. Also, because the DSSC utilizes TiO₂ nanoparticles, solar cells of much smaller sizes can be produced and they can even be flexible. In the DSSC, light is absorbed by a colored dye (commonly ruthenium based dye), to produce an excited singlet state. Excited electrons from the dye are then injected into the conduction band of the TiO₂ support. Following successful injection, the electron percolates through the oxide layer onto the working electrode. Once the electron reaches the electrode, it will travel to the counter electrode, therefore generating an electrical current (Cheng *et al.*, 2013).

2.5. Mechanism of Photocatalysis

The overall heterogeneous photocatalysis process can be summarized in the following five steps: (1) reactant diffusion to catalyst surface, (2) adsorption of reactant onto the surface, (3) chemical reaction on the catalyst surface, (4) desorption of final products off the catalyst surface, and (5) diffusion of final products from the catalyst surface (Tan *et al.*, 2011).

The basis of photocatalysis is the photo-excitation of a semiconductor that is solid as a result of the absorption of electromagnetic radiation in the near UV spectrum. When the energy (photon) supplied is equal to or greater than the band gap energy, ΔE_g of the photocatalyst, the excited electron in the valence band is transferred to the empty conduction band. The band gap energy is the difference in energy between the valence band and the conduction band of the photocatalyst. This leads to the generation of a positive hole (h_{vb}^+) in the valence band and an electron (e_{cb}^-) in the conduction band. As a result, electron-hole pairs are generated in the photocatalytic reaction.

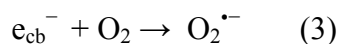


where $h\nu$ is energy required to transfer the excited electron from the valence band to the empty conduction band.

In this reaction, the positive hole and the electron are powerful oxidizing and reducing agents, respectively. Generally, the positive hole reacts with either surface-bound water (H₂O) to produce hydroxyl radical ($\bullet\text{OH}$).



Furthermore, the electron in the conduction band is picked up by an electron acceptor, such as oxygen, to produce a superoxide radical anion ($O_2^{\bullet-}$).



On the other hand, e^- and h^+ are able to recombine again which can occur at the bulk and at the surface. The recombination process is usually considered as the deactivation process in a photocatalytic reaction.

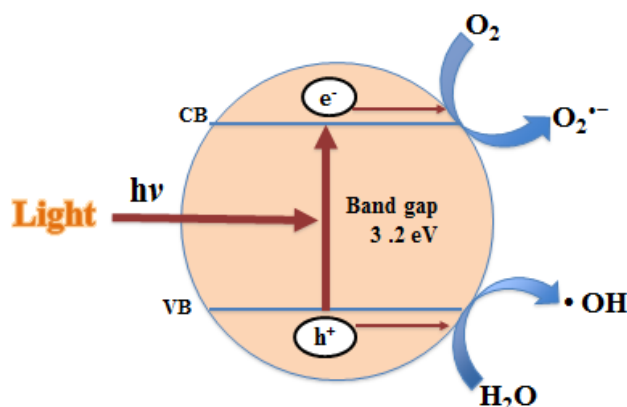
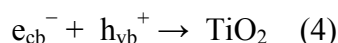


Fig. 2.2 Mechanism of TiO₂ photocatalysis.

2.6. Photocatalytic of Sugar Conversion

Sugar (glucose) oxidation on illuminated titania was studied by Zmudzinsk *et al.* (2010). Acidic derivatives were formed during the photocatalytic reaction confirming the results of pH measurements ($pH < 5$). The formation of acidic intermediates is not surprising. According to literature, oxidation of glucose in the presence of illuminated titania proceeds via formation of $OH\bullet$ radicals. The attack of $OH\bullet$ radicals on hydroxylated carbon atom in sugar leads firstly to formation of a new carbonyl group. The reaction of $OH\bullet$ with the carbonyl group causes formation of a carboxyl group. And acid derivatives of sugar could be obtained from this reaction, i.e. gluconic and glucuronic acid. Moreover, high-value chemicals obtained from selective photo-oxidation of glucose in the presence of TiO₂ photocatalysts, i.e. glucaric acid, gluconic acid and arabitol in the liquid phase and mostly CO₂ and traces of light hydrocarbons were detected in the gas phase (Colmenares *et al.*, 2011).

2.7. Preparation of Photocatalysts

2.7.1. Sol-Gel Method: a route for TiO₂ synthesis

Sol-gel is one of the most successful techniques for preparing nano-sized metallic oxide materials with high photocatalytic activities, and most recent works usually use this method. The sol-gel process, as the name implies, involves the evolution of inorganic networks through the formation of a colloidal suspension (sol) and gelation of the sol to form a network in a continuous liquid phase (gel) (Su *et al.*, 2004).

The inherent advantages of the sol-gel process are summarized as follows (Tseng *et al.*, 2010):

1. Better homogeneity from raw materials.
2. Better purity from raw materials.
3. Lower temperature of preparation.
4. Good mixing for multi-component systems.
5. Effective control of particle size, shape, and properties.
6. Better products from the special properties of the gel.
7. The creation of special products such as films.
8. Flexible to introduce dopants in large concentrations.

Generally, there are two known types of titania precursors, non-alkoxide and alkoxide, utilized in the sol-gel method. The alkoxide route uses metal alkoxides as a starting material. This route has highly been used for preparing metal oxide because metal alkoxide precursors are commercially available in high purity and are easily handled at ambient temperature.

2.7.1.1. The sol-gel process is composed of a series of steps as follows (Su *et al.*, 2004);

Step 1 A starting material will be hydrolyzed and partially condensed in order to form sol, which is a liquid suspension in solid particles.

Step 2 Gelation resulting from the formation of an oxide- or alcohol- bridged network (the gel) by a polycondensation reaction that results in a dramatic increase in the viscosity of the solution. Condensation pulls together the constitute particles of the gel into a compact mass, thus building up the metal oxide crystal.

Step 3 Aging of the gel: the gel is left to continue constructing more networks, causing stronger cross-linkages.

Step 4 Drying of the gel: in order to remove organic solvents or hydrolyzed molecules, the metal oxide needs to be heated to a sufficient temperature to dispose of them.

Step 5 Calcination: this final step emphasizes the crystallization of metal oxide. Calcination is used in order to remove the dormant organic part and to crystallize the phase of metal oxide.

2.7.1.2. Fundamental Chemical Reactions in the Sol-Gel Process

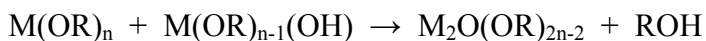
In sol-gel processes, TiO_2 is usually prepared by the reactions of hydrolysis and polycondensation of titanium alkoxides, $\text{Ti}(\text{OR})_n$ as follows:

1. Hydrolysis



2. Condensation

Dehydration



Dealcoholation



The overall reaction is



2.7.2. Ultrasonic-assisted sol-gel preparation of TiO_2

The use of sonication irradiation methods during TiO_2 synthesis could be of help to reduce crystallite growth. The use of ultrasonic irradiation during the synthesis of TiO_2 has been reported to facilitate the formation of smaller homogeneous nanoparticles and to lead to an increase in surface area (Colmenares *et al.*, 2009)

Ultrasonic waves (occurring at frequencies above 20 kHz) are a branch of sound waves that exhibits all the characteristics properties of sound waves. Depending on the frequency, ultrasound is divided into three categories, namely power ultrasound (20–100 kHz), high frequency ultrasound (100 kHz – 1 MHz), and diagnostic ultrasound (1–500 MHz). Ultrasound ranging from 20 to 100 kHz is used in chemically important

systems, it has the ability to cause cavitations of bubbles. The cavitation phenomenon under ultrasonic treatment can cause the microbubbles to tend to break up into smaller ones. Sonication led to pure-anatase nanoparticles (the most active photocatalytic phase of titania). This enhancement in surface area resulted in an increase in molar conversion (Wu *et al.*, 2013).

2.7.3. Microwave-assisted of TiO₂ preparation.

Microwave-assisted TiO₂ synthesis has been widely used. Compared with conventional heating, microwave heating has many advantages, for example, offers more efficient and uniform energy transfer, that promotes the formation of mono dispersed nanoparticles, narrow size distribution and small particle sizes (Esquivel *et al.*, 2013). The other advantages of microwave heating are very short reaction time and easy control. Consequently, microwave assisted synthesis is new way for the preparation of effective photocatalysts.

2.8. Metal Doped TiO₂

Among the advantages of titania on other photocatalysts are its excellent chemical stability, low cost and non-toxicity. However, its wide band-gap energy (3.0 eV for rutile and 3.2 eV for anatase) means that only 5% of solar spectrum is used. Moreover, TiO₂ presents a high electron-hole recombination rate, which is detrimental to its photoactivity. A lot of investigations dedicated toward improving the efficiency of TiO₂ photocatalyst. One of most applicable approaches is to doping TiO₂ with metal ions. In this sense, doping with metals could make a double effect:

(1) Firstly, it could reduce the band gap energy, thus shifting the absorption band to the visible region. Metal ion species can produce impurity states lying between the valence band and the conduction band, which causes the band gap to narrow.

(2) Secondly, metals could provoke a decrease in electron-hole recombination rates, acting as electron traps. (Tseng *et al.*, 2010)

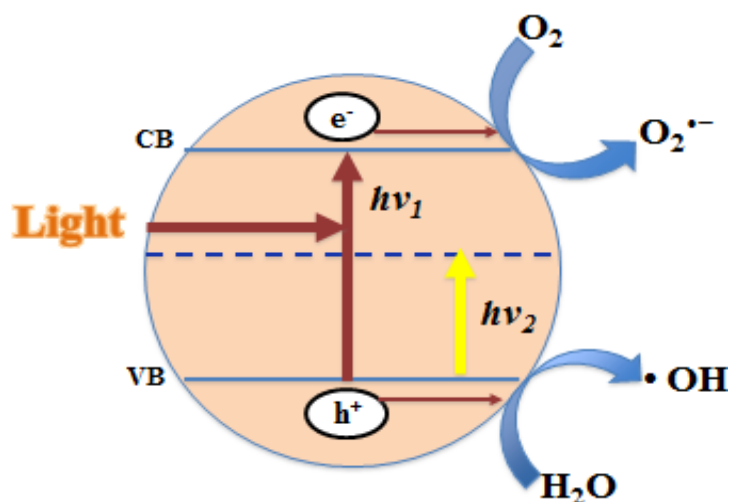


Fig. 2.3 Mechanism of TiO_2 photocatalysis: $h\nu_1$: pure TiO_2 ; $h\nu_2$: metal-doped TiO_2 (Zaleska *et al.*, 2008).

It was discovered that doping with Ag (Rengaraj *et al.*, 2006) and Cu in TiO_2 (Wang *et al.*, 2014) could lead to the absorption of photocatalysts shifting into the visible range. In addition, it was believed that doping with metal would enhance the trapping of electrons and decrease the rate of electron-hole recombination during illumination. Longer wavelengths indicate the decrease of the band gap.

2.9. Glucose

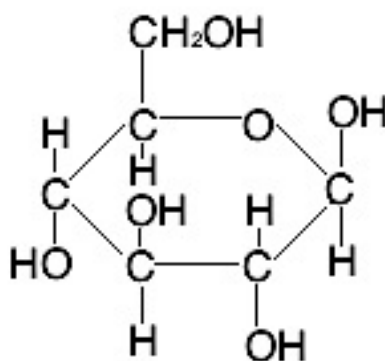


Fig. 2.4 Structure of glucose.

Glucose is a simple monosaccharide with the formula $C_6H_{12}O_6$, whose five hydroxyl (OH) groups are arranged in a specific way along its six-carbon backbone, as shown in Fig. 2.4. Glucose is also sometimes called dextrose. Glucose is one of the primary molecules that serve as energy sources for plants and animals. It is found in the sap of plants. Glucose is manufactured by plants with the aid of energy from the sun in the process called photosynthesis. This synthesis is carried out in the small energy factories called chloroplasts in plant leaves. The chloroplasts capture the energy from light and fabricate glucose molecules from carbon dioxide from the air and water from the soil.

In addition, glucose can also be found in a linear form. Aldehyde (-CHO) is a functional group that is present in glucose molecule (Fig. 2.5).

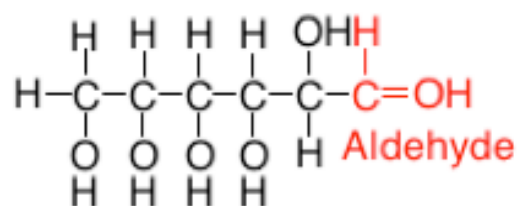


Fig. 2.5 Structure of glucose (linear form).

CHAPTER 3

METHODOLOGY

3.1. Materials

The chemicals in this research include titanium (IV) butoxide ($\text{Ti}(\text{OC}_4\text{H}_9)_4$), Isopropyl alcohol ($\text{C}_3\text{H}_7\text{OH}$), acetylacetone ($\text{CH}_3\text{CH}_2\text{COCH}_2\text{CH}_3$), metal ion salts $\text{Ag}(\text{NO}_3)$ and $\text{Cu}(\text{NO}_3)_2 \cdot 3\text{H}_2\text{O}$, and glucose, all chemicals are commercial grade supplied from Sigma-Aldrich.

3.2. Titanium Dioxide Synthesis

3.2.1. Sol-gel method

The titanium dioxide (TiO_2) particles were fabricated with the sol-gel method. The molar ratio of the precursors and solvents were, 0.032:0.784:0.032:4.444 for TiBu :i-PrOH:ACA: H_2O , respectively. The procedures of synthesis are followed by

- The titanium (IV) butoxide ($\text{Ti}(\text{OC}_4\text{H}_9)_4$) was used as the precursor of TiO_2 that was mixed with acetylacetone (ACA) to slowdown the rate of hydrolysis and the condensation.
- The distilled water was added dropwise into the solution under mechanical stirring at room temperature. After that, the isopropyl alcohol was added in the mixture solution to form titanium dioxide hydrosol.
- The prepared titanium dioxide hydrosol was gelled at room temperature for 24 h.
- The gel of titanium dioxide was dried at 80°C for 24 h. The fabricated TiO_2 was pulverized into a fine powder (as-synthesized TiO_2).
- The powder of the as-synthesized TiO_2 was calcined at 500°C for 5 h.

3.2.2. The ultrasonic-assisted sol-gel method

The modified TiO_2 with ultrasonic assistance was synthesized in the same manner mentioned above. The titanium dioxide hydrosol was treated with ultrasonics in the

ultrasonic bath (35 kHz, 320 W, Sonorex Digitec, Bandelin) under room temperature for 1 in 5 and 10 min per cycles (2 min ultrasound off between cycles). The gel of TiO₂ was kept at the room temperature for 24 h, then it was dried at 80 °C for 24 h. The ultrasound assisted TiO₂ was calcined at 500 °C for 5 h.

3.2.3. The sol-microwave method

The modified TiO₂ with sol-microwave method can be synthesized with the same manner mentioned above. The titanium dioxide hydrosol was treated with microwave irradiation (30% power) for 4 min (Whirlpool, 2.45 GHz, 970W). Then, it was dried at 80 °C for 24 h. The sol-microwave TiO₂ was calcined at 400-600 °C for 2 and 5 h.

3.2.4. Metal doped TiO₂

3.2.4.1. Wet impregnation method

The metal doped TiO₂ catalysts were prepared by aqueous wet impregnation of TiO₂ using metal ion salts, Ag(NO₃) and Cu(NO₃)₂•3H₂O, as the precursors for Ag and Cu loading, respectively. Accordingly, a solution of metal ion salts in distilled water was stirred, and then added it to TiO₂. The solvent was evaporated slowly at 80 °C under continuous stirring. The 1, 3, and 10wt.% of metal ion was introduced as the dopant. The sample was dried in oven at 120 °C over night and then calcined at 400 °C for 4 h.

3.2.4.2. Microwave assisted wet impregnation method

The metal doped TiO₂ was synthesized in the same manner mentioned above. The solvent was treated with microwave irradiation (40% power) for 5 min (Whirlpool, 2.45 GHz, 970W). After that, sample was calcined at 400 °C for 4 h.

All methods of TiO₂ and metal doped TiO₂ are summarized in Fig. 3.1.

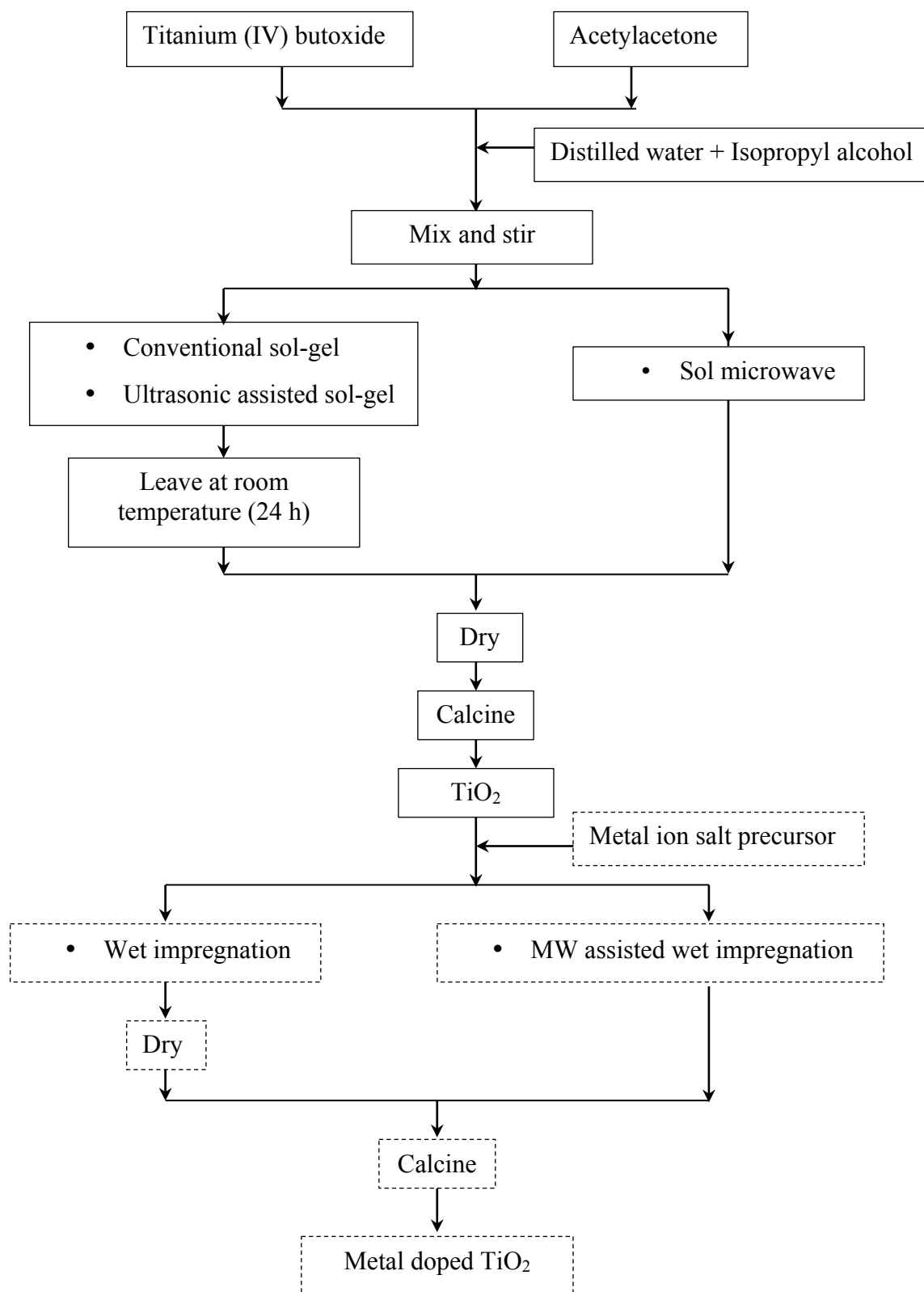


Fig. 3.1 The procedure of TiO₂ synthesis with sol-gel method, ultrasonic assisted sol-gel method, sol-microwave method, wet impregnation method of metal-TiO₂ and microwave assisted wet impregnation method of metal-TiO₂.

3.2.5. TiO₂ photocatalyst characterization

The TiO₂ photocatalysts in this study were characterized by the X-ray Diffraction (XRD; RIGAKU RINT 2100) technique with Cu-K α radiation ($\lambda=0.15418$ nm) at 40 kV and 30 mA to analyze the crystalline structure of TiO₂; Scanning Electron Microscopy (SEM; JEOL JSM-6500FE) to analyze the microstructure of the prepared TiO₂; and UV-vis spectrophotometer to monitor the light absorption of TiO₂.

3.3. Photocatalytic Study

3.3.1. Photocatalytic reaction

The glucose solution was prepared in a mixture of distilled water and acetonitrile (10:90 v/v) (Colmenares *et al.*, 2011). The 500 ml of prepared solution was transferred into a Pyrex cylindrical double-walled reactor. The TiO₂ photocatalyst was used in photocatalytic reaction. The glucose solution (1 g/l) and TiO₂ particles (1 g/l) were mixed under dark condition and continuous stirring for 30 min to obtain a homogenous suspension of the photocatalyst. A mercury lamp as a light source to irradiate the sample that located beside the reactor was turned on to start the reaction. The photocatalytic system was continuously stirred in the wood box that was coated with the aluminium foil inside. The reaction temperature was maintained by cooling water system. Then, the samples were taken from the photoreactor at specified times for analysis.

3.3.2. The products analysis

Approx. 10 ml of the samples were taken from the photoreactor at specified times. The liquid product was filtrated by 0.45 μ m nylon filter before analysis. The generated products were monitored by High performance liquid chromatography (HPLC, Shimudzu, LC-20AD pump) equipped with a refractive index detector (Shimudzu RID-10A). Separation was performed on a Aminex HPX-87H column (300 x 7.8 mm) (Bio-Rad). The mobile phase was 5 mM sulfuric acid at a flow rate of 0.5 mL/min and injection volume was 20 μ L. HPLC was used for analysis of the content of organic products and glucose conversion.

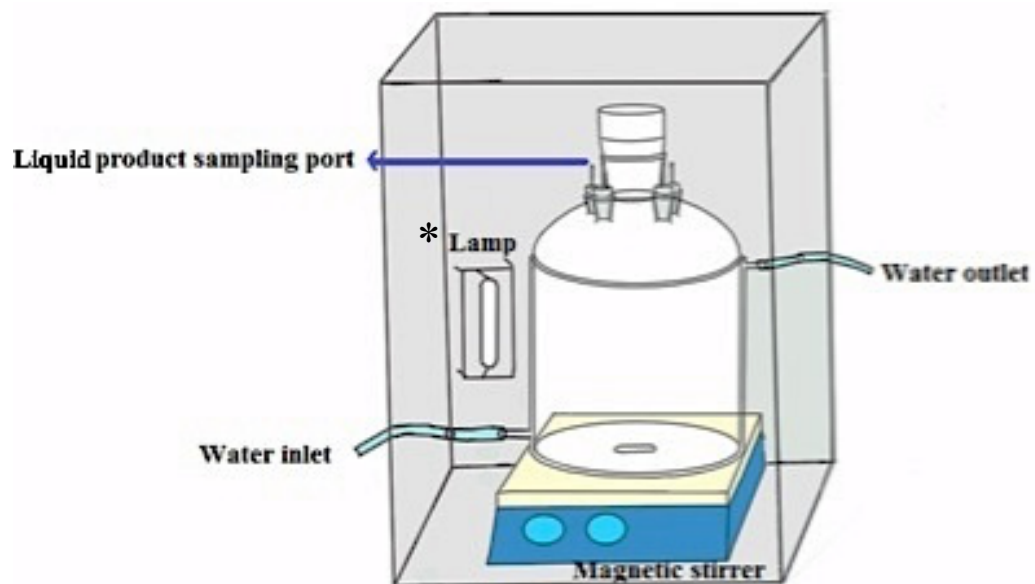


Fig. 3.2 Photocatalytic reactor.

* Mercury lamp (400 W, $\lambda_{max} = 365 \text{ nm}$)

CHAPTER 4

RESULTS AND DISCUSSION

4.1. Effect of TiO₂ Preparation Methods on Its Photocatalytic Activity

4.1.1. Material characterizations

The effect of TiO₂ synthesis methods i.e. sol-gel (SG), microwave (MW) and ultrasonic irradiation (US) on material crystal phase and crystallite size were firstly investigated. The XRD patterns of the TiO₂ synthesized by sol-gel, ultrasonic assisted sol-gel and sol-microwave method that calcined at 500 °C for 5 h are shown in Fig. 4.1, while the phase identification, crystallite size from XRD analysis and S_{BET} of the photocatalysts are shown in Table 4.2. X-ray diffraction is used to determine the phase composition and crystallite size of TiO₂. XRD patterns of photocatalyst post-annealed at 873 K are shown in Fig. 4.1. All of TiO₂ photocatalysts presented peaks of anatase at 2θ of 25.2°, 37.0°, 37.7°, 38.5°, 47.8°, 53.8°, 55.0°, 62.6°, 68.9°, 70.4° and 75.0° were observed, corresponding to reflections from A(101), A(103), A(004), A(112), A(200), A(105), A(211), A(204), A(116), A(220), and A(215) planes were observed, respectively. The peaks located at 27.5°, 36.1°, 41.3°, and 56.6° respond to the (110), (101), (111), and (220) planes of the rutile phase, respectively.

TiO₂(SG), TiO₂(US), and TiO₂(MW) photocatalysts exhibited the same crystallite size of 25.1 nm (Table 4.1), which indicates that ultrasonic and microwave treatment did not significantly affect the crystallite size of anatase. Moreover, TiO₂(US) and TiO₂(SG) exhibited pure anatase phase. Conversely, TiO₂(MW) showed the mixture of anatase and rutile. There were 86% of anatase and 14% of rutile, with crystallite sizes of 25.1 and 84.03 nm, respectively. This result implied that heat treatment under microwave radiation facilitated the transformation of anatase to rutile phase. Similarly, P25 also consisted of mix phase between 79% of anatase and 21% of rutile, with large crystallite size of 57.5 and 100.7 nm, respectively.

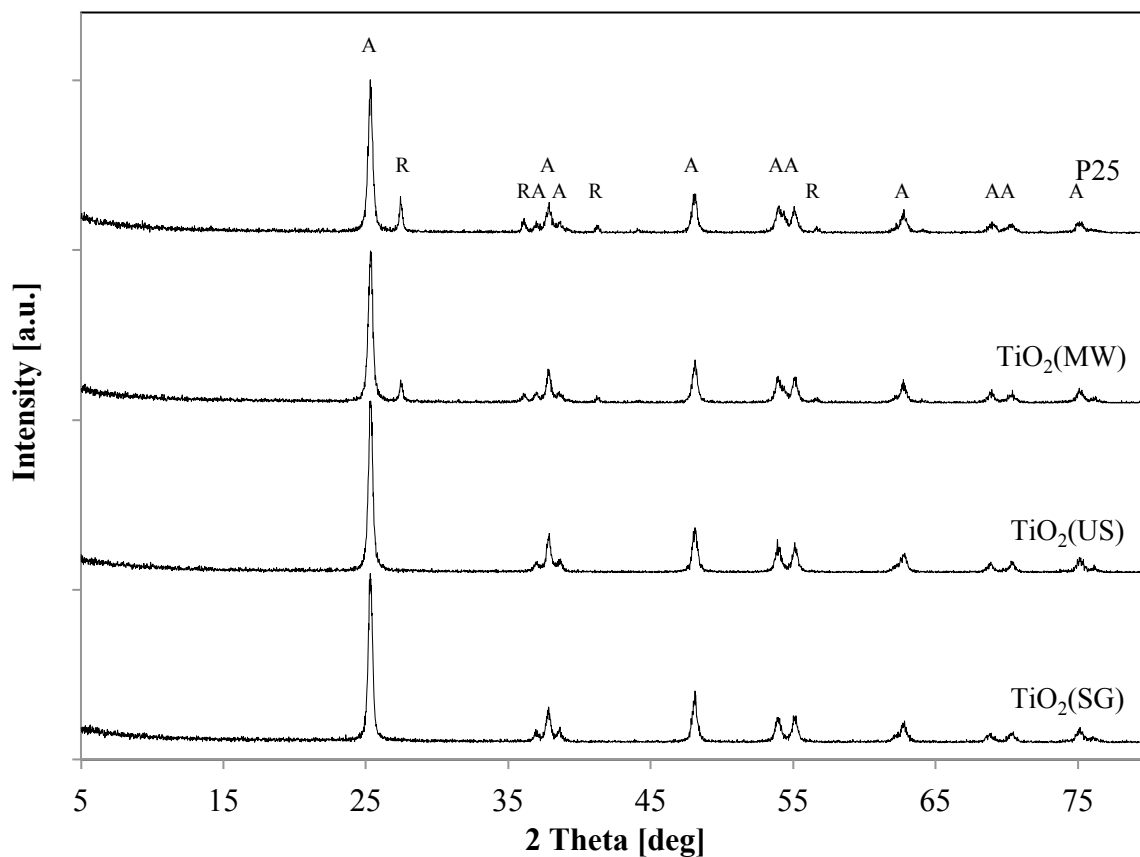


Fig. 4.1 X-ray diffraction patterns of $\text{TiO}_2(\text{SG})$, $\text{TiO}_2(\text{US})$, $\text{TiO}_2(\text{MW})$, and P25.

Table 4.1 Summary of XRD, SEM and S_{BET} characterizations of the synthesized TiO_2 : $\text{TiO}_2(\text{SG})$, $\text{TiO}_2(\text{US})$, $\text{TiO}_2(\text{MW})$, calcined at 500 °C for 5 h and P25.

Photocatalyst	Crystal phase ^a (%)	Crystallite size (nm)	Particle size (μm)	S_{BET} (m^2/g)
$\text{TiO}_2(\text{SG})$	A(100)	25.1	3.0	7.2
$\text{TiO}_2(\text{US})$	A(100)	25.1	2.2	19.5
$\text{TiO}_2(\text{MW})$	A(86)/R(14)	25.1/84.0	0.4	24.3
P25	A(79)/R(21)	57.5/100.7	0.052	-

^a A and R denote anatase and rutile, respectively.

SEM images of $\text{TiO}_2(\text{SG})$, $\text{TiO}_2(\text{US})$, $\text{TiO}_2(\text{MW})$ and P25 are represented in Fig. 4.2. The particle size of TiO_2 was spherical shape and monodispersion. The smallest particle size was obtained from P25. Among the synthesized TiO_2 (SG, US, and MW), particle size of TiO_2 that was treated with microwave radiation (0.4 μm) was the smallest,

and the particle size of $\text{TiO}_2(\text{US})$ ($2.2 \mu\text{m}$) was smaller than that of $\text{TiO}_2(\text{SG})$ ($3.0 \mu\text{m}$) (as seen in Table 4.1), which indicates that microwave irradiation had greatly facilitated the morphology of TiO_2 , the distribution of spherical particles more uniform and smallest particle size compared with $\text{TiO}_2(\text{US})$ and $\text{TiO}_2(\text{SG})$ were obtained. This could be ascribed to the effect of strong polarization of the microwaves (Li *et al.*, 2014).

The S_{BET} of all the samples are listed in Table 4.1. The results show that small particle size induced larger specific surface areas and $\text{TiO}_2(\text{MW})$ represented the largest specific surface area of $24.3 \text{ m}^2/\text{g}$.

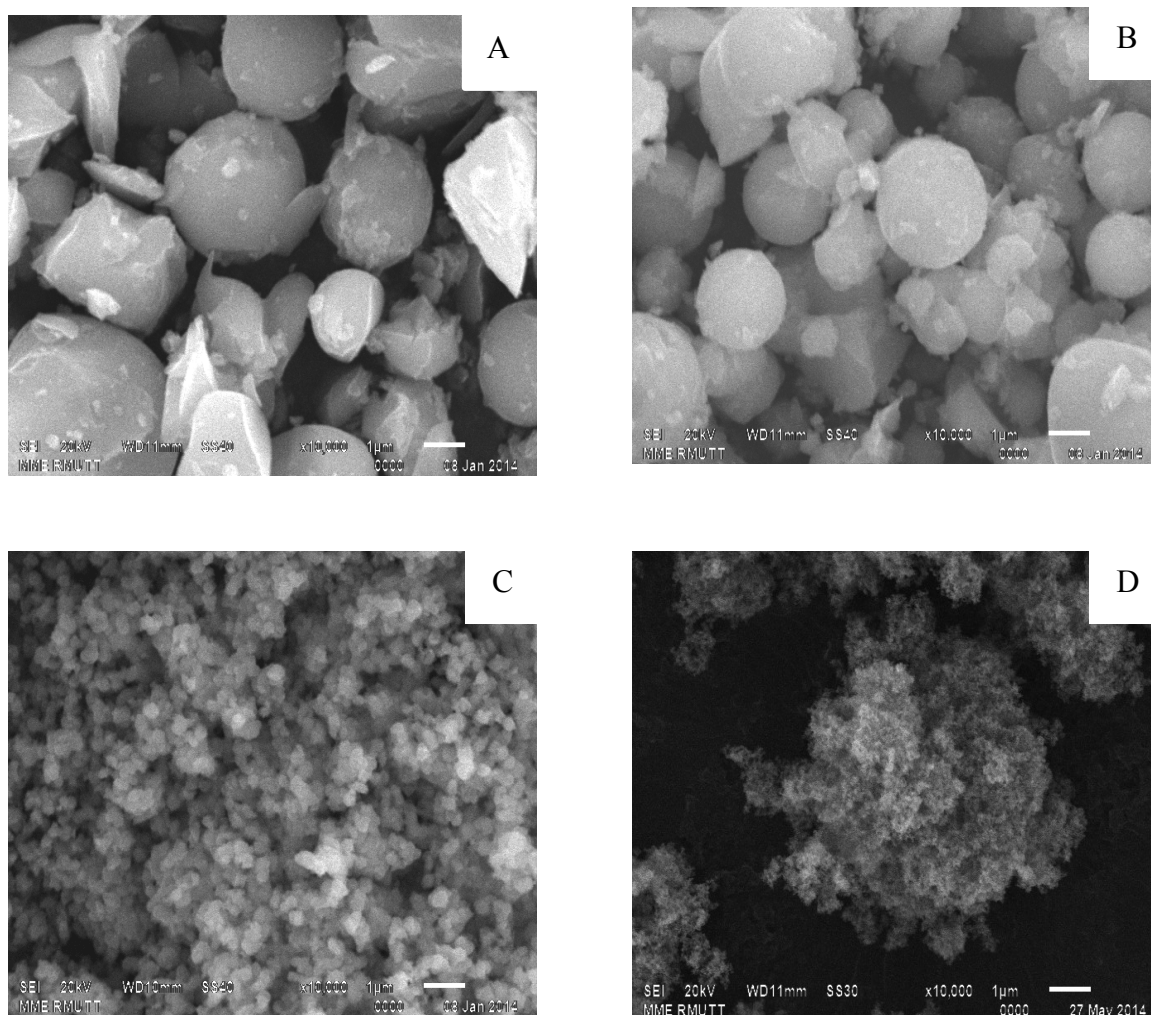


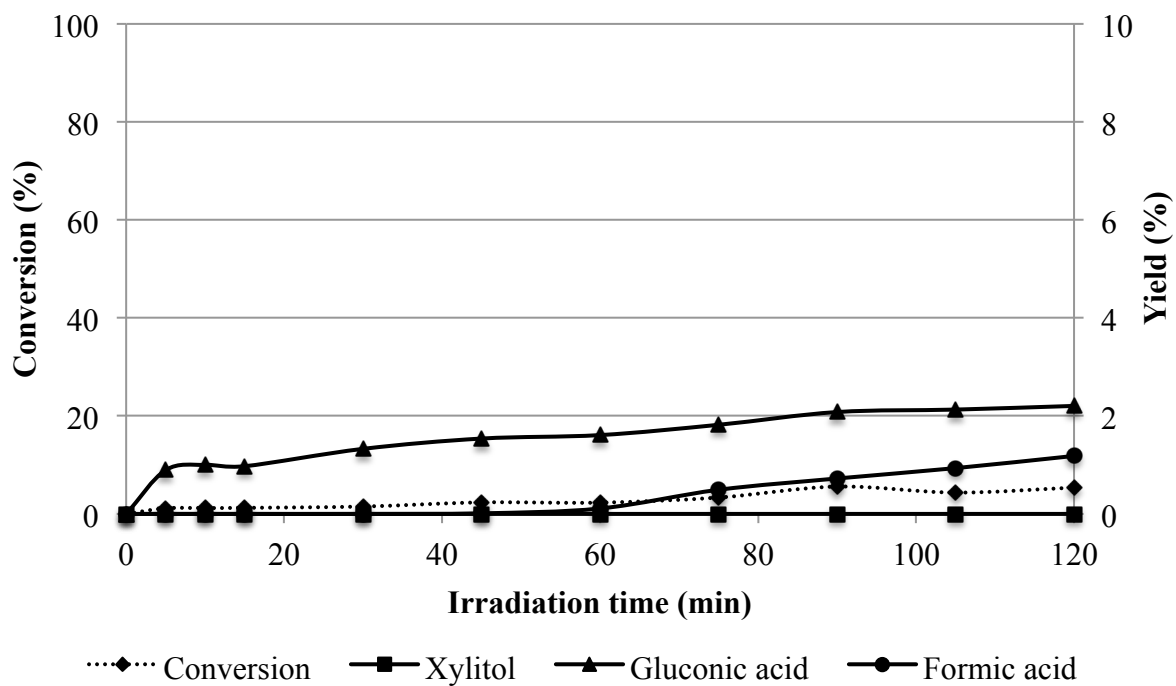
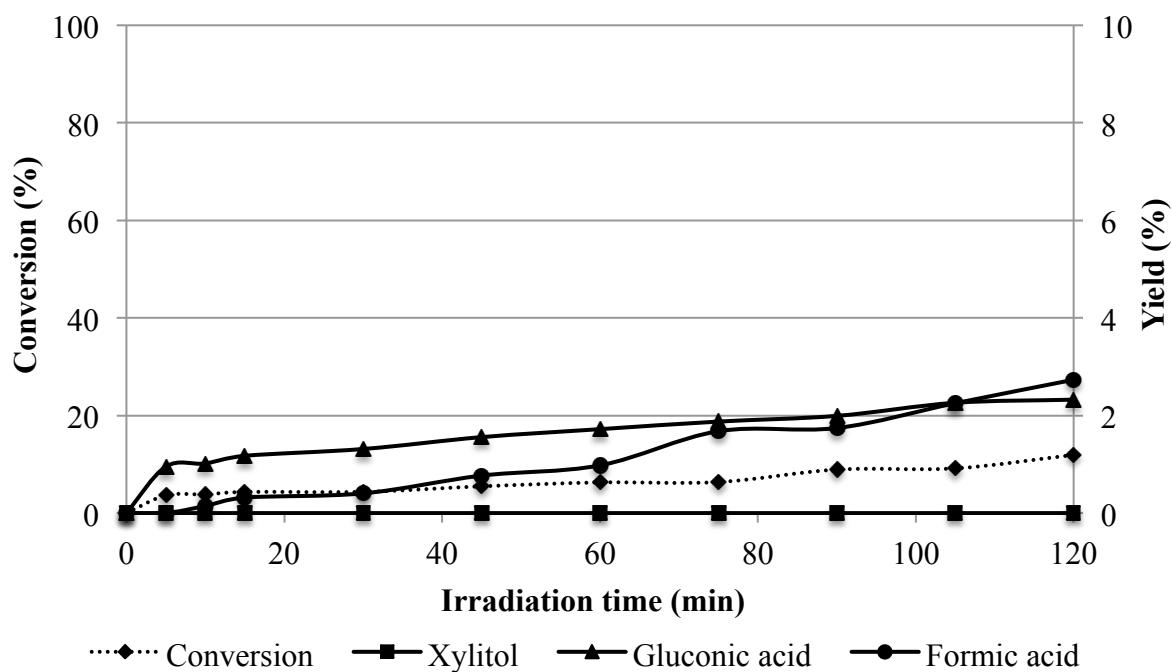
Fig. 4.2 SEM images (10000x) of (A) $\text{TiO}_2(\text{SG})$, (B) $\text{TiO}_2(\text{US})$, (C) $\text{TiO}_2(\text{MW})$, and (D) P25.

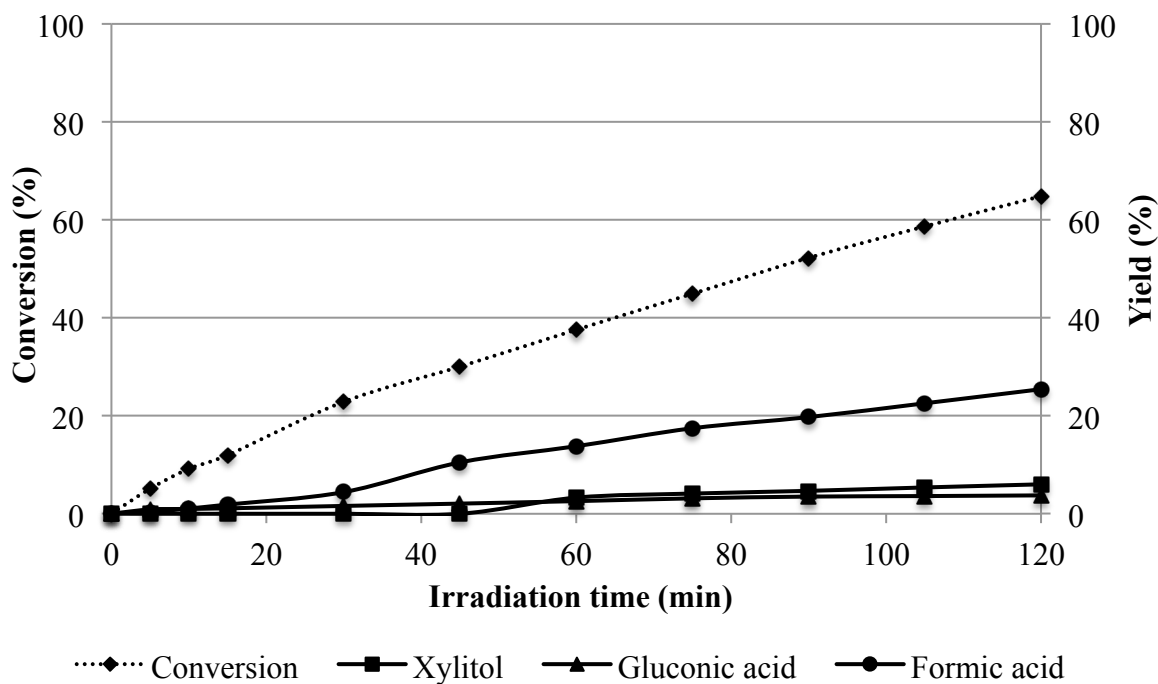
4.1.2. Photocatalytic conversion of glucose

The glucose conversion with initial concentration of 1 g/L on TiO₂(SG), TiO₂(US), TiO₂(MW) and P25 base catalysts was carried out for 120 min. Eleven samples were collected at the time intervals of 0, 5, 10, 15, 30, 45, 60, 75, 90, 105, and 120 min, respectively, and analyzed for glucose conversion and organic compound yields by HPLC.

The photocatalytic conversion of glucose and the yield of the products after 120 min irradiation time, including xylitol, gluconic acid and formic acid, are shown in Fig. 4.3. The glucose conversion and organic compound yields increased with long irradiation time and maximum at 120 min. It also indicated that the highest glucose conversion (90.72%) and the yield of products including 11.46% of xylitol, 5.49% of gluconic acid, and 39.66% of formic acid (12.64%, 10.09%, and 43.72% of selectivity of xylitol, gluconic acid, and formic acid, respectively) were obtained from commercial photocatalyst P25. Between photocatalysts which synthesized from by different techniques (SG, US, and MW), among them TiO₂(MW) shows the highest glucose conversion (64.82%) and yield of products including 6.01% of xylitol, 3.76% of gluconic acid and 25.43% of formic acid (9.28%, 5.79%, and 39.23% of selectivity of xylitol, gluconic acid, and formic acid, respectively). It could be implied that smaller particles of TiO₂, well dispersion of particles and large surface area of TiO₂(MW), so, its photocatalytic conversion and yield was high. Moreover, TiO₂(MW) shows the mixture of anatase and rutile (86:14) similar P25 that might induce higher photocatalytic activity. Nevertheless, the photocactivity of TiO₂(MW) is still lower P25.

Moreover, TiO₂(SG) shows the lowest glucose conversion (5.37%). After 120 min of irradiation, under the presence of TiO₂(SG), 2.20% of gluconic acid and 1.18% of formic were obtained. Comparatively, 2.33% of gluconic acid and 2.73% of formic were obtained from TiO₂(US).

(a) TiO₂(SG)(b) TiO₂(US)

(c) TiO₂(MW)

(d) P25

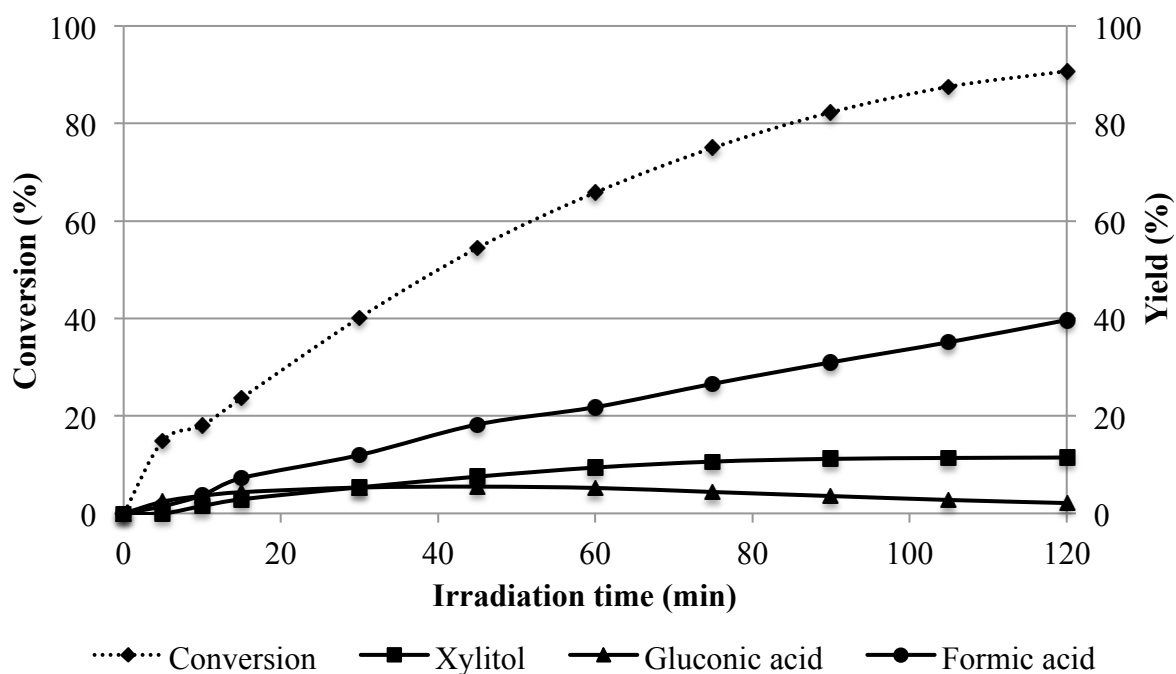


Fig. 4.3 Effect of TiO₂ synthesis methods on organic compounds in liquid phase after 120 min illumination: (a) TiO₂(SG), (b) TiO₂(US), (c) TiO₂(MW), and (d) P25.

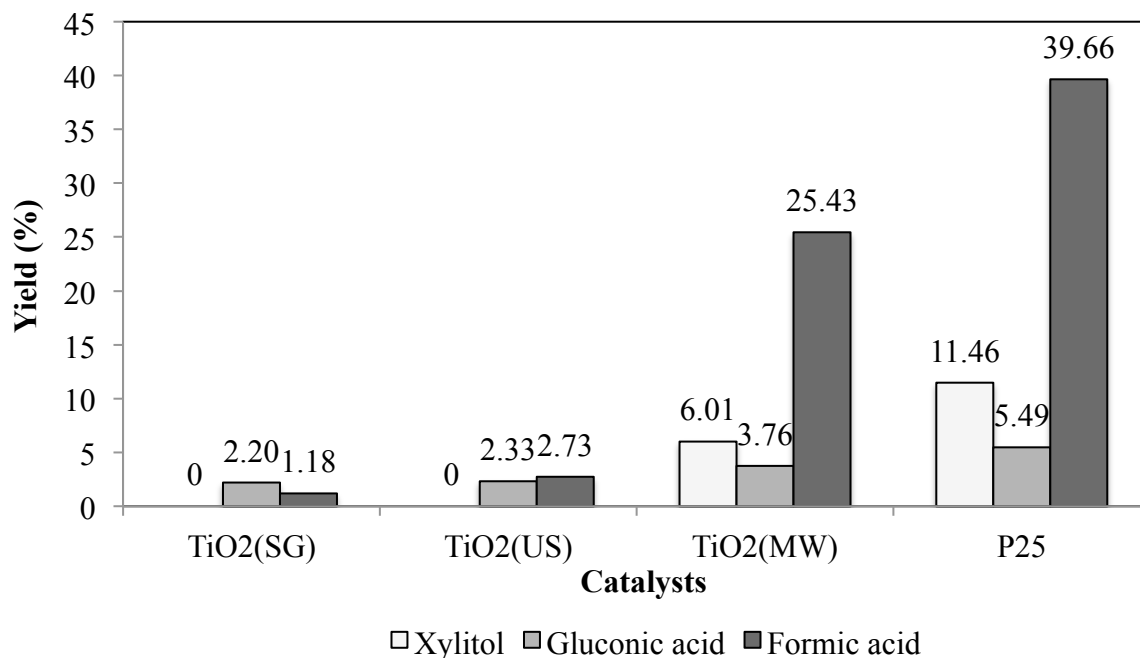


Fig. 4.4 Effect of TiO₂ synthesis methods on maximum yields of xylitol, gluconic acid, and formic acid: TiO₂(SG), TiO₂(US), and TiO₂(MW).

Li *et al.* (2010) suggested that the intermediate gluconic acid was obtained from photocatalytic H₂ production in the presence of glucose. Glucose molecules adsorbed on TiO₂ that can react with hydroxyl radicals (\bullet OH) to produce gluconic acid. After that, gluconic acid (C₆) would react further with hydroxyl radicals and xylitol with formic acid were detected. It was indicated that C₆ compounds are converted to C₅ compounds by the further hydroxyl radical attack.

4.2. Effect of TiO₂ Calcination Temperature

4.2.1. Material characterizations

The thermal treatment significantly affects the crystal phase and crystallite size of anatase and rutile. The XRD patterns of the TiO₂ synthesized by sol-microwave method that calcined at 400 °C to 600 °C for 5 h are shown in Fig. 4.5. The phase identification and crystallite size of the photocatalyst from XRD analysis are shown in Table 4.2. The increasing of calcination temperature resulted in higher crystallinity, as shown in Fig. 4.5. The TiO₂ (400 °C) consisted of only anatase phase. While the samples calcined at 500 °C

and 600 °C, composed of the anatase and rutile phases. The higher crystallinity increased with increasing calcination temperature.

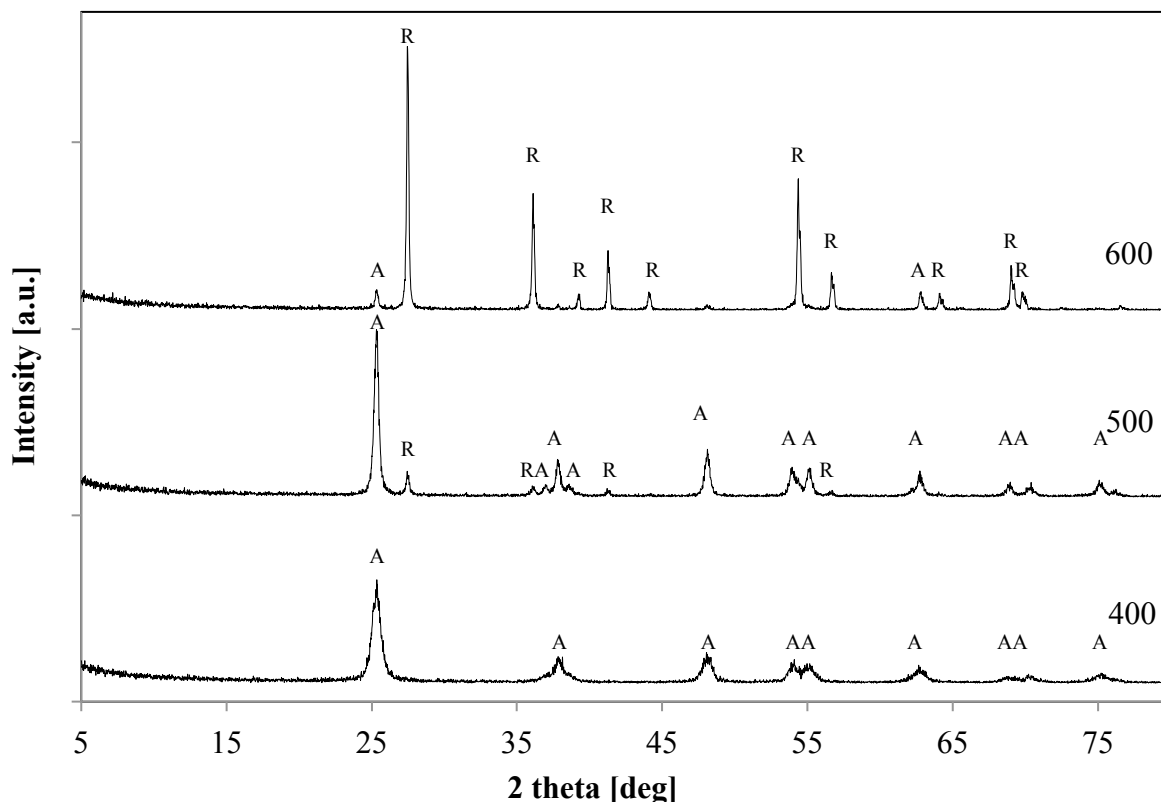


Fig. 4.5 X-ray diffraction patterns of TiO₂: 400 °C, 500 °C, and 600 °C.

Table 4.2 Summary of XRD characterizations of the synthesized TiO₂: catalysts synthesized by sol-microwave method, calcined at 400 °C, 500 °C, and 600 °C for 5 h.

Photocatalyst	Crystal phase ^a (%)	Crystallite size (nm)
TiO ₂ (400 °C)	A(100)	A(12.6)
TiO ₂ (500 °C)	A(86)/R(14)	A(25.1)/R(84.0)
TiO ₂ (600 °C)	A(5)/R(95)	A(40.2)/R(204.8)

^a A and R denote anatase and rutile, respectively.

For the TiO₂ (500 °C), partial phase transformation from anatase to rutile occurred, resulting in the mixed phases of anatase and rutile: A(86)/R(14) as shown in Table 4.2. Furthermore, 95% of rutile phase was obtained from TiO₂ (600 °C), almost all of the anatase phase was transformed into the rutile phase. The dominant peaks at 2θ of 27.41°,

36.11°, 41.21°, and 54.31° are rutile phase, correspond to (110), (101), (111), and (211) planes, respectively. From Table 4.2, it is clearly shown that, when calcination temperature increased, crystalline of TiO₂ aggregated upon annealing, resulted in the growth of crystallite size, corresponding to 12.6-40.2 nm for the anatase, 84-204.8 nm for the rutile.

4.2.2. Photocatalytic conversion of glucose

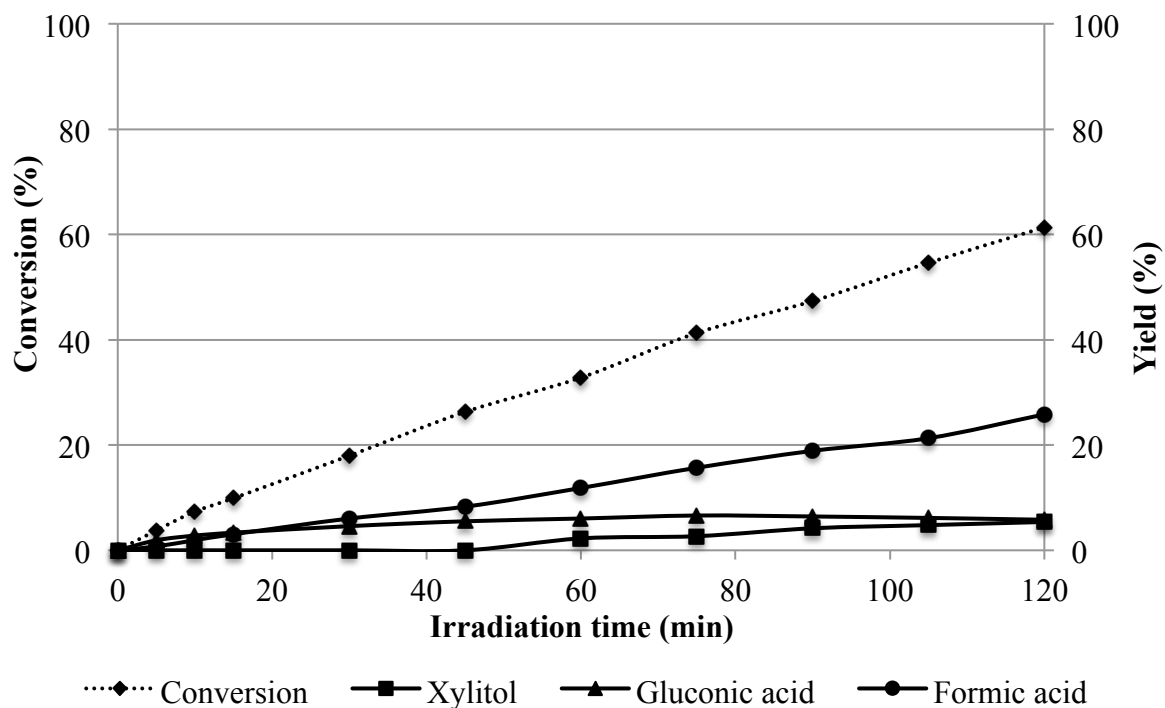
The glucose conversions on TiO₂ (calcined at 400 °C, 500 °C, and 600 °C) based catalysts were carried out for 120 min. The photocatalytic conversion of glucose and yield of organic compounds are shown in Fig. 4.6. The glucose conversion increased with long irradiation time (120 min). The highest glucose conversion (64.82%) was obtained from TiO₂ calcined at 500°C, whereas the TiO₂ calcined at 400°C provided much higher conversion than TiO₂ calcined at 600°C.

The results indicated that calcination temperature affects glucose conversion. The effect of calcination temperature on the yields of products: xylitol, gluconic acid, and formic acid are shown in Fig. 4.7. It represents that the highest xylitol yield of 6.01% with selectivity of 9.28% was obtained from TiO₂(500°C). Xylitol is one of 12 top value chemicals, it is building blocks for many compounds like xylaric acid or glycols (Werpy *et al.*, 2004) and can be used as sweetener but xylitol has 40% less calories than sugar. The highest in photocatalytic activity of TiO₂ calcined at 500 °C attributed to the small crystallite size (25.1 nm) promoted high surface area, consequently resulted in high photocatalytic activity.

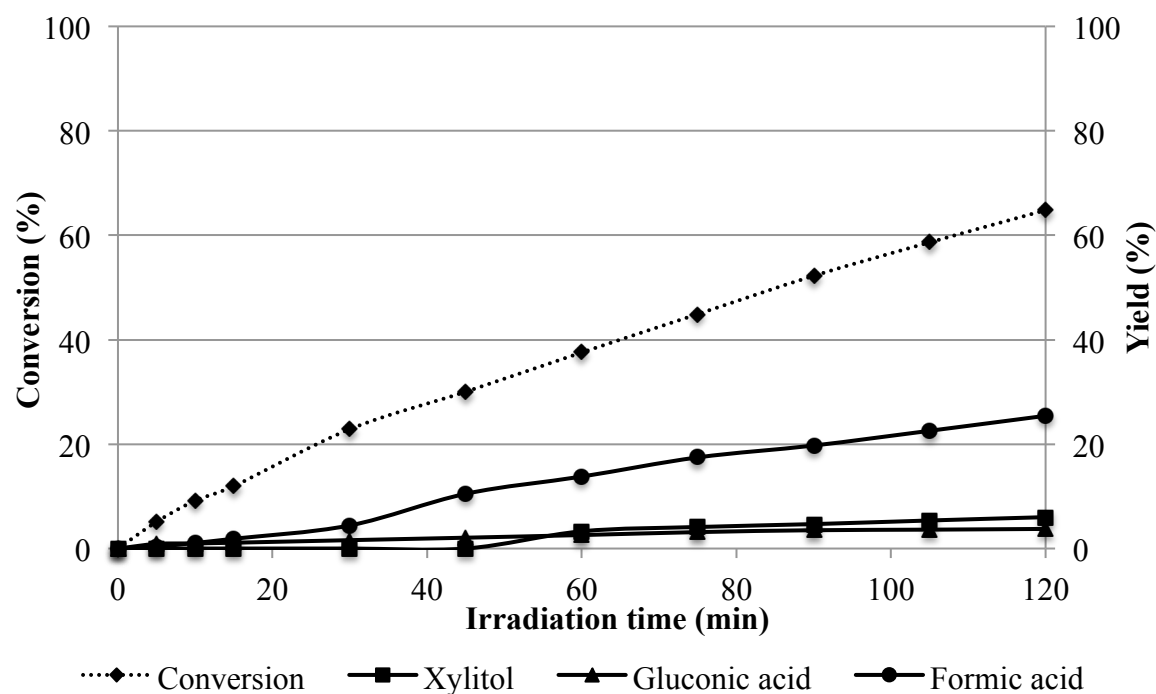
Although TiO₂ (400°C) provided the smallest crystallite size, it had poor crystallinity, which facilitated low photocatalytic activity. It was found that poor crystallinity of TiO₂ could increase the number of lattice defects and then inhibit the transport of electron that react with water molecule leading to decrease photocatalytic activity (Jittputti *et al.*, 2007). Moreover, it has been reported that pure anatase phase of TiO₂ shows a highest photocatalytic activity due to its low recombination rate of electrons and holes (Yu *et al.*, 2007). However, 86:14 of mixed phase between anatase and rutile in case of TiO₂ (500°C) exhibits the highest photocatalytic activity. This is because electrons can easily transfer from the conduction band of anatase to the conduction band of rutile since the conduction band level of rutile is lower than conduction band level of anatase,

called the synergistic effect between anatase and rutile phases (Gao *et al.*, 2014), resulting in the increased photocatalytic activity. Furthermore, the lowest in photocatalytic activity of TiO₂ calcined at 600 °C attributed to the large crystallite size affects low surface area and the presence of high content of rutile phase promoted faster recombination rate, consequently resulted in low photocatalytic activity.

(a) 400 °C



(b) 500 °C



(c) 600 °C

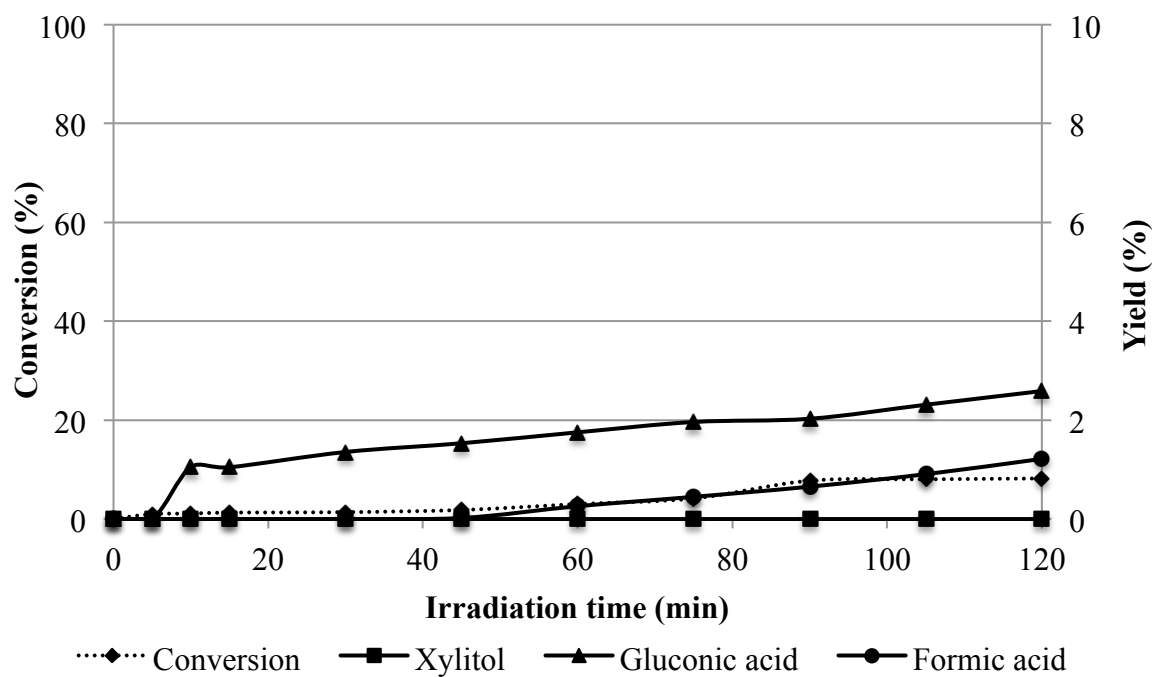


Fig. 4.6 Effect of calcination temperature on organic compounds in liquid phase and glucose conversion after 120 min illumination: (a) 400 °C, (b) 500 °C, and (c) 600 °C.

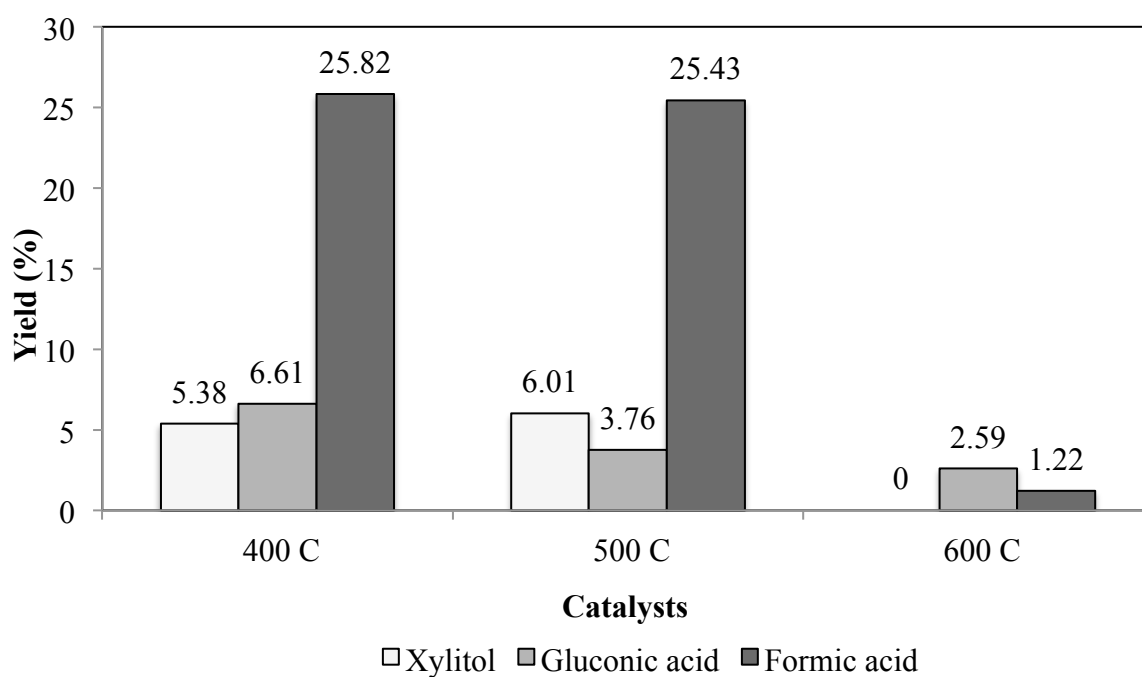


Fig. 4.7 Effect of calcination temperature on maximum yields of xylitol, gluconic acid and formic acid: TiO₂ calcined at 400 °C, TiO₂ calcined at 500 °C, and TiO₂ calcined at 600 °C.

4.3. Effect of TiO₂ Calcination Time

4.3.1. Photocatalyst characterization

The thermal treatment duration significantly affects crystallinity, phase composition and the crystallite size of rutile. The XRD patterns of the TiO₂ synthesized by sol-microwave method that calcined at 500 °C for 2 and 5 h are represented in Fig. 4.8. The phase identification and crystallite size of the photocatalyst from XRD analysis are shown in Table 4.3. An increase of the heat treatment time from 2 h to 5 h at 500 °C resulted in higher crystallinity as shown in Fig. 4.8. In this case, different calcination duration changed phase composition of TiO₂. The TiO₂ calcined for 5 h of shows higher phase transformation from anatase to rutile than TiO₂ calcined for 2 h, suggesting that phase transformation from anatase to the rutile increased at the elevated calcination time. Moreover, TiO₂ calcined for 2 and 5 h exhibit the same anatase crystallite size of 25.1 nm as shown in Table. 4.3. It indicated increasing of calcination time did not affect crystallite size of anatase. However, crystallite size of rutile was larger when calcination time increased from 2 h to 5 h, corresponding to 39.7-84.0 nm. It indicated that, the calcination time affected only rutile crystallite size. During 5 h of heat treatment, rutile crystal aggregation increased upon annealing as a result the crystals grow.

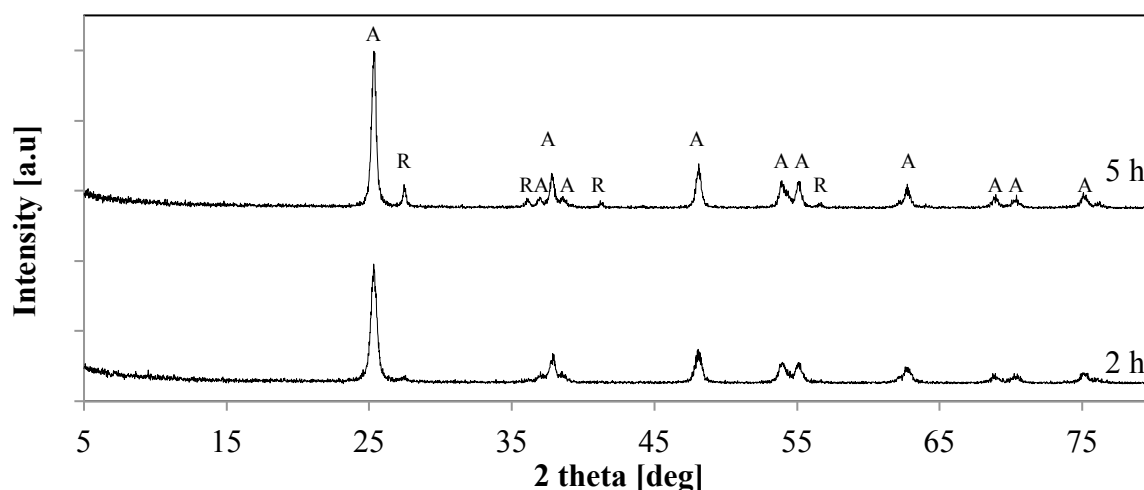


Fig. 4.8 X-ray diffraction patterns of TiO₂: 2 and 5 h.

Table 4.3 Summary of XRD characterizations of the synthesized TiO₂: catalysts synthesized by sol-microwave method, calcined at 500 °C for 2 and 5 h.

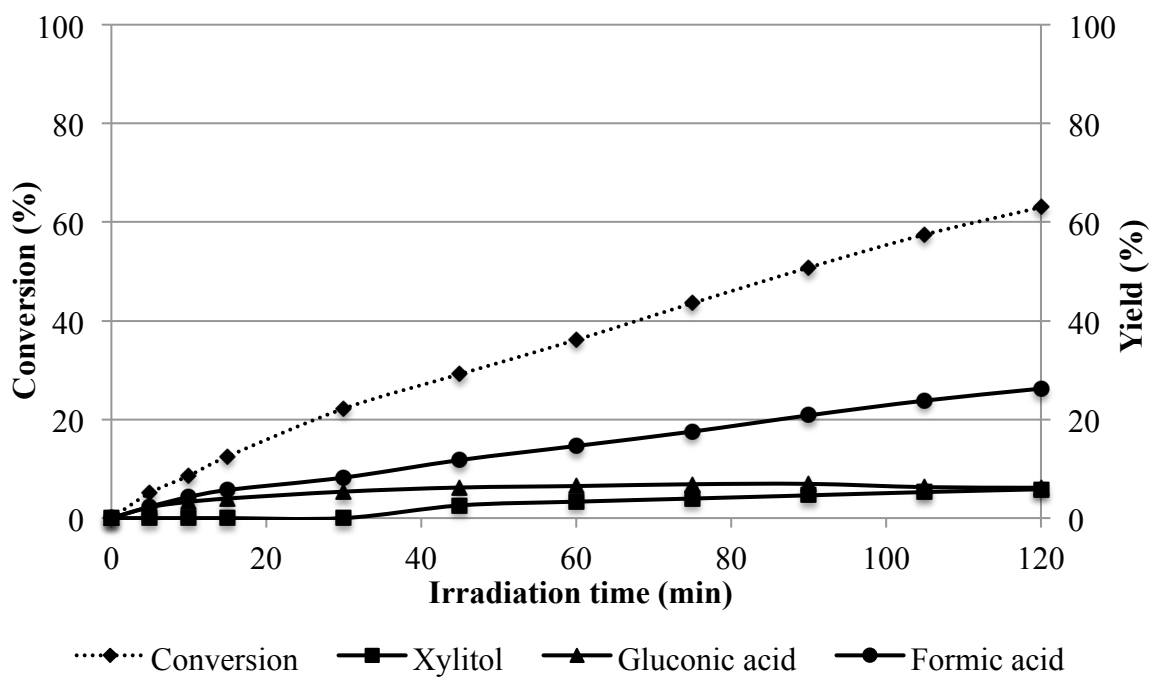
Photocatalyst	Crystal phase ^a (%)	Crystallite size (nm)
TiO ₂ (2 h)	A(96)/R(4)	A(25.1)/R(39.7)
TiO ₂ (5 h)	A(86)/R(14)	A(25.1)/R(84.0)

^aA and R denote anatase and rutile, respectively.

4.3.2. Photocatalytic conversion of glucose

The glucose conversions on the TiO₂ (calcined for 2 and 5 h) base catalysts were carried out for 120 min. The photocatalytic conversion of glucose and yield of organic compounds over the TiO₂ calcined at various durations (2 and 5 h) are shown in Fig. 4.9. The glucose conversion increased with long irradiation time. The highest glucose conversion was obtained from TiO₂ calcined for 5 h of 64.82%. The maximum yield of products: xylitol, gluconic acid and formic acid are shown in Fig. 4.10. It represents that the highest xylitol yield of 6.01% with selectivity of 9.28% were obtained from TiO₂ (500°C). Although the large rutile crystallite size was obtained from TiO₂ calcined for 5 h, which could be the cause of low photocatalytic activity, but TiO₂ calcined for 5 h provided high crystallization that facilitated higher photocatalytic activity (Jittputti *et al.*, 2007). Moreover, the 14% rutile-TiO₂ (5 h) sample exhibits the higher glucose conversion than 4% rutile-TiO₂ (2 h) as shown in Fig. 4.9. It indicated that optimal mixed phases content of anatase and rutile led to greater photocatalytic activity. Conversely, TiO₂ calcined for 2 h showed more yield of gluconic acid and formic acid production than TiO₂ calcined for 5 h. Gluconic acid is important building blocks for food and pharmaceutical industry (Ramachandran *et al.* 2006). Formic acid is important intermediate in chemical reactions and can have medical applications (Gibson *et al.*, 1969).

(a) 2 h



(b) 5 h

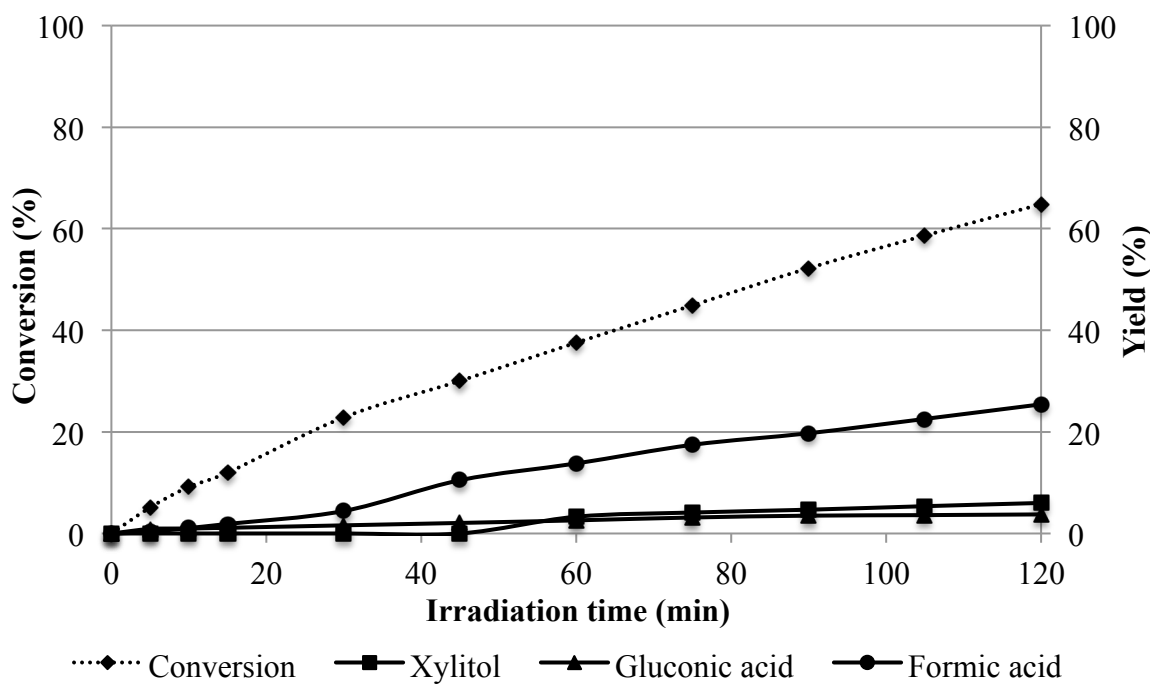


Fig. 4.9 Effect of calcination time on organic compounds in liquid phase and glucose conversion after 120 min illumination: (a) 2 h and (b) 5 h.

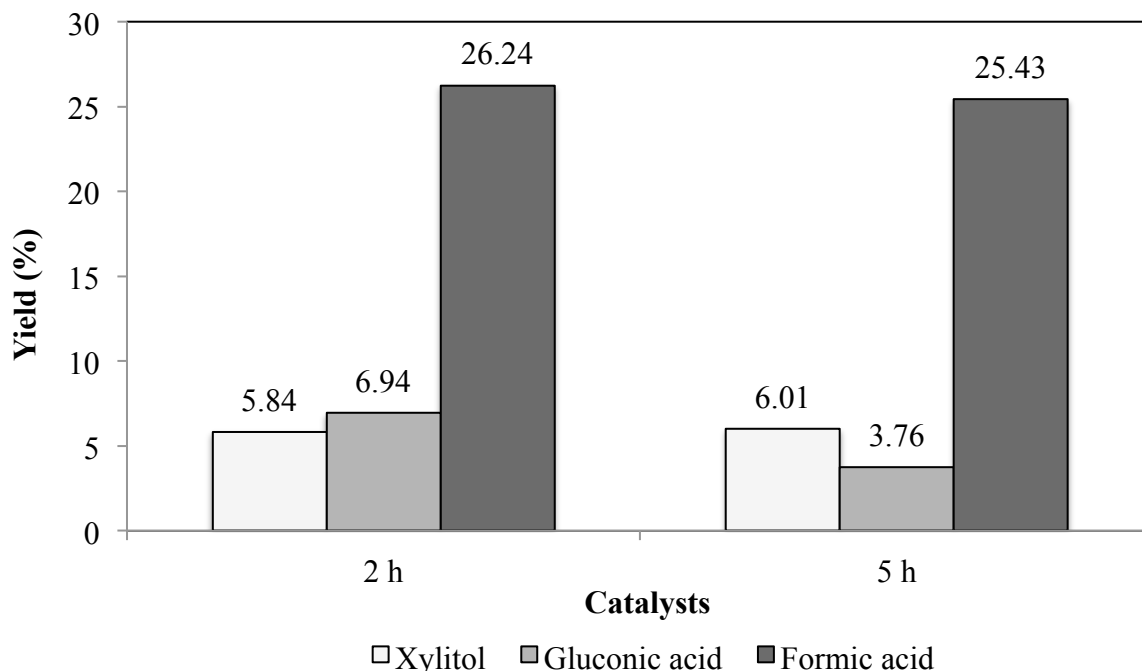


Fig. 4.10 Effect of calcination time on maximum yields of xylitol, gluconic acid and formic acid: TiO₂ calcined for 2 h and TiO₂ calcined for 5 h.

4.4. Effect of Metal Doped TiO₂

4.4.1. Ag doped TiO₂

4.4.1.1. Material characterizations

The Ag doped TiO₂ affects the crystal phase and the crystallite size of anatase and rutile. The XRD patterns of 1, 3, 10wt.% Ag doped TiO₂ and pure TiO₂ synthesized by sol-microwave method that calcined at 500 °C for 5 h are shown in Fig. 4.11. The phase identification, crystallite size of the photocatalyst from XRD analysis and S_{BET} are shown in Table 4.4. X-ray diffraction was used to determine the phase composition and crystallite size of Ag doped TiO₂. XRD patterns of 1, 3, 10wt.% Ag doped TiO₂ and pure TiO₂ are shown in Fig. 4.11. All of TiO₂ photocatalysts presented peaks of anatase at 2θ of 25.2°, 37.0°, 37.7°, 38.5°, 47.8°, 53.8°, 55.0°, 62.6°, 68.9°, 70.4°, and 75.0° were observed, corresponding to reflections from A(101), A(103), A(004), A(112), A(200), A(105), A(211), A(204), A(116), A(220), and A(215) planes were observed, respectively. The peaks located at 27.5°, 36.1°, 41.3°, 44.7, 56.6°, and 65.0° respond to the (110), (101), (111), (210), (220), and (002) planes of the rutile phase, respectively.

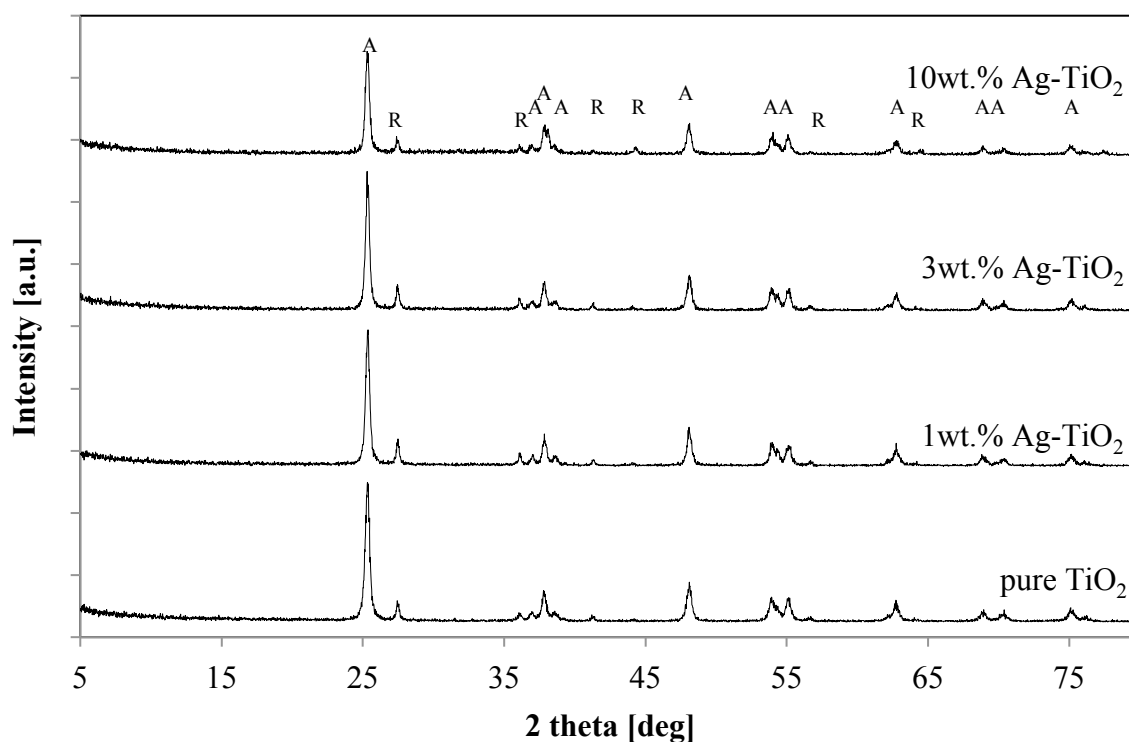


Fig. 4.11 X-ray diffraction patterns of pure TiO₂, 1wt.% Ag-TiO₂, 3wt.% Ag-TiO₂, and 10wt.% Ag-TiO₂.

Table 4.4 Summary of XRD characterizations and S_{BET} of the catalysts synthesized by sol-microwave method, calcined at 500 °C for 5 h: pure TiO₂, 1wt.% Ag-TiO₂, 3wt.% Ag-TiO₂, and 10wt.% Ag-TiO₂.

Photocatalyst	Phase ^a (%)	Crystallite size (nm)	S_{BET} (m ² /g)
pure TiO ₂	A(86)/R(14)	A(25.1)/R(84.0)	24.3
1wt.% Ag-TiO ₂	A(83)/R(17)	A(25.1)/R(129.1)	43.6
3wt.% Ag-TiO ₂	A(80)/R(20)	A(28.7)/R(102.5)	37.0
10wt.% Ag-TiO ₂	A(89)/R(11)	A(28.7)/R(83.8)	19.7

^aA and R denote anatase and rutile, respectively.

As shown in Fig. 4.11, the mixture phases of anatase and rutile were found in the Ag-doped TiO₂ samples. For the Ag doped TiO₂, no diffraction peaks of Ag (1 1 1) plane at $2\theta = 38.1^\circ$ and Ag (2 0 0) plane at $2\theta = 44^\circ$ occurred in the XRD patterns, possibly resulting from low Ag loading content and also appropriate dispersion of Ag was doped into interstitial positions of TiO₂ lattice that might be integrated into the basic structure of TiO₂ (Sun *et al*, 2013). It can be found that 1 and 3wt.% Ag could induce phase

transformation from anatase to rutile, as shown in Table 4.4. Rutile phase increased from 14 to 20% when TiO₂ was doped with 3wt.% Ag due to some perturbation in the anatase crystalline phase. The Ag⁺ (1.15 Å) has ionic radii larger than Ti⁴⁺ (0.68 Å). It is thermodynamically possible for Ag ions to reside in the interstitial positions of TiO₂ lattice (Chang *et al*, 2014). According to $r_{\text{Ti}} < r_{\text{Cu}}$ produce the strain of the TiO₂ lattice resulting defects of grains occurred. Defects increased with the increase of Ag doping content from 1wt.% to 3wt.%, which facilitated the rearrangement of structure for rutile and promoted the phase transformation (Li *et al*, 2010). For case of 10wt.% Ag-TiO₂, rutile phase decreased from 14% to 11% compared with pure TiO₂ as shown in Table 4.4. It is possible that Ag might exist in the form of Ti-O-Ag three elements around the anatase crystallites, possibly inhibiting the production of the rutile phase (Francisco *et al*, 2002).

Based on the XRD results, the crystallite sizes of the pure TiO₂ and Ag-TiO₂ catalysts were calculated by the Scherrer equation as shown in Table 4.4. The pure TiO₂ and 1wt.% Ag-TiO₂ indicated the same anatase crystallite size of 25.1 nm. The anatase crystallite size of 3wt.% Ag-TiO₂ was larger than 1wt.% Ag-TiO₂. Moreover, 3wt.% Ag-TiO₂ and 10wt.% Ag-TiO₂ display the same anatase crystallite size of 28.7 nm. It indicated the crystallite size of anatase slightly increased or unchanged with the increase of Ag from 0 to 10%. This could be explained by the rearrangement of titanium and oxygen ions in anatase grain boundaries, which would be greatly disturbed by the silver ions. The transferring of material in anatase grains were hindered affected energy for the movement of anatase grain boundary must increase, resulting slower grain growth (Li *et al*, 2010). In addition, the rutile crystallite size increased with increase of Ag loading from 0-1wt.%. Ag⁺ ions might cause of defects and anion vacancies on the surface of rutile grains, which would facilitate larger rutile grains (Li *et al*, 2010). Furthermore, rutile crystallite size decreased with increase of Ag loading from 3-10wt.% compared with 1wt.% Ag. The smallest rutile crystallite size was obtained from 10wt.% Ag-TiO₂ of 83.8 nm. The results imply that excess Ag from high Ag loading content might deposited on the face of rutile, which hinder the rutile crystal growth (Bokare *et al.*, 2013).

Moreover, 1wt.% Ag-TiO₂ and 3wt.% Ag-TiO₂ displayed higher BET surface area than did pure TiO₂ as shown in Table 4.4. Among them, 1wt.% Ag-TiO₂ represented the highest BET surface area of 43.6 m²/g. It could be explained by some Ag ion might remain near the boundary of the particles, obstructing their growth that facilitated an increase of

BET surface area. On the other hand, the lowest BET surface area was obtained from 10wt.% Ag-TiO₂ due to too many of Ag dopant might agglomerate on TiO₂ surface that induce large TiO₂ particle cause of low BET surface area.

The effect of Ag doping content on the absorption threshold and the band gap energy of TiO₂ were also examined with UV-Visible Diffuse Reflectance spectroscopies. The optical absorbance spectra of pure TiO₂, 1wt.% Ag-TiO₂, 3wt.% Ag-TiO₂, and 10wt.% Ag-TiO₂ are shown in Fig. 4.12. Compared with pure TiO₂, the absorption edges of 1wt.% Ag-TiO₂, 3wt.% Ag-TiO₂ and 10wt.% Ag-TiO₂ shifted to longer wavelength in the UV-vis region, indicating that Ag doped TiO₂ with broadened the absorption edge of TiO₂. To estimate the band gap energies (E_g), the absorption band of Ag-doped TiO₂ were calculated using the following equation $E_g = 1240/\lambda_g$ where λ_g is the wavelength at the overlap of vertical and horizontal portions of the spectra. The band gap energy (E_g) of 1wt.% Ag-TiO₂, 3wt.% Ag-TiO₂ and 10wt.% Ag-TiO₂ were 2.85, 2.83 and 2.77 eV, respectively, as shown in Table 4.5. It indicated that when Ag doping content is increased, the absorption edge shifts towards a longer wavelength, which affects the decrease of the band gap. The band gaps are shown in Table 4.5. The shortening of band gap induced TiO₂ more photocatalytic activity, due to the yield of photogenerated electron-hole pair decreases and it possibly increased the photocatalytic activity of TiO₂. (Rengaraj *et al.*, 2006).

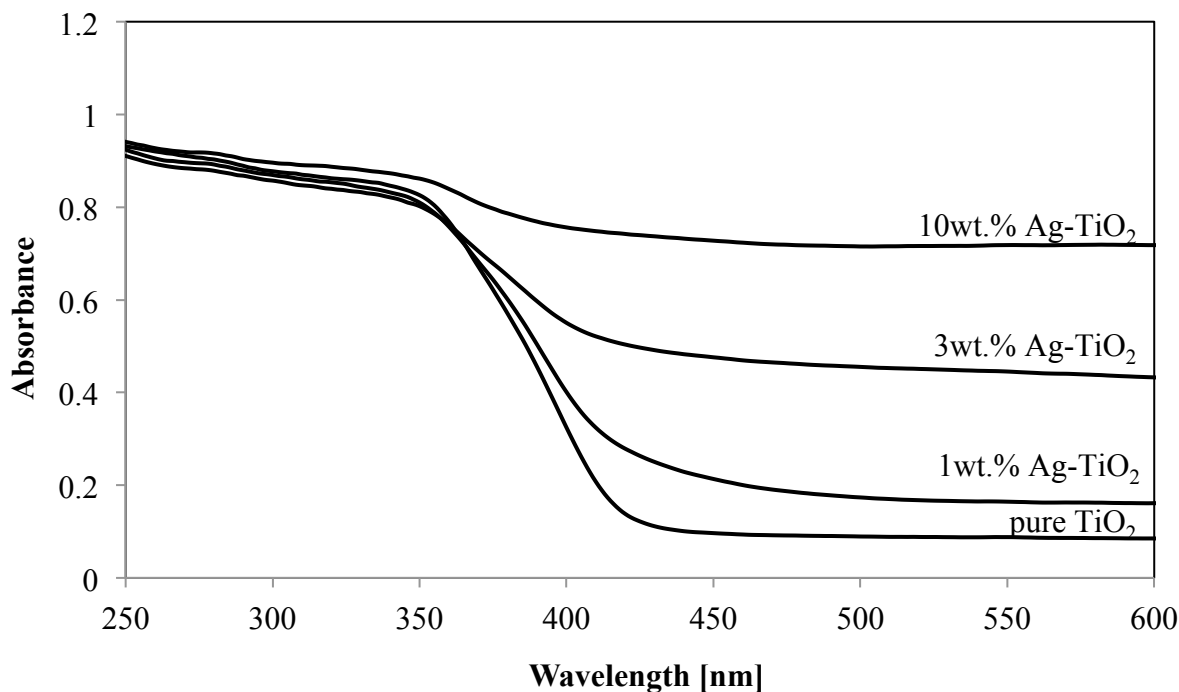


Fig. 4.12 UV-visible diffuse reflectance spectra of pure TiO₂, 1wt.% Ag-TiO₂, 3wt.% Ag-TiO₂, and 10wt.% Ag-TiO₂.

Table 4.5 Summary of UV-vis DR characterizations of the synthesized TiO₂: pure TiO₂, 1wt.% Ag-TiO₂, 3wt.% Ag-TiO₂, and 10wt.% Ag-TiO₂.

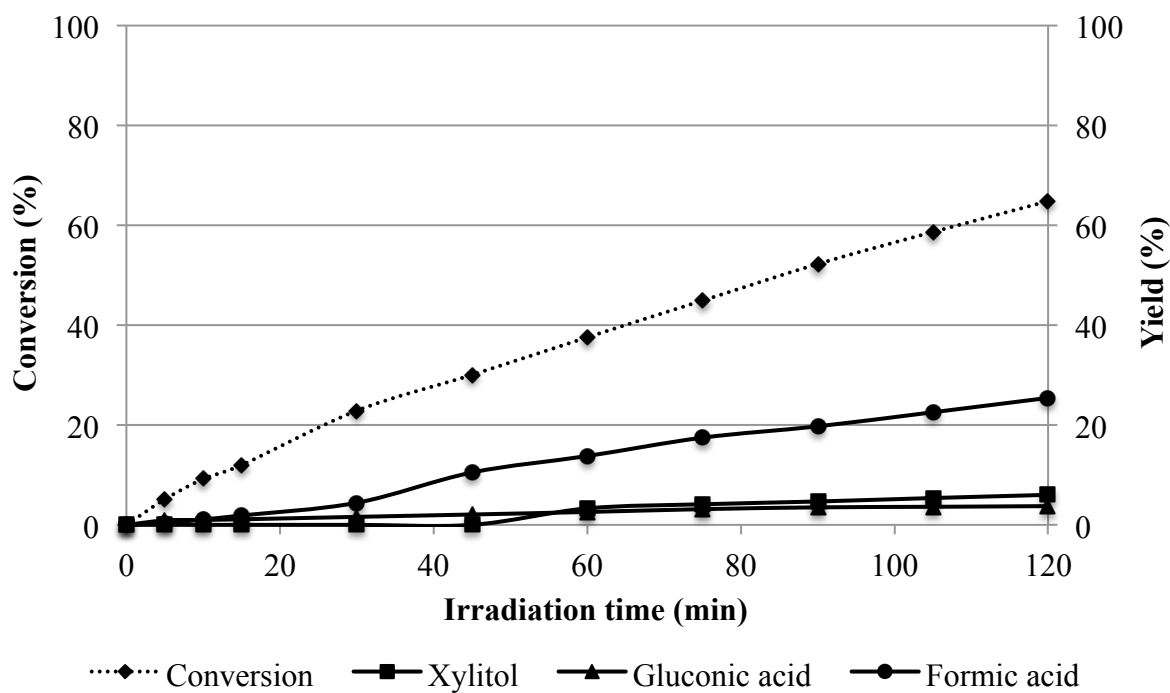
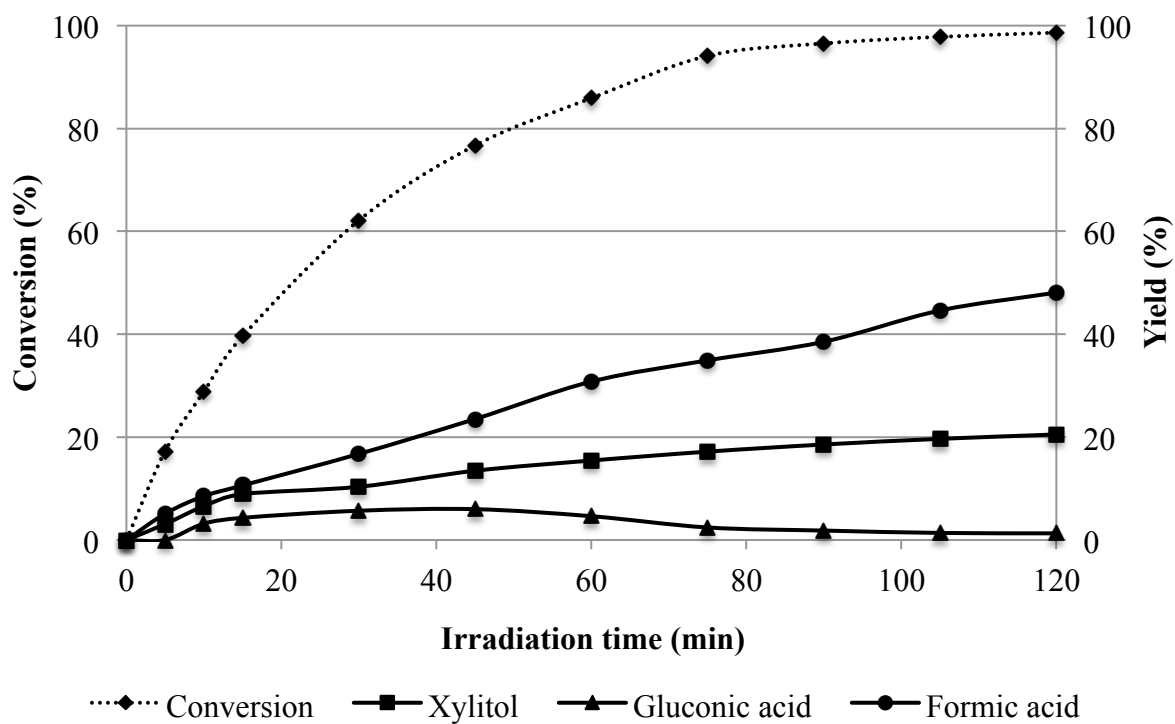
Photocatalyst	Band gap (eV)	Absorption threshold (nm)
pure TiO ₂	2.95	421
1wt.% Ag-TiO ₂	2.85	436
3wt.% Ag-TiO ₂	2.83	439
10wt.% Ag-TiO ₂	2.77	448

4.4.1.2. Photocatalytic conversion of glucose

The glucose conversion on the Ag-TiO₂ base catalyst was carried out for 120 min. The photocatalytic activity of pure TiO₂ and Ag-TiO₂ catalysts with metal loading content 1, 3, and 10 wt.% are shown in Fig. 4.13. And the effect of Ag doped TiO₂ on maximum yields of xylitol, gluconic acid and formic acid: 0wt.% Ag, 1wt.% Ag, 3wt.% Ag, and 10wt.% Ag doped TiO₂ are shown in Fig. 4.14.

The experimental results indicated that after 120 min reaction, 3 organic compounds were produced: xylitol, gluconic acid and formic acid. It was found that 1wt.% Ag-TiO₂ achieved the highest glucose conversion of 98.63%. The maximum yield of products: xylitol, gluconic acid and formic acid are showed in Fig. 4.14. The highest xylitol yield of 20.51% with selectivity of 20.80% was obtained from 1wt.% Ag-TiO₂ after 120 min illumination time. It indicated that high surface area (43.6 m²/g), mixed phase of anatase and rutile (83% of anatase : 17% of rutile) and small band gap (2.85 eV) of 1wt.% Ag-TiO₂ could promote high photocatalytic activity. The small band gap facilitated yield of photogenerated electron-hole increased and electrons easily transferred (Rengaraj *et al.*, 2006). It was reported that Ag dopant could insert into TiO₂ lattice as Ag impurity state, over the valance band and below the conduction band of TiO₂, forms in its optical band gap. For photocatalytic reaction of glucose under mercury lamp irradiation, electrons in valence band were excited to Ag impurity state, left holes in valence band, and after that these electrons transferred from impurity state to conduction band. Ag impurity state like intermediate band that electrons stay there for a short time and then transferred again facilitated the photoactivity in the visible light region (Sun *et al.*, 2013). On the other hand, 10wt.% Ag-TiO₂ achieved the lowest glucose conversion because it had the lowest BET surface area. Too many Ag loading content might close active site of catalyst, so, phtocatalytic activity was low. Moreover, Ag might defect into the TiO₂ lattice resulting in too many oxygen vacancies in lattice. Oxygen vacancies act as recombination centers of generated electron-hole pairs, resulting decreased photocatalytic activity (Pham *et al.*, 2014).

Moreover, the 17% rutile of the 1wt.% Ag-TiO₂ sample exhibited the highest photocatalytic activity, indicating that the optimal mixed phase contents of anatase and rutile (83% of anatase : 17% of rutile) that was quite similar to Degussa-P25 and led to the highest photocatalytic activity.

(a) pure TiO₂(b) 1wt.% Ag-TiO₂

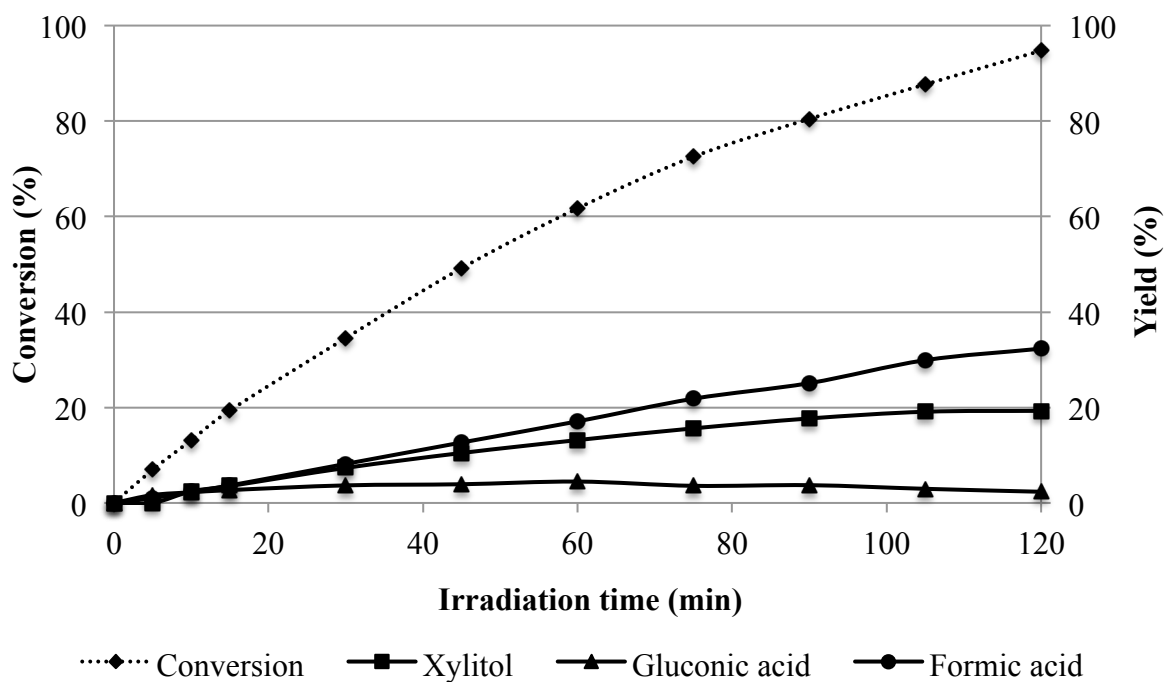
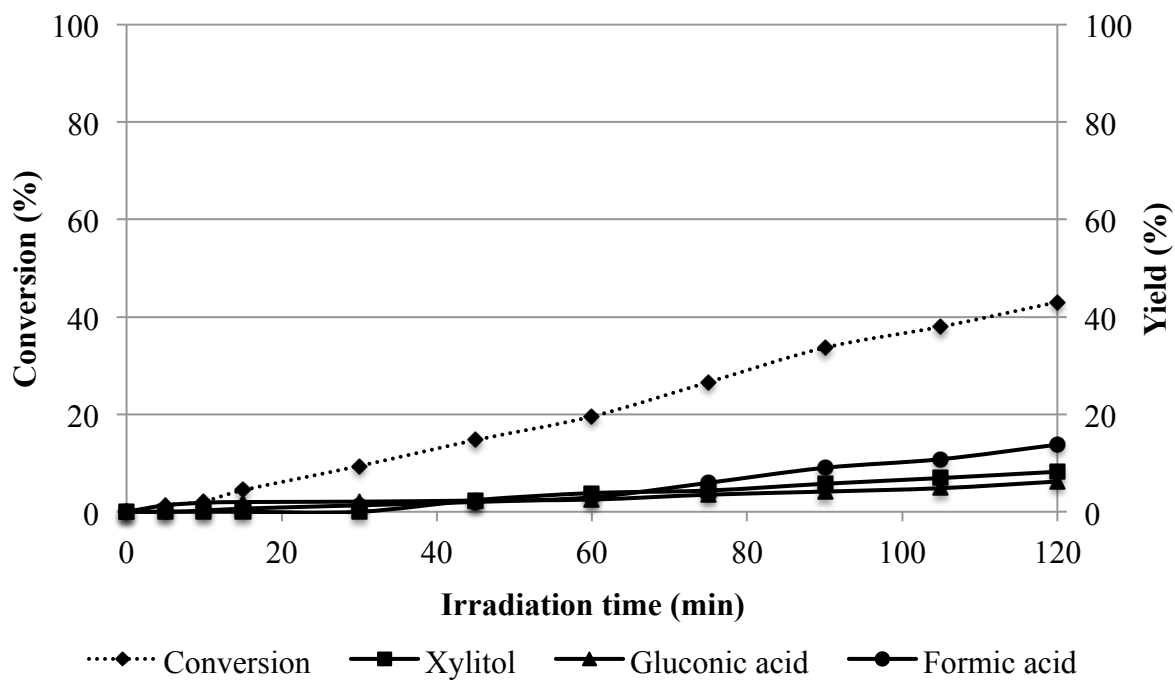
(c) 3wt.% Ag-TiO₂(d) 10wt.% Ag-TiO₂

Fig. 4.13 Effect of Ag doped TiO₂ on glucose conversion and yields of xylitol, gluconic acid, and formic acid after 120 min illumination: (a) pure TiO₂, (b) 1wt.% Ag-TiO₂, (c) 3wt.% Ag-TiO₂, and (d) 10wt.% Ag-TiO₂.

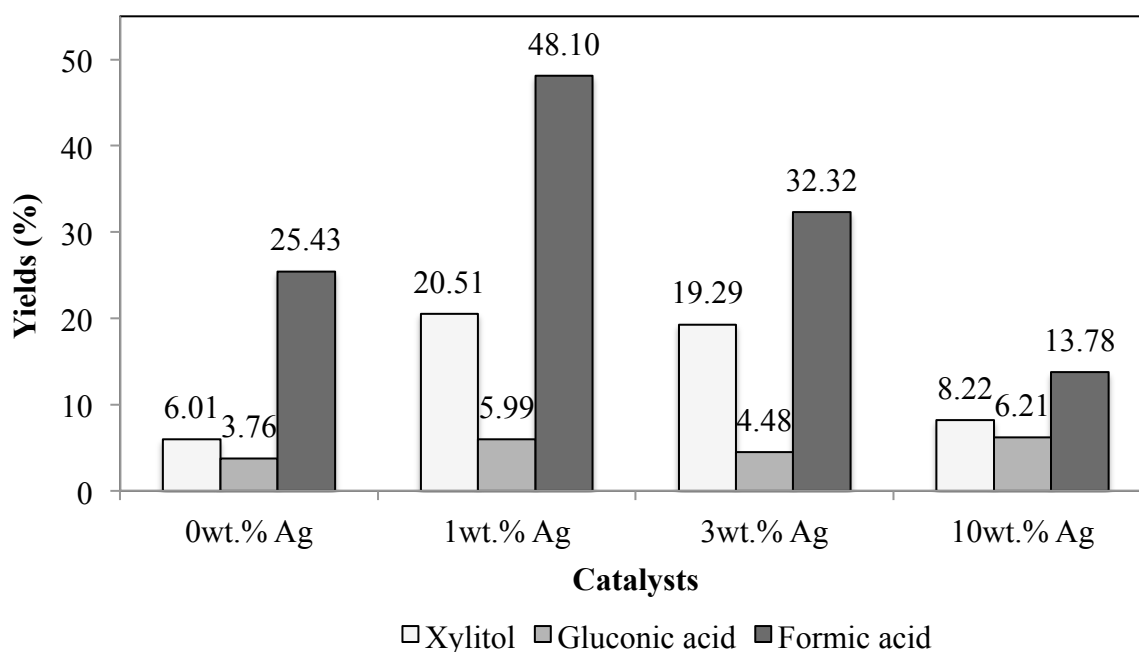


Fig. 4.14 Effect of Ag doped TiO₂ on maximum yields of xylitol, gluconic acid, and formic acid: 0wt.% Ag, 1wt.% Ag, 3wt.% Ag, and 10wt.% Ag doped TiO₂.

4.4.2 Cu doped TiO₂

4.4.2.1. Photocatalyst characterization

The Cu doped TiO₂ affects the crystal phase and the crystallite sizes of anatase and rutile. The XRD patterns of 1, 3, 10wt.% Cu-TiO₂ and pure TiO₂ synthesized by sol-microwave method that calcined at 500 °C for 5 h are shown in Fig. 4.15. The phase identification, crystallite size of the photocatalyst from XRD analysis and S_{BET} are shown in Table 4.6.

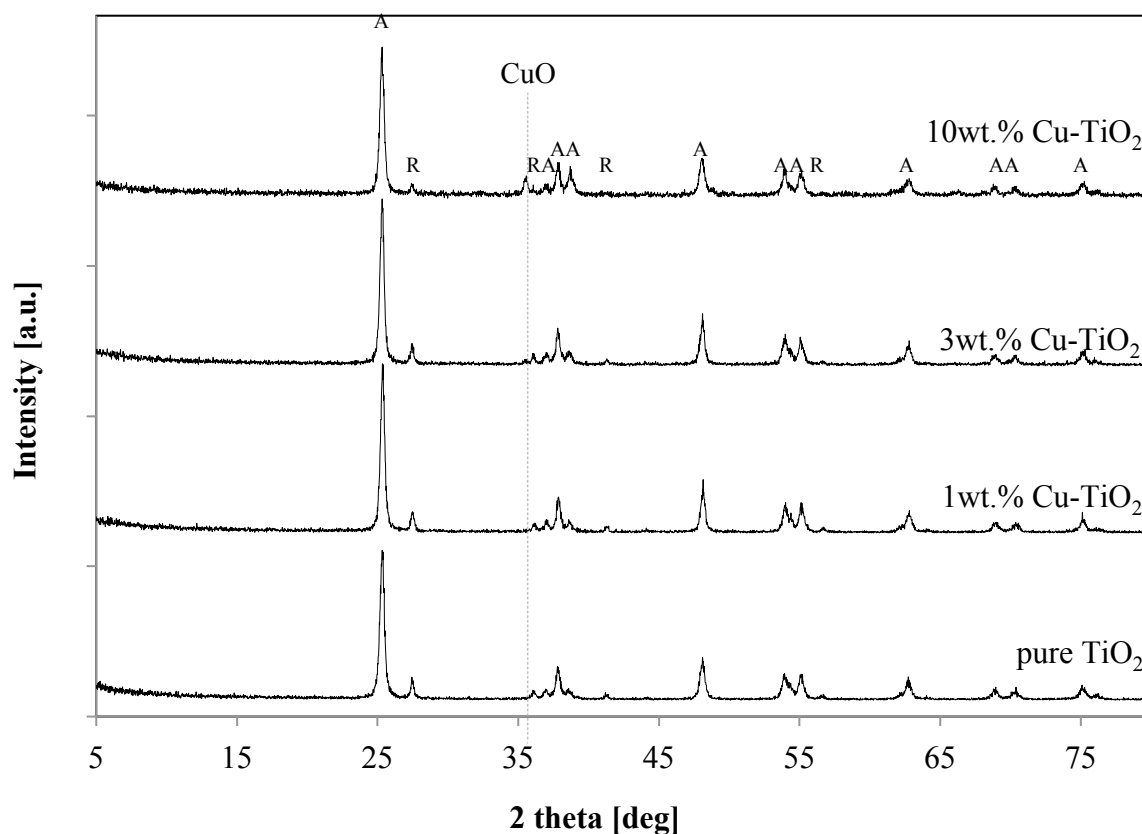


Fig. 4.15 X-ray diffraction patterns of pure TiO₂, 1wt.% Cu-TiO₂, 3wt.% Cu-TiO₂, and 10wt.% Cu-TiO₂.

Table 4.6 Summary of XRD characterizations and S_{BET} of the catalysts synthesized by the sol-microwave method, calcined at 500 °C for 5 h: pure TiO₂, 1wt.% Cu-TiO₂, 3wt.% Cu-TiO₂, and 10wt.% Cu-TiO₂.

Photocatalyst	Phase ^a (%)	Crystallite size (nm)	S_{BET} (m ² /g)
pure TiO ₂	A(86)/R(14)	A(25.1)/R(84.0)	24.3
1wt.% Cu-TiO ₂	A(88)/R(12)	A(25.1)/R(73.9)	38.2
3wt.% Cu-TiO ₂	A(88)/R(12)	A(50.3)/R(103.3)	43.0
10wt.% Cu-TiO ₂	A(93)/R(7)	A(57.3)/R(82.5)	31.2

^a A and R denote anatase and rutile, respectively.

The mixtures of the anatase and rutile peaks of TiO₂ were found in the Cu-doped TiO₂ samples. For Cu doped TiO₂, diffraction peaks of CuO (0 0 2) plane at $2\theta = 35.5^\circ$ only occurred in the XRD patterns of 10wt.% Cu-TiO₂. Furthermore, rutile phase decreased with the increase of Cu doped content as shown in Table 4.6. The lowest rutile

content was obtained from 10wt.% Cu-TiO₂. It indicated that Cu dopant inhibit phase transformation from anatase to rutile. The phenomena occurred due to the incorporation of Cu into the TiO₂ lattice. Due to Cu²⁺ (0.73Å) and Ti⁴⁺ (0.64Å) have similarity in the ionic radius, so, the Cu ions can substitutionally replace Ti ions in TiO₂ lattice and might exist in the form of Ti-O-Cu three elements around the anatase crystallites possibly inhibited the transformation to rutile phase (Francisco *et al.*, 2002). It has previously been argued that Cu dopant created higher number of defects inside the anatase phase, resulting in faster phase transformation from anatase to rutile (Wang *et al.*, 2014). The crystallites size of pure TiO₂ and 1,3,10wt.% Cu doped TiO₂ were presented in Table 4.6. It indicated that anatase crystallite size increased with increase of Cu loading. It can be explained by Cu²⁺ might cause of defects on anatase lattice, which would facilitate larger anatase grains (Li *et al.*, 2010). In case of pure TiO₂ and 1wt.% Cu-TiO₂ indicated the same anatase crystallite size of 25.1 nm.

Moreover, Cu-TiO₂ displayed higher BET surface area than pure TiO₂ as shown in Table 4.6. Among them, 3wt.% Cu-TiO₂ represented the highest BET surface area of 43.0 m²/g, It could be explained by some Cu ion might obstruct particles growth that facilitated an increase of BET surface area. Similarly, Wand *et al.*, 2014 found that the larger Cu²⁺ ions preferred to remain near the boundary or on the surface of the particles, inhibit their particles growth. Among Cu-TiO₂, 10wt.% Cu-TiO₂ achieved the lowest BET surface area.

The effect of Cu doping content on the absorption threshold and the band gap energy were also examined with UV-Visible Diffuse Reflectance spectroscopic. The UV-visible diffuse reflectance spectra of pure TiO₂, 1wt.% Cu-TiO₂, 3wt.% Cu-TiO₂ and 10wt.% Cu-TiO₂ are shown in Fig. 4.16. The absorption spectrum for Cu-doped TiO₂ shifted to an energy region lower than pure TiO₂. It indicated that when Cu doping content is increased, the absorption edge shifts towards a longer wavelength. The red shift of the absorbance edge toward longer wavelengths of Cu-TiO₂ promoted the decrease in band gap energy of TiO₂. Accordingly, the values of E_g for pure TiO₂, 1wt.% Cu-TiO₂, 3wt.% Cu-TiO₂, and 10wt.% Cu-TiO₂ were 2.95, 2.90, 2.86, and 1.98 eV, respectively as shown in Table 4.7. It indicated that E_g values decreased with the increase of Cu dopant. Theelectron could be easily transferred when Cu-TiO₂ has low band gap energy, resulting in the increase photocatalytic activity (Pham *et al.*, 2014).

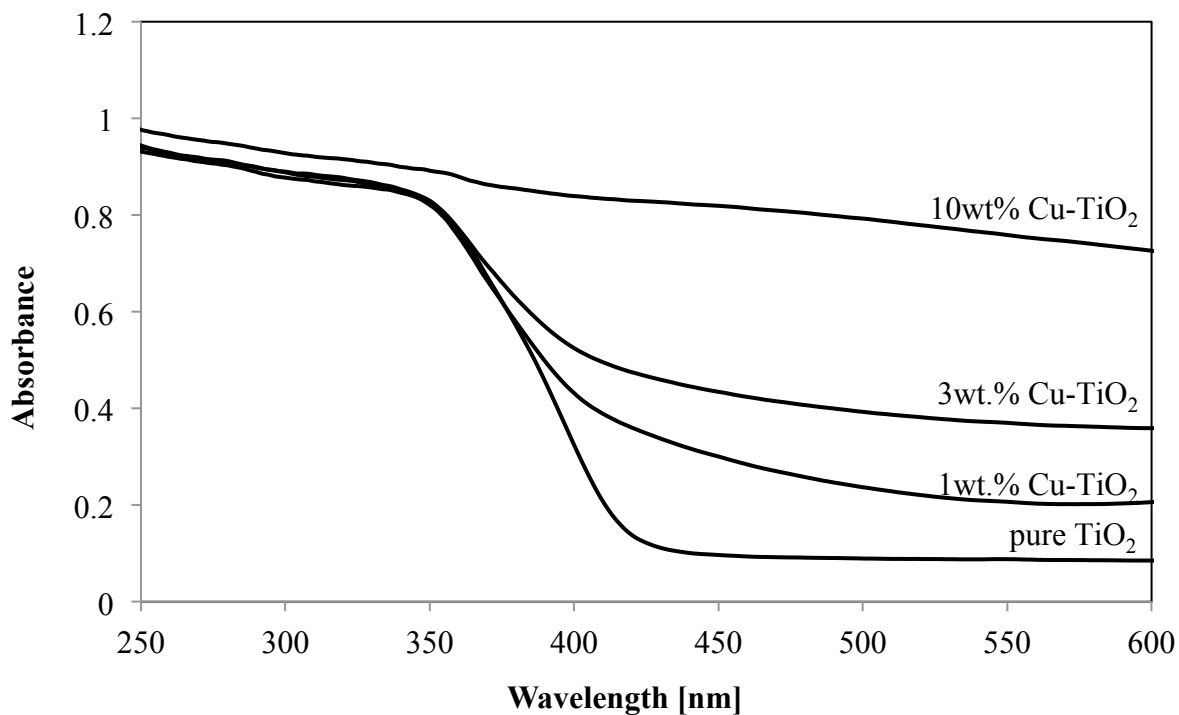


Fig. 4.16 UV-visible diffuse reflectance spectra of pure TiO₂, 1wt.% Cu-TiO₂, 3wt.% Cu-TiO₂, and 10wt.% Cu-TiO₂.

Table 4.7 Summary of UV-vis DR characterizations of the synthesized TiO₂: pure TiO₂, 1wt.% Cu-TiO₂, 3wt.% Cu-TiO₂, and 10wt.% Cu-TiO₂.

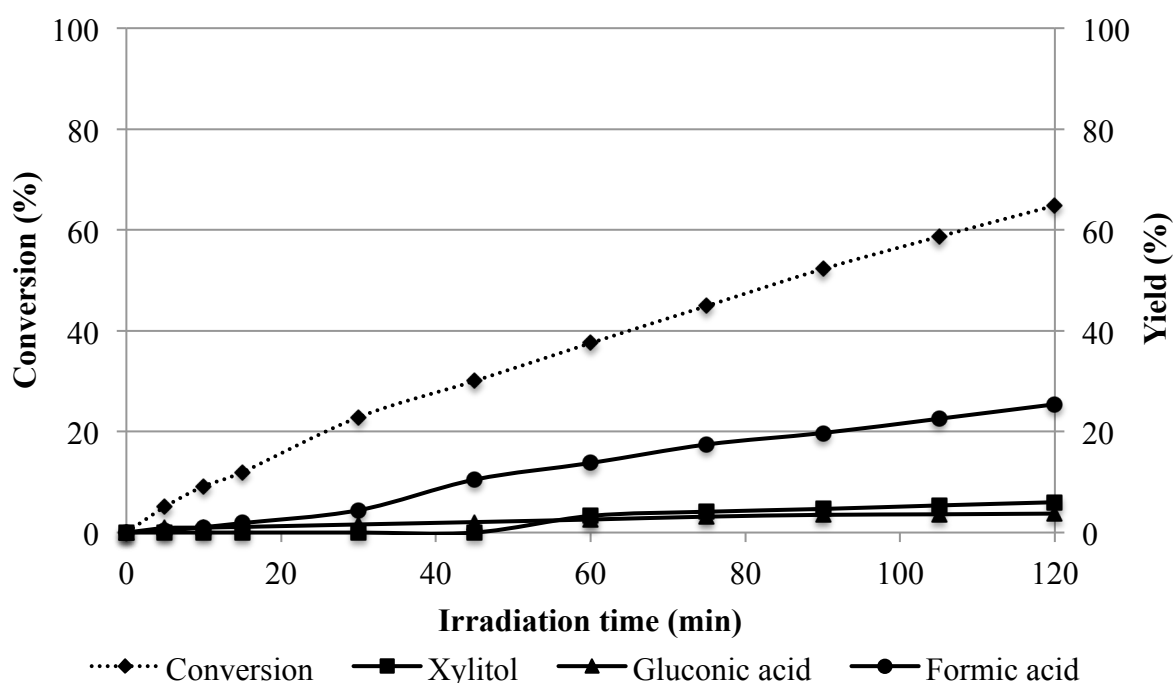
Photocatalyst	Band gap (eV)	Absorption threshold (nm)
0wt.% Cu-TiO ₂	2.95	421
1wt.% Cu-TiO ₂	2.90	429
3wt.% Cu-TiO ₂	2.86	435
10wt.% Cu-TiO ₂	1.98	629

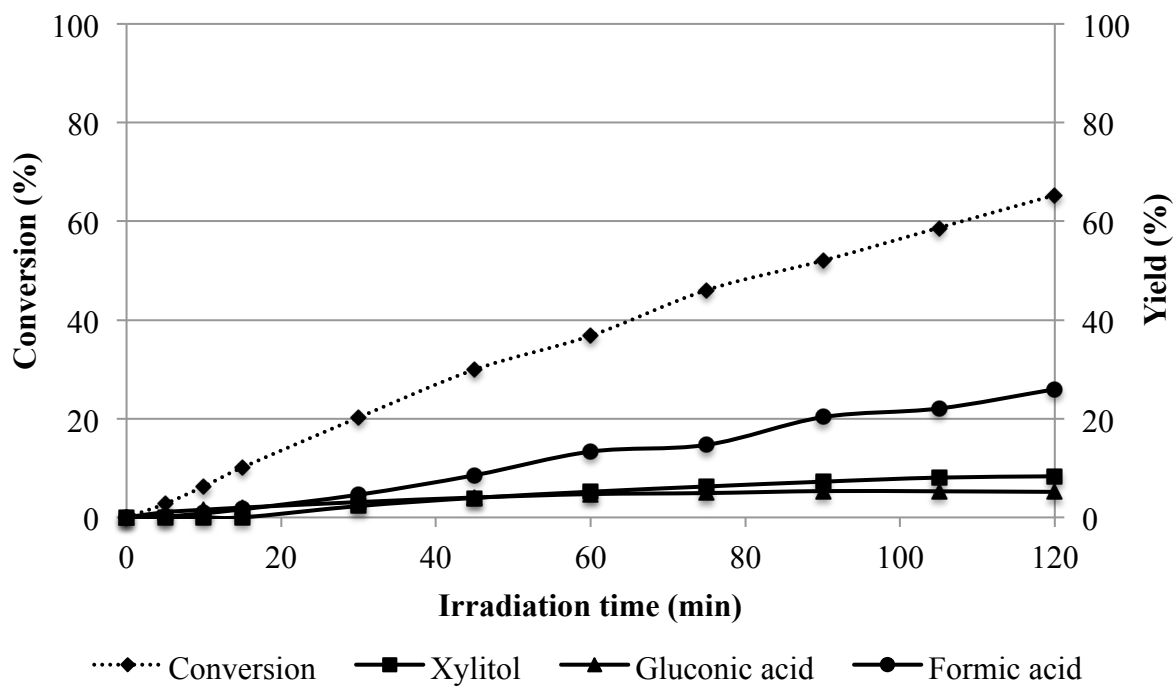
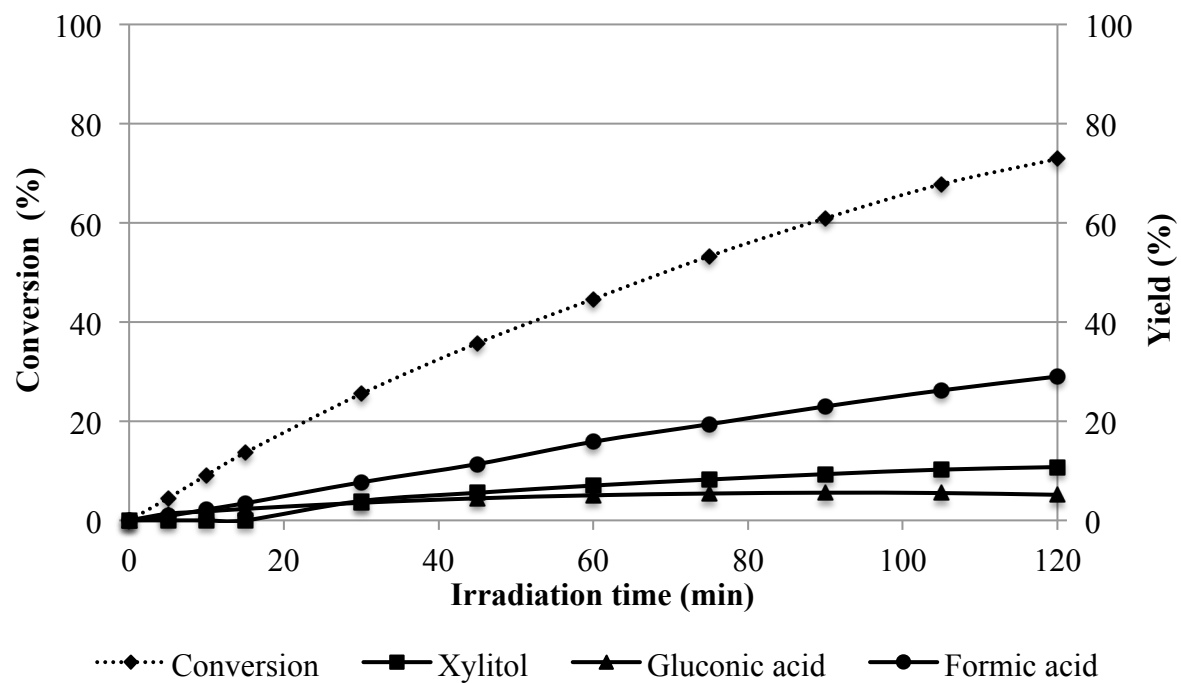
4.4.2.2. Photocatalytic conversion of glucose

The glucose conversion on the Cu-TiO₂ base catalyst was carried out for 120 min. The photocatalytic activity of pure TiO₂ and Cu-TiO₂ catalysts with metal loading content 1, 3 and 10 wt.% are shown in Fig. 4.17. The effect of Cu doped TiO₂ on maximum yields of xylitol, gluconic acid, and formic acid: 0wt.% Cu, 1wt.% Cu, 3wt.% Cu, and 10wt.% Cu doped TiO₂ are shown in Fig. 4.18. Glucose conversion of pure TiO₂, 1wt.% Cu-TiO₂, 3wt.% Cu-TiO₂, and 10wt.% Cu-TiO₂ were achieved by

64.82, 65.30, 72.87, and 82.21%, respectively after 120 min of irradiation time. Among them, 10wt.% Cu-TiO₂ achieved the highest glucose conversion. It possible concluded that the smallest band gap induced TiO₂ photocatalytic activity in term of conversion, due to small band gap facilitated yield of photogenerated electron–hole pair increased and electrons easily transferred (Rengaraj *et al*, 2006). It has been reported that Cu act as impurity state in TiO₂ nanocrystals that promoted photocatalytic activity of glucose and facilitated the photocatalytic reaction in the visible light region. Conversely, highest BET surface area (43.0 m²/g) of 3wt.% Cu-TiO₂ promoted the highest xylitol yield of 10.75% with selectivity of 14.75%. Moreover, it indicated that 10wt.% Cu-TiO₂ achieved the higher level of glucose mineralization (oxidation to other intermediate products, i.e. formic acid, CO₂, H₂O) than 3wt.% Cu-TiO₂, so, xylitol yield of 3wt.% Cu-TiO₂ was higher.

(a) pure TiO₂



(b) 1wt.% Cu-TiO₂(c) 3wt.% Cu-TiO₂

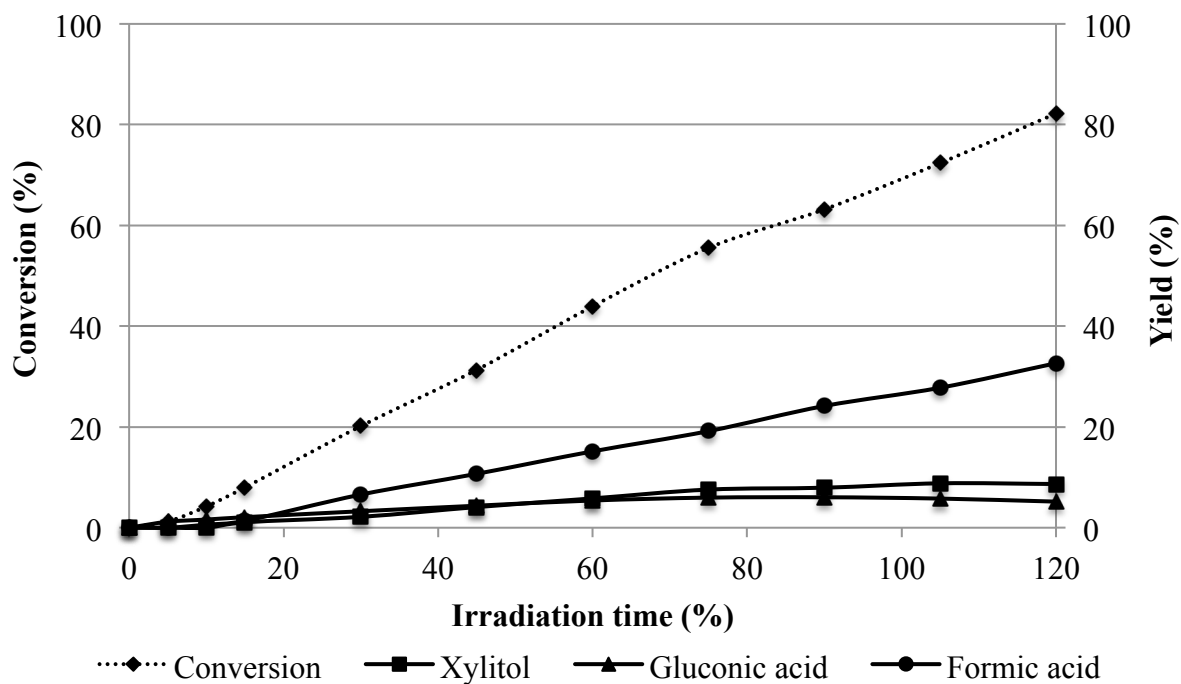
(d) 10wt.% Cu-TiO₂

Fig. 4.17 Effect of Cu doped TiO₂ on glucose conversion and yields of xylitol, gluconic acid, and formic acid after 120 min illumination: (a) pure TiO₂, (b) 1wt.% Cu-TiO₂, (c) 3wt.% Cu-TiO₂, and (d) 10wt.% Cu-TiO₂.

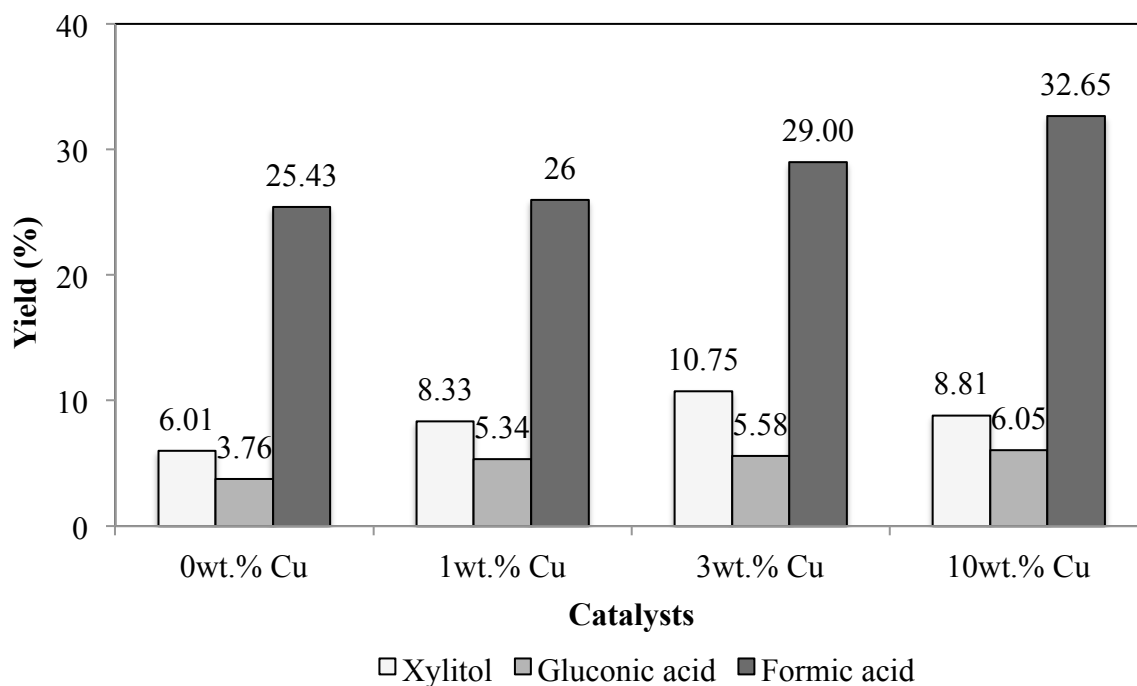


Fig. 4.18 Effect of Cu doped TiO₂ on maximum yields of xylitol, gluconic acid, and formic acid: 0wt.% Cu, 1wt.% Cu, 3wt.% Cu, and 10.wt% Cu doped TiO₂.

4.4.3. Ag and Cu Co-doped TiO₂

4.4.3.1. Photocatalyst characterization

The effects of Ag-Cu co-doped TiO₂ on the phase composition and crystallite sizes of anatase and rutile were studied. The XRD patterns 1wt.% Ag-TiO₂, 3wt.% Cu-TiO₂, and 1wt.% Ag-3wt.% Cu-TiO₂ synthesized by sol-microwave method that calcined at 500 °C for 5 h are shown in Fig. 4.19. The phase identification, crystallite size of the photocatalyst from XRD analysis and S_{BET} are shown in Table 4.8.

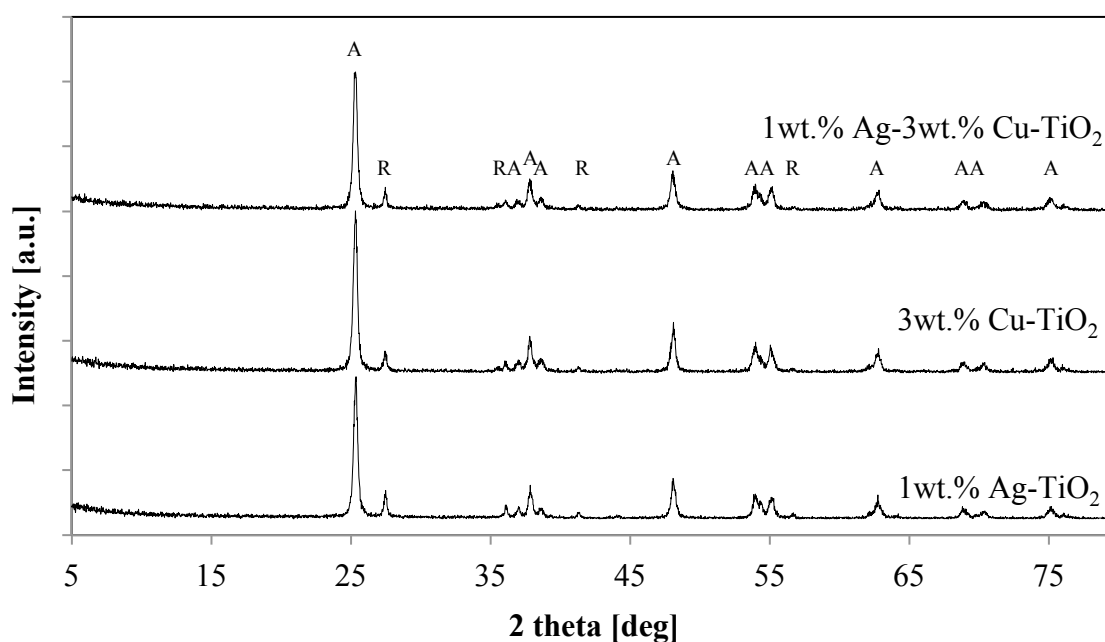


Fig. 4.19 X-ray diffraction patterns of TiO₂: 1wt.% Ag-TiO₂, 3wt.% Cu-TiO₂, and 1wt.% Ag-3wt.% Cu-TiO₂.

Table 4.8 Summary of XRD characterizations and S_{BET} of the catalysts synthesized by the sol-microwave method, calcined at 500 °C for 5 h: 1wt.% Ag-TiO₂, 3wt.% Cu-TiO₂, and 1wt.% Ag-3wt.% Cu-TiO₂.

Photocatalyst	Phase ^a (%)	Crystallite size (nm)	S _{BET} (m ² /g)
1wt.% Ag-TiO ₂	A(83)/R(17)	A(25.1)/R(129.1)	43.6
3wt.% Cu-TiO ₂	A(88)/R(12)	A(50.3)/R(103.3)	43.0
1wt.% Ag-3wt.% Cu-TiO ₂	A(87)/R(13)	A(28.7)/R(104.6)	18.7

^a A and R denote anatase and rutile, respectively.

The mixture of the anatase and rutile phases was found in all TiO₂ samples. For 1wt.% Ag-3wt.% Cu-TiO₂, no diffraction peaks of Ag₂O and CuO occurred in the XRD patterns possibly resulting from low metal loading content. In case of 3wt.% Cu-TiO₂ contained 12% of rutile phase and this phase increased to 13% when 3wt.% Cu co-doped with 1wt.% Ag-TiO₂ as shown in Table 4.8. It indicated that 1wt.% Ag didn't significantly induce the phase transformation from anatase to rutile.

Based on the XRD results, the crystallite sizes of the 1wt.% Ag-TiO₂, 3wt.% Cu-TiO₂, and 1wt.% Ag-3wt.% Cu-TiO₂ catalysts are shown in Table 4.8. The 1wt.% Ag-3wt.% Cu-TiO₂ indicated the larger anatase crystallite size than 1wt.% Ag-TiO₂. It indicated that Cu dopant induced large crystallite size of Ag-Cu co doped TiO₂. Nevertheless, the anatase crystallite size of 3wt.% Cu-TiO₂ decreased when 3wt.% Cu co-doped 1wt.% Ag-TiO₂ from 50.3 to 28.7 nm because Ag from might deposited on anatase grain boundary, which hinders the anatase crystal growth (Bokare *et al.*, 2013). Moreover co-doped 1wt.% Ag-3wt.% Cu-TiO₂ achieved the lowest BET surface area due to Ag and Cu dopant might agglomerate on TiO₂ surface cause of low BET surface area.

The effect of Ag-Cu co doping content on the absorption threshold and the band gap energy of TiO₂ were also examined with UV-Visible Diffuse Reflectance spectroscopic. The UV-visible diffuse reflectance spectra of 1wt.% Ag-TiO₂, 3wt.% Cu-TiO₂, and 1wt.% Ag-3wt.% Cu-TiO₂ are shown in Fig. 4.20. The absorption spectrum for 1wt.% Ag-3wt.% Cu-TiO₂ shifted to an energy region lower than 1wt.% Ag-TiO₂ and 3wt.% Cu-TiO₂. The red shift of the absorbance edge toward longer wavelengths of 1wt.% Ag-3wt.% Cu-TiO₂ facilitated the decrease in band gap energy of TiO₂. Accordingly, the values of E_g for 1wt.% Ag-TiO₂, 3wt.% Cu-TiO₂, and 1wt.% Ag-3wt.% Cu-TiO₂ were 2.85, 2.86, and 2.62 eV, respectively as shown in Table 4.9. It indicated that E_g values decreased when 1wt.% Ag was co-doped with 3wt.% Cu.

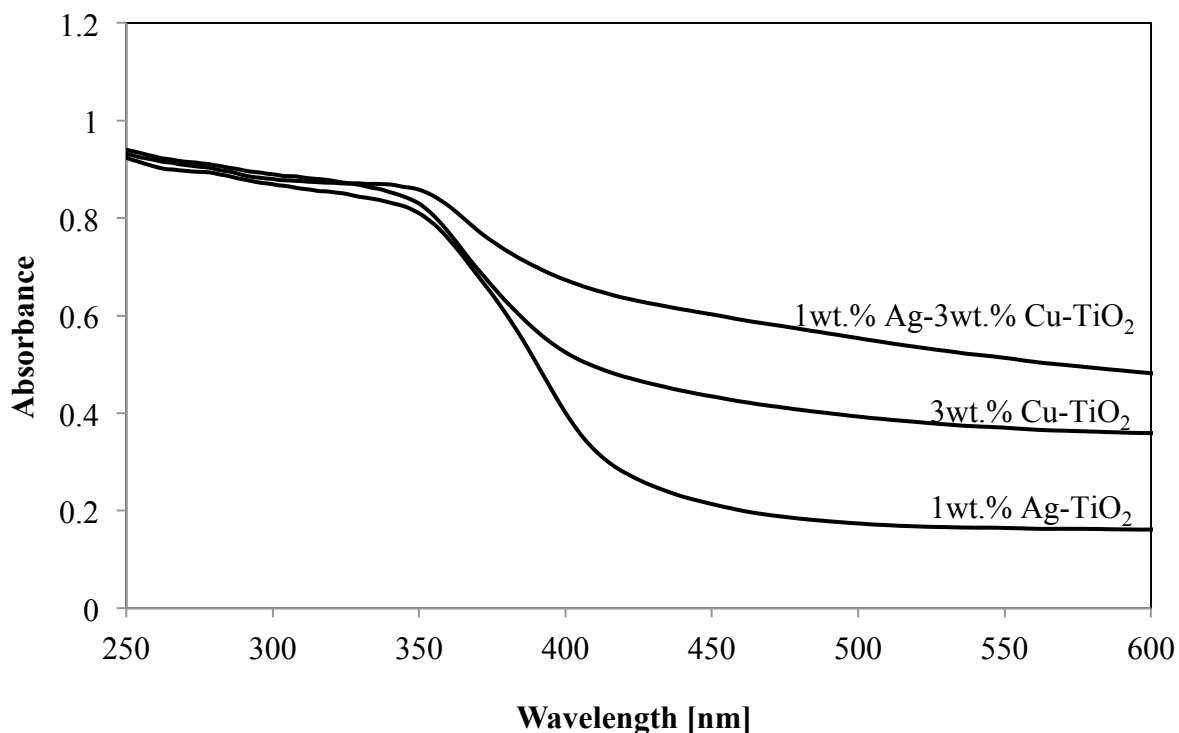


Fig. 4.20 UV–visible diffuse reflectance spectra of 1wt.% Ag-TiO₂, 3wt.% Cu-TiO₂, and 1wt.% Ag-3wt.% Cu-TiO₂.

Table 4.9 Summary of UV-vis DR characterizations of the synthesized TiO₂: 1wt.% Ag-TiO₂, 3wt.% Cu-TiO₂, and 1wt.% Ag-3wt.% Cu-TiO₂.

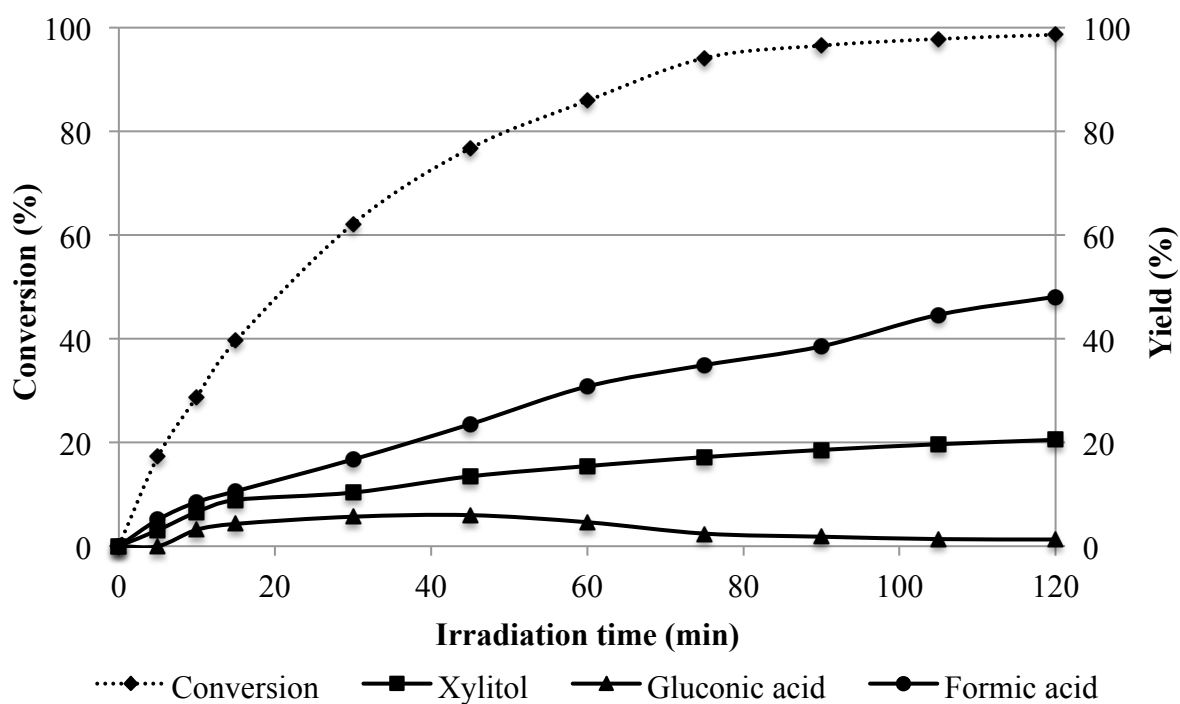
Photocatalyst	Band gap (eV)	Absorption threshold (nm)
1wt.% Ag-TiO ₂	2.85	436
3wt.% Cu-TiO ₂	2.86	435
1wt.% Ag-3wt.% Cu-TiO ₂	2.62	475

4.4.3.2 Photocatalytic conversion of glucose

The photocatalytic activity of Ag-Cu-TiO₂ compared to Ag-TiO₂ and Cu-TiO₂ catalysts are shown in Fig. 4.21. The experimental results indicated that after 120 min reaction, 3 organic compounds were produced: xylitol, gluconic acid and formic acid. It was found that glucose conversion with 1wt.% Ag-TiO₂, 3wt.% Cu-TiO₂ and 1wt.% Ag-3wt.% Cu-TiO₂ were achieved by 98.63, 72.87, and 61.85%, respectively. Among them, 1wt.% Ag-3wt.% Cu-TiO₂ achieved lowest glucose conversion. The

maximum yield of products: xylitol, gluconic acid, and formic acid are shown in Fig. 4.22. The lowest xylitol yield was obtained from 1wt.% Ag-3wt.% Cu-TiO₂ of 8.33%. This is because 1wt.% Ag-3wt.% Cu had lowest BET surface area and co-doped defected to TiO₂ lattice resulting in too many oxygen vacancies as recombination centers of electron-hole pairs, affected low photocatalytic activity. On the other hand, highest xylitol yield was obtained from 1wt.% Ag-TiO₂ of 20.51% with selectivity of 20.80%.

(a) 1wt.% Ag-TiO₂



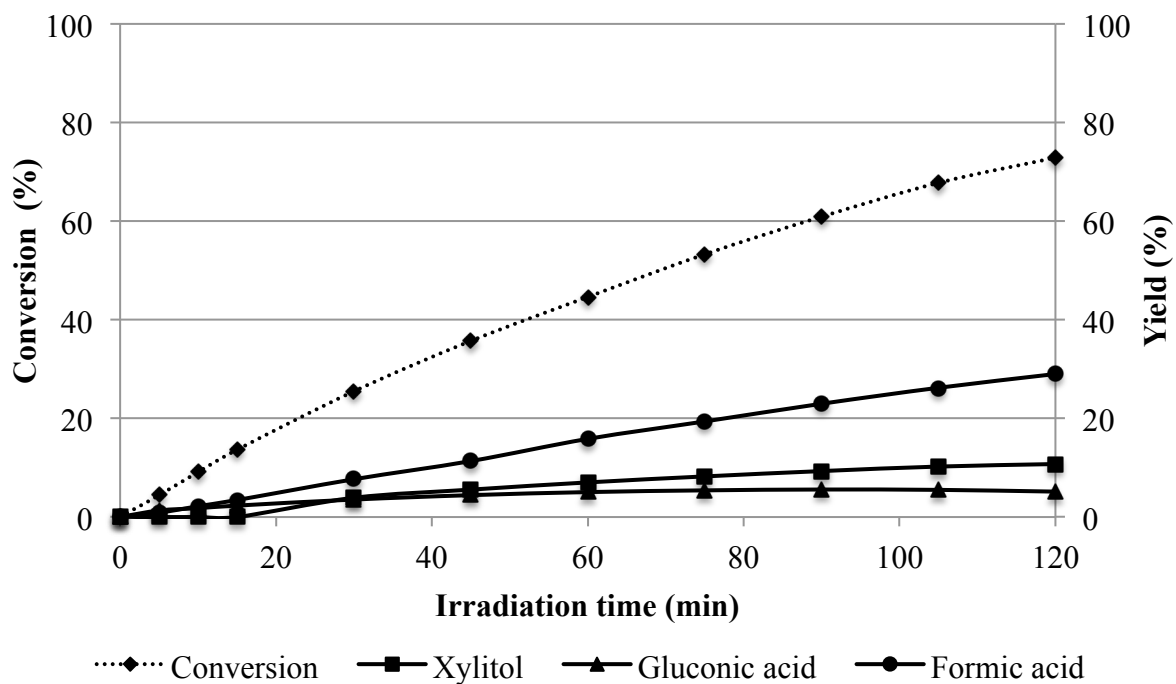
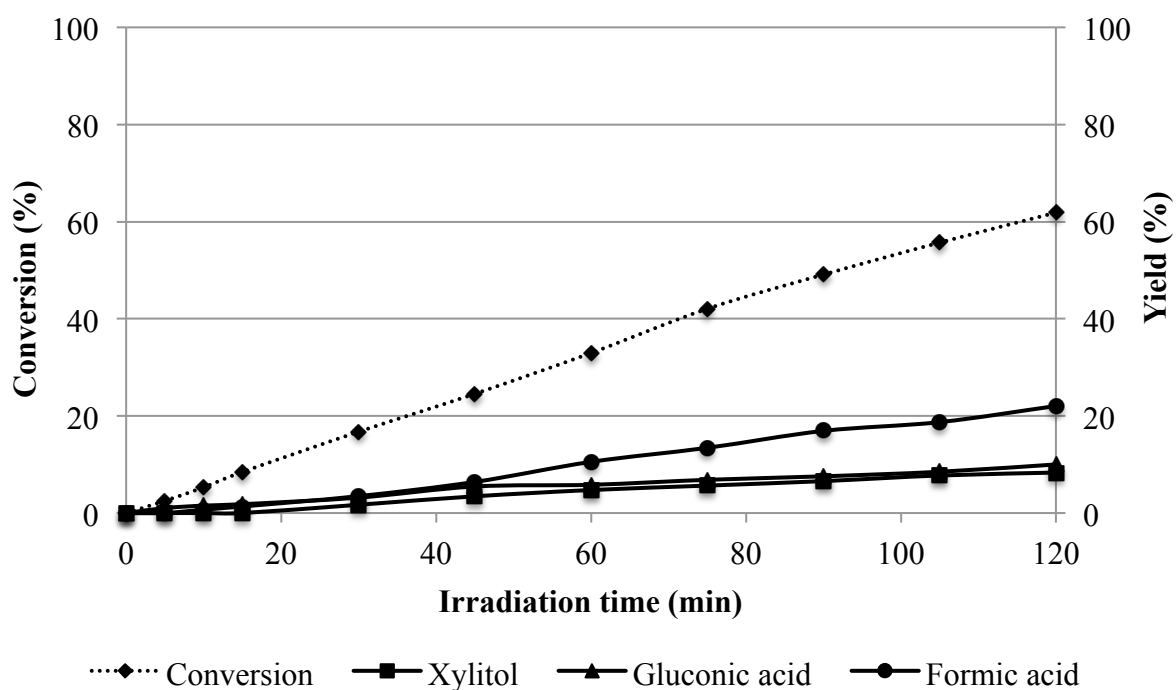
(b) 3wt.% Cu-TiO₂(c) 1wt.% Ag-3wt.% Cu-TiO₂

Fig. 4.21 Effects of Ag, Cu and Ag-Cu doped TiO₂ on glucose conversion and yields of xylitol, gluconic acid, and formic acid after 120 min illumination: (a) 1wt.% Ag-TiO₂, (b) 3wt.% Cu-TiO₂, and (c) 1wt.% Ag-3wt.% Cu-TiO₂.

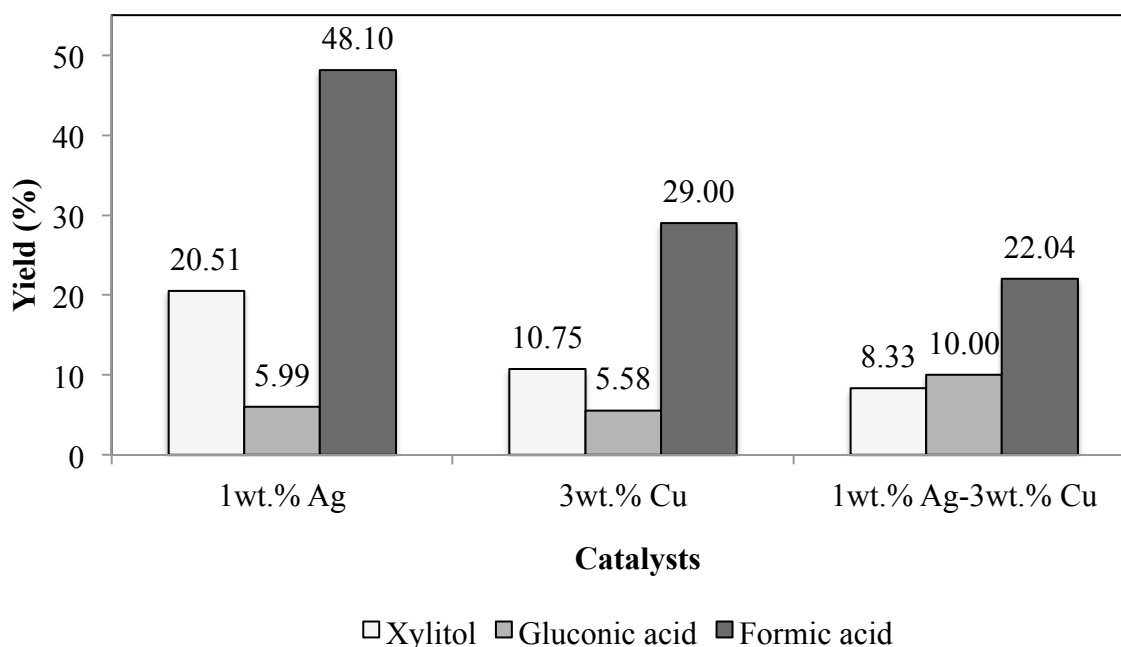


Fig. 4.22 Effects of Ag, Cu and Ag-Cu doped TiO₂ on maximum yields of xylitol, gluconic acid and formic acid: 1wt.% Ag-TiO₂, 3wt.% Cu-TiO₂, and 1wt.% Ag-3wt.% Cu-TiO₂.

4.4.4. Effect of metal doping techniques

4.4.4.1. Photocatalyst characterization

The effects of microwave assisted wet impregnation of 1wt.% Ag doped TiO₂ on the phase compositions and crystallite sizes of anatase and rutile were studied. The XRD patterns of 1wt.% Ag-TiO₂(wet impregnation) and 1wt.% Ag-TiO₂ (microwave assisted wet impregnation) synthesized by sol-microwave method that calcined at 500 °C for 5 h are shown in Fig. 4.23. The phase identification, crystallite size of the photocatalyst from XRD analysis and S_{BET} are shown in Table 4.10.

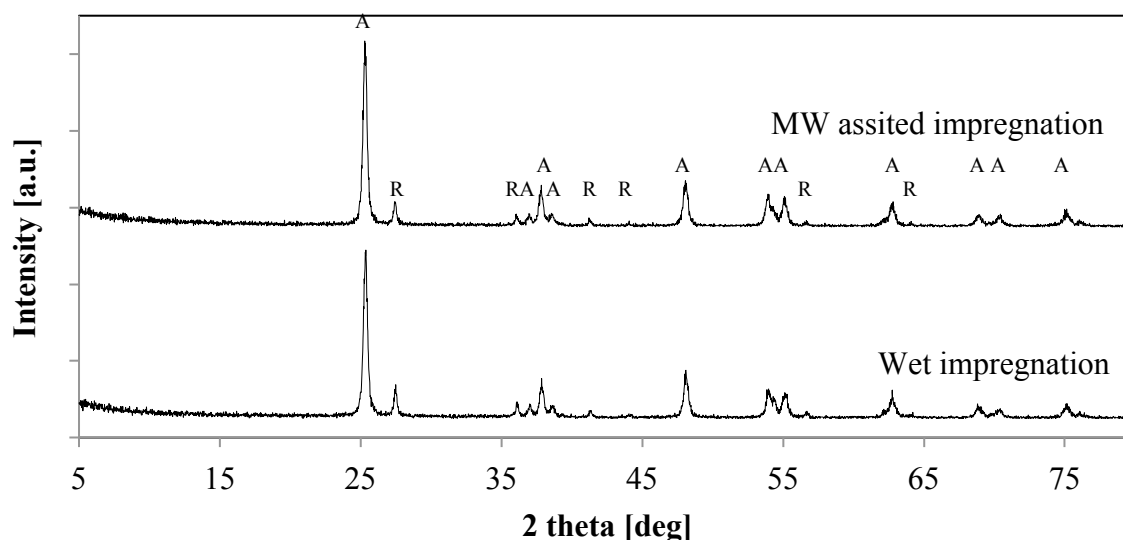


Fig. 4.23 X-ray diffraction patterns of TiO₂: 1wt.% Ag-TiO₂(wet impregnation) and 1wt.% Ag-TiO₂ (microwave assisted wet impregnation).

Table 4.10 Summary of XRD characterizations and S_{BET} of the catalysts synthesized by sol-microwave method, calcined at 500 °C for 5 h: 1wt.% Ag-TiO₂ (wet impregnation) and 1wt.% Ag-TiO₂ (microwave assisted wet impregnation).

Photocatalyst	Phase ^a (%)	Crystallite size	S_{BET} (m ² /g)
1wt.% Ag-TiO ₂ (wet impregnation)	A(83)/R(17)	A(25.1)/R(129.1)	43.6
1wt.% Ag-TiO ₂ (MW assisted wet impregnation)	A(87)/R(13)	A(50.1)/R(101.0)	20.4

^a A and R denote anatase and rutile, respectively.

The mixtures of anatase and rutile phase were found in all TiO₂ samples. In case of 1wt.% Ag-TiO₂ doped by wet impregnation contained 17% of rutile phase and this phase decreased to 13% when MW assisted wet impregnation was applied as shown in Table 4.10. It indicated that MW assisted wet impregnation retarded phase transformation from anatase to rutile.

Based on the XRD results, the crystallite sizes of 1wt.% Ag-TiO₂ (wet impregnation) and 1wt.% Ag-TiO₂ (microwave assisted wet impregnation) catalysts were

shown in Table 4.10. The anatase crystallite size of 1wt.% Ag-TiO₂ (microwave assisted wet impregnation) was larger than and 1wt.% Ag-TiO₂ (wet impregnation). It indicated that microwave assisted wet impregnation induced larger crystallite size of 1wt.% Ag-TiO₂ due to high heat of microwave irradiation promoted higher densities of defects on anatase grains, and result in larger anatase grains.

The effect of microwave assisted wet impregnation on the absorption threshold and the band gap energy of TiO₂ were also examined with UV-Visible Diffuse Reflectance spectroscopic. The UV-visible diffuse reflectance spectra of 1wt.% Ag-TiO₂ (wet impregnation) and 1wt.% Ag-TiO₂ (microwave assisted wet impregnation) are shown in Fig. 4.24. The absorption spectrum for 1wt.% Ag-TiO₂ (wet impregnation) shifted to an energy region slightly lower than 1wt.% Ag-TiO₂ (microwave assisted wet impregnation). Moreover, 1wt.% Ag-TiO₂ (microwave assisted wet impregnation) achieved the lowest BET surface area due to the high heating rate of microwave might cause of Ag aggregation during impregnation step, induced low BET surface area.

The red shift of the absorbance edge toward longer wavelengths of 1wt.%Ag-TiO₂ (wet impregnation) facilitated the decrease in band gap energy of TiO₂. Accordingly, the values of E_g for 1wt% Ag-TiO₂ (wet impregnation) and 1wt.%Ag-TiO₂ (microwave assisted wet impregnation) were 2.85 and 2.92 eV, respectively as shown in Table 4.11. It indicated that microwave assisted wet impregnation did not promote the decrease of E_g values.

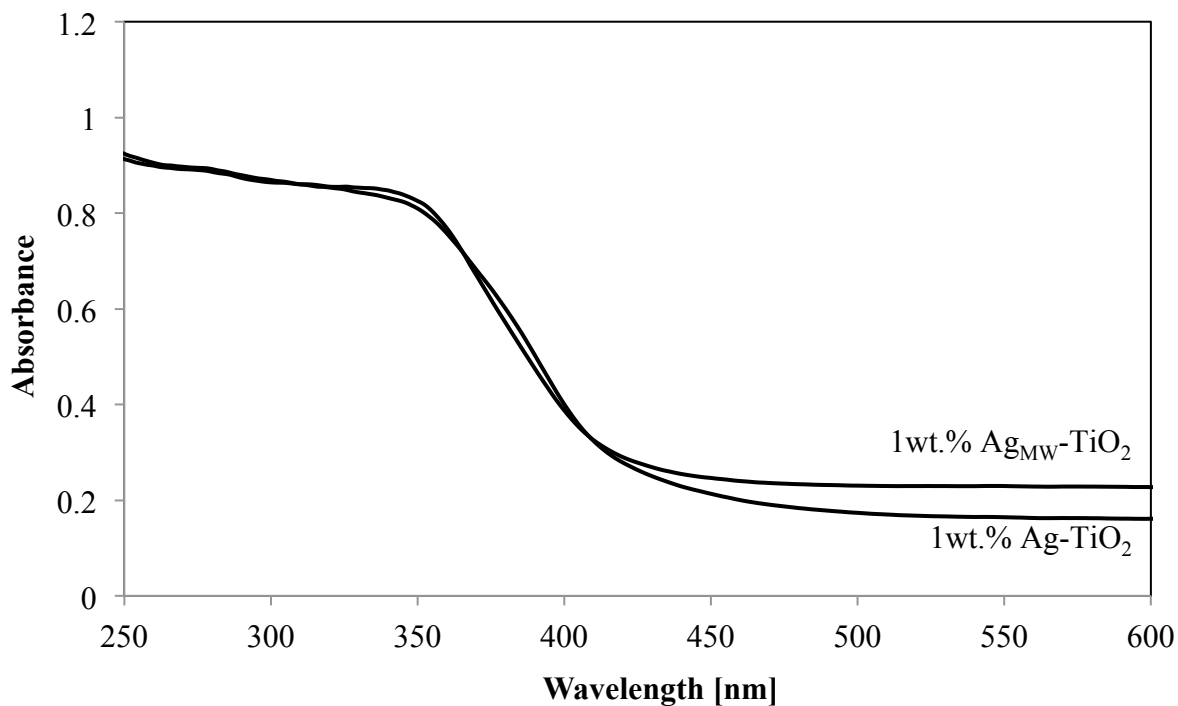


Fig. 4.24 UV–visible diffuse reflectance spectra of 1wt.% Ag-TiO₂(wet impregnation) and 1wt.% Ag-TiO₂ (microwave assisted wet impregnation).

Table 4.11 Summary of UV-vis DR characterizations of the synthesized TiO₂: 1wt.% Ag-TiO₂ (wet impregnation) and 1wt.% Ag-TiO₂ (microwave assisted wet impregnation).

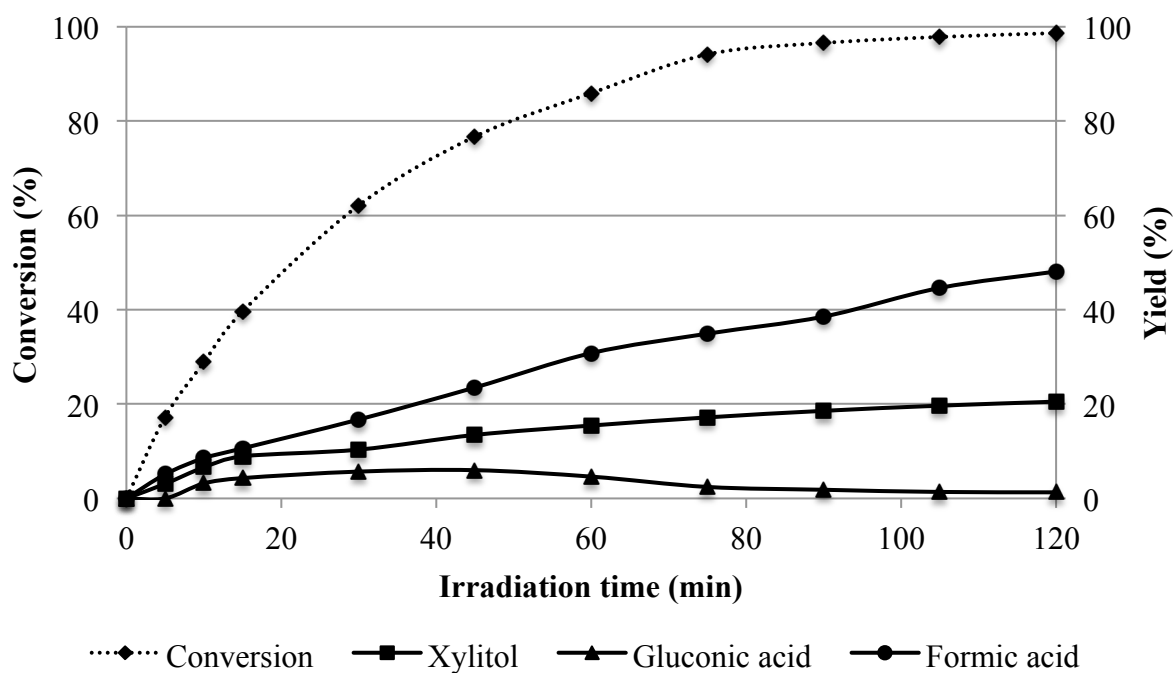
Photocatalyst	Band gap (eV)	Absorption threshold (nm)
1wt.% Ag-TiO ₂ (wet impregnation)	2.85	436
1wt.% Ag-TiO ₂ (MW assisted wet impregnation)	2.92	425

4.4.4.2. Photocatalytic conversion of glucose

The photocatalytic activity of 1wt.% Ag-TiO₂ (wet impregnation) and 1wt.% Ag-TiO₂ (microwave assisted wet impregnation) are shown in Fig. 4.25. The effect of Cu photocatalysts on maximum yields of xylitol, gluconic acid and formic acid: 1wt.% Ag-TiO₂ (wet impregnation) and 1wt.% Ag-TiO₂ (microwave assisted wet impregnation) are shown in Fig. 4.26. Three organic compounds were produced: xylitol, gluconic acid and formic acid after 120 min. It was found that glucose conversion with

1wt.% Ag-TiO₂ (wet impregnation) and 1wt.% Ag-TiO₂ (microwave assisted wet impregnation) were achieved by 98.63 and 95.07%, respectively, after 120 min reaction. The highest yield of xylitol and formic acid of 20.51% and 48.10%, respectively, (20.80% and 48.76% selectivity of xylitol and formic acid, respectively) were obtained from 1wt.% Ag-TiO₂ (wet impregnation). It indicated that 1wt.% Ag-TiO₂ under microwave assisted wet impregnation of could not promote greater photocatalytic activity because microwave irradiation caused low S_{BET}, and might have caused too many oxygen vacancies as the recombination centers of electron-hole pairs, resulting in low photocatalytic activity.

(a) 1wt.% Ag-TiO₂ (wet impregnation)



(b) 1wt.% Ag-TiO₂ (microwave assisted wet impregnation)

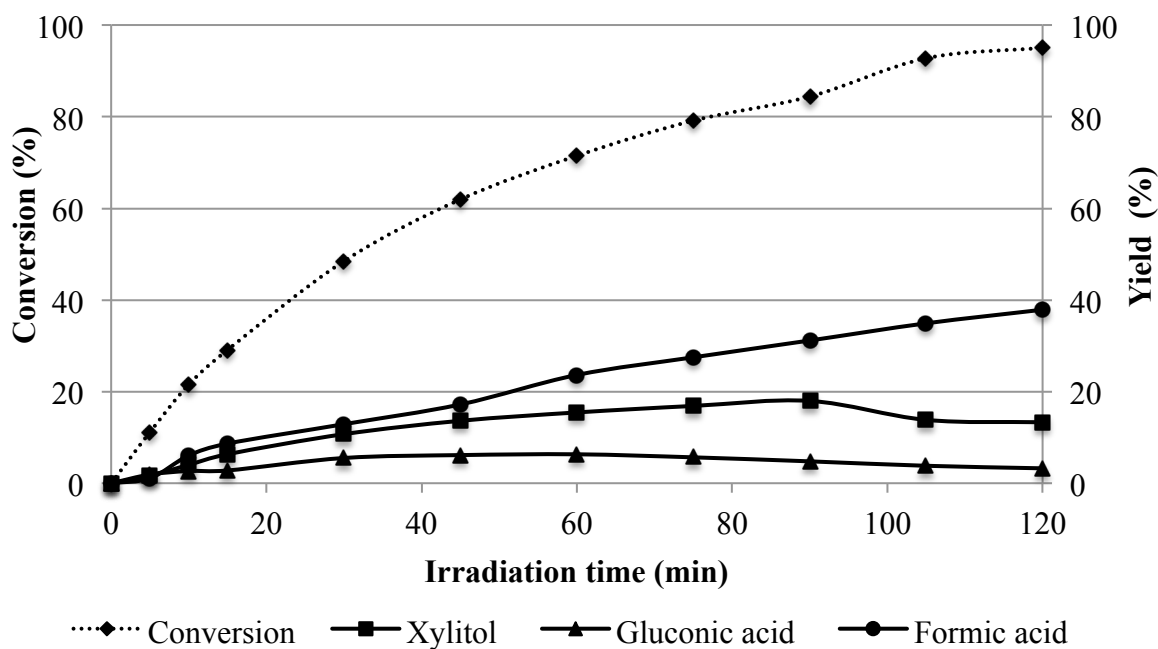


Fig. 4.25 Effect of microwave assisted wet impregnation of Ag doped TiO₂ on maximum yields of xylitol, gluconic acid and formic acid: (a) 1wt.% Ag-TiO₂ (wet impregnation) (b) 1wt.% Ag-TiO₂ (microwave assisted wet impregnation).

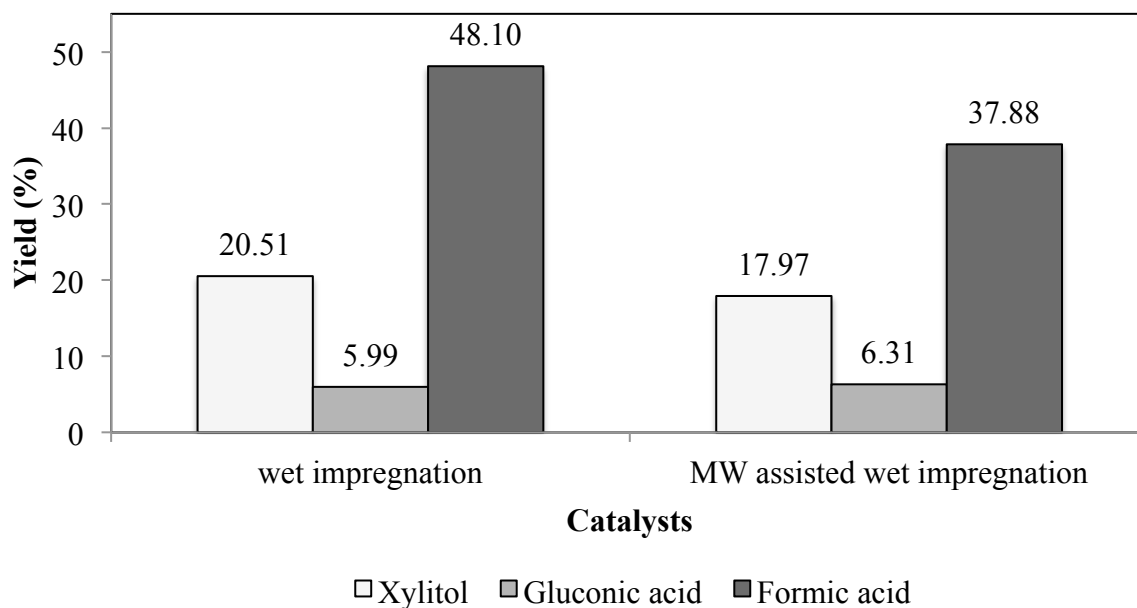


Fig. 4.26 Effect of microwave assisted wet impregnation of TiO₂ on maximum yields of xylitol, gluconic acid and formic acid: 1wt.% Ag-TiO₂ (wet impregnation) and 1wt.% Ag-TiO₂ (microwave assisted wet impregnation).

CHAPTER 4

CONCLUSION

In this thesis, several TiO₂ catalysts were fabricated. They were characterized by XRD, SEM, BET and UV–vis and their photocatalytic activities were tested for the conversion of glucose to produce high value chemicals (xylitol, gluconic acid, and formic acid). The results are summarized as follows:

1. TiO₂ can be successfully synthesized by sol-gel, ultrasonic assisted sol-gel and sol-microwave (MW) methods (calcined at 500 °C for 5 h). Among them, the smallest particle size (400 nm), the highest S_{BET} (24.3 m²/g) and suitable mixed phase (anatase and rutile in ratio of 86:14) were obtained from TiO₂(MW). The highest glucose conversion of 64.82% and the highest xylitol, gluconic acid, and formic acid yields of 6.01, 3.76, and 25.43%, respectively, were obtained from TiO₂(MW).

2. TiO₂(MW) was calcined at various temperatures (400 °C, 500 °C, 600 °C) and the effect of the calcination time between 2 h and 5 h on TiO₂(MW) was also investigated. Among them, TiO₂(MW) calcined at 500 °C for 5 h provided the highest photocatalytic activity. Due to their small anatase crystallite size (25.1 nm), high crystallinity and appropriate anatase-rutile ratio (86:14) promoted to greater photocatalytic activity.

3. Ag-TiO₂, Cu-TiO₂, and Ag-Cu-TiO₂ photocatalysts were synthesized. Among them, the highest glucose conversion of 98.63%, the highest xylitol, gluconic acid and formic acid yields of 20.51, 5.99, and 48.10%, respectively, were obtained from 1wt.% Ag-TiO₂. 1wt.% Ag-TiO₂ provided the smallest anatase crystallite size (25.1 nm), the highest S_{BET} (43.6 m²/g), relatively small band gap (2.85 eV) and mix phase of anatase-rutile (83:17). These good characteristics of 1wt.% Ag-TiO₂ promoted the highest photocatalytic activity.

4. The effect of microwave assisted wet impregnation of 1wt.% Ag-TiO₂ was studied. The 95.07% of glucose conversion, as well as 17.97, 6.31, and 37.88% of xylitol, gluconic acid, and formic acid respectively were obtained from 1wt.% Ag-TiO₂ under microwave assisted wet impregnation. It was found that microwave irradiation did not promote greater photocatalytic activity because it achieved large anatase crystallite size (50.1 nm) and lowest S_{BET} (20.4 m²/g), resulting in low photocatalytic activity.

RECOMMENDATIONS

1. According to the results obtained from high-performance liquid chromatography (HPLC), three unknown products still cannot be identified, so these products should be examined by liquid chromatography tandem-mass spectrometry (LC-MS/MS).

2. For the metal ion doped TiO_2 , it should be determined by scanning electron microscopy with energy dispersive X-ray spectroscopy (SEM/EDX), X-ray photoelectron spectroscopy (XPS), inductively coupled plasma (ICP) spectroscopy, and atomic absorption spectroscopy (AA) to confirm the metal doping results.

3. In the case of metal-doped TiO_2 , the reaction time should be longer than 120 min, because the trend of product yields continually increased.

4. The morphology of the photocatalyst, should be examined by transmission electron microscopy (TEM).

5. To improve activity of photocatalyst, the supports (i.e. zeolite and silica) should be used. More experiments on this issue should be conducted.

6. The heating rate and radiation time of the microwaves should be studied.

7. To increase the yield of xylitol (the highest value chemical compared with others) should be increased, the solvent composition of acetonitrile and distilled water should be further studied.

REFERENCES

- Aramendia, M.A., Marinas, A., Colmenares, J.C., Marinas, J.M., Urbano, F.J., 2006, "Synthesis, characterization and photocatalytic activity of different metal-doped titania systems", **Applied Catalysis A: General**, Vol. 306, pp. 120–127.
- Bokare, A., Sanap, A., Pai, M., Sabharwal, S., Athawale, A.A., 2013, "Antibacterial activities of Nd doped and Ag coated TiO₂ nanoparticles under solar light irradiation", **Colloids and Surfaces B: Biointerfaces**, Vol. 102, pp. 273–280.
- Bridgwater, A.V., 2012, "Review of fast pyrolysis of biomass and product upgrading", **Biomass and Bioenergy**, Vol. 38, pp. 68–94.
- Cao, L., Gao, Z., Suib, S.L., Obee, T.N., Hay, S.O., Freihaut, J.D., 2000, "Photocatalytic oxidation of toluene on nanoscale TiO₂ catalysts: Studies of deactivation and regeneration", **J. Catal.**, Vol. 196, pp. 253–261.
- Chang, S.M., Liu, W.S., 2014, "The roles of surface-doped metal ions (V, Mn, Fe, Cu, Ce, and W) in the interfacial behavior of TiO₂ photocatalysts", **Applied Catalysis B: Environmental**, Vol. 156–157, pp. 466–475.
- Chaudhary, V., Srivastava, A.K., Kumar, J., 2011, "On the Sol-gel Synthesis and Characterization of Titanium Oxide Nanoparticles", **Materials Research Society**, Vol. 1352.
- Chen, J., 1997, "Advanced oxidation technologies photocatalytic treatment of waste water", Thesis with acknowledgement in China.
- Chen, X., Mao, S.S., 2007, "Titanium dioxide nano-materials: Synthesis, Properties, Modifications, and Applications", **Chem. Rev**, Vol. 107, pp. 2891-2959.
- Cheng, G., Akhtar, M.S., Yang, O.B., Stadler, F.J., 2013, "Structure modification of anatase TiO₂ nanomaterials-based photoanodes for efficient dye-sensitized solar cells", **Electrochimica acta**, Vol. 113, pp. 527-535.

- Chong, M.N., Jin, B., Chow, C.W.K., Saint, C., 2010, "Recent developments in photocatalytic water treatment technology: A review", **Water Research**, Vol. 44, pp. 2997-3027.
- Colmenares, J.C., Luque, R., Campelo, J.M., Colmenares, F., Karpiński, Z., Romero, A.A., 2009, "Nanostructured photocatalysts and their applications in the photocatalytic transformation of lignocellulosic biomass: An Overview", **Materials**, Vol. 2, pp. 2228-2258.
- Colmenares, J.C., Magdziarz, A., Bielejewska, A., 2011, "High-value chemicals obtained from selective photo-oxidation of glucose in the presence of nanostructured titanium photocatalysts", **Bioresource Technology**, Vol. 102, pp. 11254–11257.
- Devi, L.G., Kottam, N., Murthy, B.N., Kumar, S.G., 2010, "Enhanced photocatalytic activity of transition metal ions Mn^{2+} , Ni^{2+} and Zn^{2+} doped polycrystalline titania for the degradation of Aniline Blue under UV/solar light", **Journal of molecular catalysis A: Chemical**, Vol. 328, pp. 44–52.
- Erkiaga, A., Lopez, G., Amutio, M., Bilbao, J., Olazar, M., 2013, "Influence of operating conditions on the steam gasification of biomass in a conical spouted bed reactor", **Chemical engineering journal**, Vol. 237, pp. 259-267.
- Esquivel, K., Nava, R., Méndez, A.Z., González, M.V., Acuna, O.E.J., Alarcón, L.E., Hernández, J.M.P., Pawelec, B., Fierro, J.L.G., 2013, "Microwave-assisted synthesis of (S)Fe/TiO₂ systems: Effects of synthesis conditions and dopant concentration on photoactivity", **Applied Catalysis B: Environmental**, Vol. 140–141, pp. 213–224.
- Francisco, M.S.P., Mastelaro, V.R., 2002, "Inhibition of the Anatase-Rutile Phase Transformation with Addition of CeO₂ to CuO-TiO₂ System: Raman Spectroscopy, X-ray Diffraction, and Textural Studies", **Chem. Mater.**, Vol. 14, pp. 2514-2518.
- Fua, X., Longa, J., Wanga, X., Leungb, D.Y.C., Dinga, Z., Wua, L., Zhanga, Z., Lia, Z., 2008, "Photocatalytic reforming of biomass: A systematic study of hydrogen evolution from glucose solution", **International Journal of Hydrogen Energy**, Vol. 33, pp. 6484–6491.

- Gao, Y., Wang, H., Wu, J., Zhao, R., Lu, Y., Xin, B., 2014, "Controlled facile synthesis and photocatalytic activity of ultrafine high crystallinity TiO₂ nanocrystals with tunable anatase/rutile ratios", **Applied Surface Science**, Vol. 294, pp. 36–41.
- Gibson, H.W., 1969, "The Chemistry Of Formic Acid and its Simple Derivatives", Chemicals and Plastics Division, Union Carbide Corporation, Tarrytown, New York.
- Gomathisankar, P., Yamamoto, D., Katsumata, H., Suzuki, T., Kaneco, S., 2013, "Photocatalytic hydrogen production with aid of simultaneous metal deposition using titanium dioxide from aqueous glucose solution", **International Journal of Hydrogen Energy**, Vol. 38, pp. 5517-5524.
- Hanaor, D.A.H., Sorrell, C.C., 2011, "Review of the anatase to rutile phase transformation", **J Mater Sci.**, Vol. 46, pp. 855–874.
- Hwang, K.J., Lee, J.W., Shim, W.G., Jang, H.D., Lee, S.I., Yoo, S.J., 2012, "Adsorption and photocatalysis of nanocrystalline TiO₂ particles prepared by sol–gel method for methylene blue degradation", **Advance Powder Technology**, Vol. 23, pp. 414–418.
- Jitputti, J., Pavasupree, S., Suzuki, Y., Yoshikawa, S., 2007, "Synthesis and photocatalytic activity for water-splitting reaction of nanocrystalline mesoporous titania prepared by hydrothermal method", **Journal of Solid State Chemistry**, Vol. 180, pp.1743–1749
- Kobayashi, H., Komanoya, T., Guha, S.K., Hara, K., Fukuoka, A., 2011, "Conversion of cellulose into renewable chemicals by supported metal catalysis", **Applied Catalyst A: General**, Vol. 409-410, pp. 13–20.
- Latt, K.K., Kobayashi, T., 2008, "TiO₂ nanosized powders controlling by ultrasound sol–gel reaction", **Ultrasonics Sonochemistry**, Vol. 15, pp. 484–491.
- Li, L., Zhang, X., Zhang, W., Wang, L., Chen, X., Gao, Y., 2014, "Microwave-assisted synthesis of nanocomposite Ag/ZnO–TiO₂ and photocatalytic degradation Rhodamine B with different modes", **Colloids and Surfaces A: Physicochem. Eng. Aspects**, Vol. 457, pp. 134–141.

- Li, X., Wang, L., Lu, X., 2010, "Preparation of silver-modified TiO₂ via microwave-assisted method and its photocatalytic activity for toluene degradation", **Journal of Hazardous Materials**, Vol. 177, pp. 639–647.
- Li, Y., Wang, J., Peng, S., Lu, G., Li, S., 2010, "Photocatalytic hydrogen generation in the presence of glucose over ZnS-coated ZnIn₂S₄ under visible light irradiation", **Int J Hydrogen Energy**, Vol. 35, pp. 7116-7126.
- Lopez, R., Gomez, R., Llanos, M.E., 2009, "Photophysical and photocatalytic properties of nanosized copper-doped titania sol-gel catalysts", **Catalysis Today**, Vol. 148, pp. 103–108.
- Mohan, D., Pittman, C.U., Steele, P.H., 2006, "Pyrolysis of wood/biomass for bio-oil: A critical review", **Energy Fuel**, Vol. 20, pp. 848-889.
- Moziak, S., Heciak, A., Morawski, A.W., 2011, "Photocatalytic acetic acid decomposition leading to the production of hydrocarbons and hydrogen on Fe-modified TiO₂", **Catalysis Today**, Vol. 161, pp. 189–195.
- Murugan, K., Subasri, R., Rao, T.N., Gandhi, A.S., Murty, B.S., 2013, "Synthesis, characterization and demonstration of self-cleaning TiO₂ coatings on glass and glazed ceramic tiles", **Progress in Organic Coatings**, Vol. 76, pp. 1756-1760.
- Nakata, K., Fujishima, K., 2012, "TiO₂ photocatalysis: Design and applications", **Journal of Photochemistry and Photobiology C: Photochemistry Reviews**, Vol. 13, pp. 169–189.
- Nasralla, N., Yeganeh, M., Astuti, Y., Piticharoenphuna, S., Shahtahmasebi, N., Kompany, A., Karimipour, M., Mendis, B.G., Poolton, N.R.J., Siller, L., 2013, "Structural and spectroscopic study of Fe-doped TiO₂ nanoparticles prepared by sol-gel method", **Scientia Iranica**, Vol. 20, pp. 1018-1022.
- Park, J.Y., Yun, J.J., Hwang, C.H., Lee, I.H., 2010, "Influence of silver doping on the phase transformation and crystallite growth of electrospun TiO₂ nanofibers", **Materials Letters**, Vol. 64, pp. 2692–2695.

- Patel, R.N., Bandyopadhyay, S., Ganesh, A., 2011, “A simple model for super critical fluid extraction of bio oils from biomass”, **Energy Conversion and Management**, Vol. 52, pp. 652–657.
- Pelaeza, M., Nolanb, N.T., Pillai, S.C., Seery, M.K., Falaras, P., Kontos, A.G., Dunlop, P.S.M., Hamilton, J.W.J., Byrne, J.A., O’Sheaf, K., Entezari, M.H., Dionysiou, D.D., 2012, “A review on the visible light active titanium dioxide photocatalysts for environmental applications”, **Applied Catalysis B: Environmental**, Vol. 125, pp. 331–349.
- Pham, T.D., Lee, B.K., 2014, “Cu doped TiO₂/GF for photocatalytic disinfection of Escherichia coli in bioaerosols under visible light irradiation: Application and mechanism”, **Applied Surface Science**, Vol. 296, pp. 15–23.
- Ramachandran, S., Fontanille, P., Pandey, A., Larroche, C., 2006, “Gluconic Acid: Properties, Applications and Microbial Production”, Vol. 44, pp. 185–195.
- Rengaraj, S., Li, X.Z., 2006, “Enhanced photocatalytic activity of TiO₂ by doping with Ag for degradation of 2,4,6-trichlorophenol in aqueous suspension”, **Journal of Molecular Catalysis A: Chemical**, Vol. 243, pp. 60–67.
- Shojaie, A.F., Loghmani, M.H., 2010, “La³⁺ and Zr⁴⁺ co-doped anatase nano TiO₂ by sol-microwave”, **Chemical Engineering Journal**, Vol. 157, pp. 263–269.
- Su, C., Hong, B.-Y., Tseng, C.-M., 2004, “Sol–gel preparation and photocatalysis of titanium dioxide”, **Catalysis today**, Vol. 96, pp. 119–126.
- Sun, T., Fan, Jun F., Liu, E., Liu, L., Wang, Y., Dai, H., Yang, Y., Hou, W., Hu, X., Jiang, Z., 2012, “Fe and Ni co-doped TiO₂ nanoparticles prepared by alcohol-thermal method: Application in hydrogen evolution by water splitting under visible light irradiation”, **Powder Technology**, Vol. 228, pp. 210–218.
- Sun, T., Liu, E., Fan, J., Hub, X., Wua, F., Hou, W., Yang, Y., Kang, L., 2013, “High photocatalytic activity of hydrogen production from water over Fe doped and Ag deposited anatase TiO₂ catalyst synthesized by solvothermal method”, **Chemical Engineering Journal**, Vol. 228, pp. 896–906.

- Tan, Y.N., Wong, C.L., Mohamed, A.R., 2011, "An Overview on the Photocatalytic Activity of Nano-Doped-TiO₂ in the Degradation of Organic Pollutants", **International Scholarly Research Network**, Vol. 2011, Article ID 261219.
- Tseng, T.K., Lin, Y.S., Chen, Y.J., Chu, H., 2010, "A review of photocatalysts prepared by sol-gel method for VOCs removal", **Int. J. Mol. Sci.**, Vol. 11, pp. 2336-2361.
- Wang, S., Yang, X.J., Jiang, Q., Lian, J.S., 2014, "Enhanced optical absorption and photocatalytic activity of Cu/N-codopedTiO₂ nano crystals", **Materials Science in Semiconductor Processing**, Vol. 24, pp. 247–253.
- Werpy, T., Pedersen, G., 2004, "Top value chemicals from biomass. vol. 1. Results of screening for potential candidates from sugars and synthesis gas", US Department of energy report.
- Wu, T.Y., Guo, N., Teh, C.Y., Hey, Y.X.W., 2013, "Handbook on Theory and Fundamentals of Ultrasound: Chapter 2", pp. 5-12.
- Yu, J., Wang, G., Cheng, B., Zhou, M., 2007, "Effects of hydrothermal temperature and time on the photocatalytic activity and microstructures of bimodal mesoporous TiO₂ powders", **Applied Catalysis B: Environmental**, Vol. 69, pp. 171–180.
- Zaleska, A., 2008, "Doped-TiO₂: A Review", **Recent Patents on Engineering**, Vol. 2, pp. 157-164.
- Zmudzinski, W., 2010, "Preliminary results of glucose oxidation by photocatalysis on TiO₂ primary intermediates", **Physicochem. Probl. Miner. Process.**, Vol. 45, pp. 141-151.

APPENDIX

A. Calculation of Crystallite Size and Phase Composition

The crystallite size was calculated by Sherrer's equation as shown in Equation A1:

$$d = \frac{k\lambda}{\beta \cos \theta_B} \quad \dots(A1)$$

where d is the crystallite size (nm)

k is the Sherrer constant that value is 0.89

λ is the X-ray wavelength (0.15418 nm for $\text{CuK}\alpha$)

β is the full width at half maximum intensity (FWHM) (radians)

θ_B is the Bragg angle at the position at the peak maximum

The anatase and rutile contents were calculated by Spurr-Myers's equation:

$$w_A = \frac{1}{(1 + 1.26 \frac{I_R}{I_A})} \quad \dots(A2)$$

$$w_R = 1 - w_A \quad \dots(A3)$$

where w_A is weight fraction of anatase in the mixture

w_R is weight fraction of rutile in the mixture

I_A is the intensity of anatase diffraction peak (101)

I_R is the intensity of rutile diffraction peak (110)

B. Calculation of Band Gap Energy

The band gap energy was calculated with Equation B1:

$$E_g = \frac{hc}{\lambda} \quad \dots(B1)$$

where E_g is the band gap energy

h is the Planks constant (6.626×10^{-34} Joules sec)

c is the speed of light (3.0×10^8 meter/sec)

λ is the cut off wavelength

1 eV is equal 1.6×10^{-19} Joules (conversion factor)

C. Calculation of Conversion, Yield and Selectivity

The formulas of conversion, yield and selectivity:

$$\text{Conversion} = \frac{\text{The amount of reactant consumed}}{\text{The amount of reactant in}}$$

$$\text{Yield} = \frac{\text{The amount of product produced}}{\text{The maximum amount of product would be produced}}$$

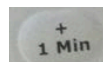
$$\text{Selectivity} = \frac{\text{The amount of product i}}{\text{The total amount of products}}$$

D. Domestic Microwave (Whirlpool AMW 585) for TiO₂(MW) Synthesis Manual



Fig. D1 Domestic microwave (Whirlpool AMW 585)

1. Place the sample into the microwave and close the door.
2. Turn the adjusting knob to set the synthesis time (4 min).
3. Turn the adjusting knob to set power (level 3).
4. Finally, press the start button.



E. Results of HPLC Analysis

Table E1 Results obtained for photocatalytic reaction of glucose with TiO₂ (synthesized by sol-gel method, calcined at 500 °C for 5 h) catalyst in terms of glucose conversion, yield and selectivity to organic compounds: gluconic acid and formic acid.

Time (min)	Glucose		Xylitol			Gluconic acid			Formic acid		
	Peak area	Conversion (%)	Peak area	Yield (%)	Selectivity (%)	Peak area	Yield (%)	Selectivity (%)	Peak area	Yield (%)	Selectivity (%)
0	308716.10	0	0.00	0.00	0.00	0	0	0	0.00	0.00	0
5	305660.50	1.15	0.00	0.00	0.00	677.90	0.89	77.66	0.00	0.00	0
10	306317.60	1.19	0.00	0.00	0.00	1743.10	1.00	83.91	0.00	0.00	0
15	306833.40	1.24	0.00	0.00	0.00	1458.50	0.97	78.29	0.00	0.00	0
30	304055.20	1.51	0.00	0.00	0.00	4965.60	1.33	88.06	0.00	0.00	0
45	301441.20	2.35	0.00	0.00	0.00	7038.50	1.54	65.34	5994.70	0.01	0.52
60	301592.40	2.31	0.00	0.00	0.00	7734.80	1.61	69.79	7939.00	0.11	4.81
75	298377.20	3.35	0.00	0.00	0.00	9808.80	1.82	54.37	15477.30	0.49	14.73
90	291476.60	5.58	0.00	0.00	0.00	12373.80	2.08	37.27	20024.10	0.72	12.96
105	295257.00	4.36	0.00	0.00	0.00	12870.30	2.13	48.89	24199.00	0.93	21.46
120	292130.90	5.37	0.00	0.00	0.00	13610.20	2.20	41.07	29108.00	1.18	22.05

Table E2 Results obtained for photocatalytic reaction of glucose with TiO₂ (synthesized by ultrasonic assisted sol-gel method, calcined at 500 °C for 5 h) catalyst in terms of glucose conversion, yield and selectivity to organic compounds: gluconic acid and formic acid.

Time (min)	Glucose		Xylitol			Gluconic acid			Formic acid		
	Peak area	Conversion (%)	Peak area	Yield (%)	Selectivity (%)	Peak area	Yield (%)	Selectivity (%)	Peak area	Yield (%)	Selectivity (%)
0	313127.30	0.00	0.00	0.00	0.00	0.00	0.00	0.00	0.00	0.00	0.00
5	301720.20	3.64	0.00	0.00	0.00	1395.20	0.95	26.18	0.00	0.00	0.00
10	301067.60	3.85	0.00	0.00	0.00	2036.60	1.02	26.43	8680.20	0.15	3.80
15	299516.30	4.34	0.00	0.00	0.00	3612.80	1.17	27.04	12123.50	0.32	7.33
30	299482.90	4.35	0.00	0.00	0.00	5008.20	1.31	30.18	13843.50	0.40	9.29
45	295928.60	5.49	0.00	0.00	0.00	7447.00	1.56	28.38	21131.10	0.77	14.00
60	293427.10	6.28	0.00	0.00	0.00	9081.70	1.72	27.38	25336.30	0.98	15.57
75	293182.20	6.36	0.00	0.00	0.00	10636.70	1.88	29.48	39353.30	1.68	26.38
90	285165.60	8.92	0.00	0.00	0.00	11804.80	1.99	22.34	40651.20	1.74	19.54
105	284384.40	9.17	0.00	0.00	0.00	14491.30	2.26	24.66	50834.00	2.25	24.56
120	275781.10	11.91	0.00	0.00	0.00	15134.60	2.33	19.52	60465.30	2.73	22.94

Table E3 Results obtained for photocatalytic reaction of glucose with TiO₂ (synthesized by sol-microwave method, calcined at 500 °C for 5 h) catalyst in terms of glucose conversion, yield and selectivity to organic compounds: xylitol, gluconic acid and formic acid.

Time (min)	Glucose		Xylitol			Gluconic acid			Formic acid		
	Peak area	Conversion (%)	Peak area	Yield (%)	Selectivity (%)	Peak area	Yield (%)	Selectivity (%)	Peak area	Yield (%)	Selectivity (%)
0	308140.20	0.00	0.00	0.00	0.00	0.00	0.00	0.00	0.00	0.00	0.00
5	292347.80	5.12	0.00	0.00	0.00	517.50	0.88	17.17	12991.10	0.37	7.18
10	279765.60	9.20	0.00	0.00	0.00	1596.70	0.99	10.75	26883.60	1.07	11.66
15	271214.90	11.97	0.00	0.00	0.00	2838.40	1.11	9.31	42787.00	1.88	15.71
30	237593.80	22.87	0.00	0.00	0.00	7657.60	1.60	7.01	92943.60	4.43	19.35
45	215465.30	30.04	0.00	0.00	0.00	12303.30	2.08	6.91	212381.40	10.49	34.91
60	192264.40	37.57	10185.10	3.30	8.78	17297.30	2.58	6.87	277340.50	13.79	36.70
75	169599.80	44.91	12859.00	4.12	9.18	22875.10	3.15	7.01	349652.70	17.46	38.87
90	146993.80	52.24	14663.10	4.68	8.96	26411.80	3.51	6.71	394453.10	19.73	37.77
105	127208.30	58.66	16913.80	5.37	9.16	27478.20	3.62	6.17	450048.30	22.56	38.45
120	108184.00	64.82	18980.60	6.01	9.28	28855.50	3.76	5.79	506634.90	25.43	39.23

Table E4 Results obtained for photocatalytic reaction of glucose with TiO₂ (synthesized by sol-microwave method, calcined at 400 °C for 5 h) catalyst in terms of glucose conversion, yield and selectivity to organic compounds: xylitol, gluconic acid and formic acid.

Time (min)	Glucose		Xylitol			Gluconic acid			Formic acid		
	Peak area	Conversion (%)	Peak area	Yield (%)	Selectivity (%)	Peak area	Yield (%)	Selectivity (%)	Peak area	Yield (%)	Selectivity (%)
0	291255.10	0.00	0.00	0.00	0.00	0.00	0.00	0.00	0.00	0.00	0.00
5	280223.60	3.78	0.00	0.00	0.00	9643.10	1.91	50.48	19499.40	0.74	19.51
10	269762.30	7.37	0.00	0.00	0.00	17878.80	2.79	37.91	41717.90	1.93	26.21
15	262375.70	9.90	0.00	0.00	0.00	23079.60	3.35	33.86	62597.90	3.05	30.82
30	238863.10	17.97	0.00	0.00	0.00	34603.50	4.59	25.55	118144.70	6.04	33.59
45	214592.40	26.29	0.00	0.00	0.00	43190.70	5.51	20.97	160074.50	8.29	31.52
60	195598.00	32.81	6422.90	2.26	6.90	48070.00	6.04	18.40	226241.10	11.84	36.09
75	170894.90	41.28	7715.50	2.68	6.50	53401.40	6.61	16.01	297726.60	15.68	37.99
90	153222.80	47.34	12316.00	4.19	8.84	51699.40	6.43	13.58	357543.00	18.89	39.91
105	132023.20	54.61	14153.70	4.79	8.76	49133.00	6.15	11.26	402256.40	21.29	38.99
120	112445.60	61.32	15989.70	5.38	8.78	45916.80	5.81	9.47	486505.2	25.82	42.10

Table E5 Results obtained for photocatalytic reaction of glucose with TiO₂ (synthesized by sol-microwave method, calcined at 600 °C for 5 h) catalyst in terms of glucose conversion, yield and selectivity to organic compounds: xylitol, gluconic acid and formic acid.

Time (min)	Glucose		Xylitol			Gluconic acid			Formic acid		
	Peak area	Conversion (%)	Peak area	Yield (%)	Selectivity (%)	Peak area	Yield (%)	Selectivity (%)	Peak area	Yield (%)	Selectivity (%)
0	306222.50	0.00	0.00	0.00	0.00	0.00	0.00	0.00	0.00	0.00	0.00
5	303119.40	1.01	0.00	0.00	0.00	0.00	0.00	0.00	0.00	0.00	0.00
10	302835.80	1.10	0.00	0.00	0.00	2152.10	1.05	95.17	0.00	0.00	0.00
15	302161.20	1.32	0.00	0.00	0.00	2114.80	1.05	79.07	0.00	0.00	0.00
30	301971.50	1.39	0.00	0.00	0.00	5140.80	1.36	97.84	0.00	0.00	0.00
45	300589.10	1.84	0.00	0.00	0.00	6868.60	1.53	83.43	6183.60	0.02	1.20
60	296944.30	3.03	0.00	0.00	0.00	9033.80	1.75	57.97	10840.70	0.26	8.59
75	293460.80	4.16	0.00	0.00	0.00	11080.50	1.96	47.17	14550.30	0.45	10.80
90	282438.10	7.76	0.00	0.00	0.00	11719.80	2.03	26.15	18577.50	0.66	8.44
105	281571.40	8.04	0.00	0.00	0.00	14492.80	2.31	28.75	23521.70	0.91	11.29
120	281062.90	8.21	0.00	0.00	0.00	17204.50	2.59	31.55	29580.50	1.22	14.83

Table E6 Results obtained for photocatalytic reaction of glucose with TiO₂ (synthesized by sol-microwave method, calcined at 500 °C for 2 h) catalyst in terms of glucose conversion, yield and selectivity to organic compounds: xylitol, gluconic acid and formic acid.

Time (min)	Glucose		Xylitol			Gluconic acid			Formic acid		
	Peak area	Conversion (%)	Peak area	Yield (%)	Selectivity (%)	Peak area	Yield (%)	Selectivity (%)	Peak area	Yield (%)	Selectivity (%)
0	298037.30	0.00	0.00	0.00	0.00	0.00	0.00	0.00	0.00	0.00	0.00
5	282708.00	5.14	0.00	0.00	0.00	12930.60	2.21	43.05	50193.60	2.33	45.40
10	272427.90	8.58	0.00	0.00	0.00	23262.10	3.30	38.40	87403.40	4.29	49.93
15	260745.40	12.50	0.00	0.00	0.00	29631.40	3.96	31.72	114354.50	5.70	45.60
30	231860.50	22.18	0.00	0.00	0.00	42949.40	5.36	24.18	162314.30	8.22	37.05
45	210950.10	29.19	7538.20	2.57	8.79	50895.20	6.20	21.23	229929.20	11.77	40.31
60	190297.00	36.11	9918.20	3.33	9.21	53724.80	6.49	17.98	284242.40	14.62	40.48
75	168085.30	43.56	11910.20	3.96	9.09	57247.90	6.86	15.76	339853.00	17.54	40.26
90	146568.90	50.77	13943.20	4.61	9.08	57936.80	6.94	13.66	402387.40	20.82	41.01
105	126586.40	57.46	16030.20	5.28	9.18	51633.30	6.27	10.92	459402.00	23.81	41.43
120	110098.40	62.99	17813.70	5.84	9.28	50466.30	6.15	9.77	505704.80	26.24	41.66

Table E7 Results obtained for photocatalytic reaction of glucose with 1wt.% Ag-TiO₂ (synthesized by sol-microwave method, calcined at 500 °C for 5 h and wet impregnation for Ag doping) catalyst in terms of glucose conversion, yield and selectivity to organic compounds: xylitol, gluconic acid and formic acid.

Time (min)	Glucose		Xylitol			Gluconic acid			Formic acid		
	Peak area	Conversion (%)	Peak area	Yield (%)	Selectivity (%)	Peak area	Yield (%)	Selectivity (%)	Peak area	Yield (%)	Selectivity (%)
0	305846.30	0.00	0.00	0.00	0.00	0.00	0.00	0.00	0.00	0.00	0.00
5	252981.30	17.27	9453.30	3.10	17.93	0.00	0.00	0.00	105722.30	5.11	29.61
10	217545.10	28.84	20694.40	6.59	22.85	23051.70	3.19	11.06	172662.10	8.54	29.60
15	184515.00	39.63	28198.60	8.92	22.52	33975.30	4.31	10.87	213231.10	10.61	26.78
30	115591.50	62.14	32774.80	10.34	16.65	47464.40	5.69	9.15	332862.80	16.73	26.92
45	70964.40	76.72	42807.70	13.46	17.55	50387.90	5.99	7.80	465563.10	23.52	30.66
60	42872.40	85.89	49187.80	15.45	17.98	37049.00	4.62	5.38	607898.90	30.80	35.86
75	17687.50	94.12	54751.50	17.18	18.25	15614.30	2.43	2.58	688504.70	34.92	37.10
90	10282.90	96.54	59224.50	18.57	19.23	9780.30	1.83	1.90	759311.60	38.54	39.92
105	6349.60	97.82	62754.70	19.66	20.10	5272.50	1.37	1.40	878164.60	44.62	45.61
120	3859.70	98.63	65492.80	20.51	20.80	4490.30	1.29	1.31	946125.00	48.10	48.76

Table E8 Results obtained for photocatalytic reaction of glucose with 3wt.% Ag-TiO₂ (synthesized by sol-microwave method, calcined at 500 °C for 5 h and wet impregnation for Ag doping) catalyst in terms of glucose conversion, yield and selectivity to organic compounds: xylitol, gluconic acid and formic acid.

Time (min)	Glucose		Xylitol			Gluconic acid			Formic acid		
	Peak area	Conversion (%)	Peak area	Yield (%)	Selectivity (%)	Peak area	Yield (%)	Selectivity (%)	Peak area	Yield (%)	Selectivity (%)
0	303344.80	0.00	0.00	0.00	0.00	0.00	0.00	0.00	0.00	0.00	0.00
5	282216.40	6.96	0.00	0.00	0.00	7876.40	1.65	23.74	24957.90	0.99	14.23
10	263409.80	13.15	7290.30	2.44	18.58	13453.10	2.23	16.93	51527.30	2.36	17.95
15	244508.70	19.38	10822.80	3.55	18.33	18010.90	2.70	13.92	76624.40	3.65	18.86
30	198452.30	34.54	22933.70	7.35	21.27	27571.60	3.68	10.66	164426.80	8.18	23.69
45	153975.00	49.19	32878.80	10.46	21.27	29842.40	3.92	7.96	251316.80	12.66	25.74
60	115949.10	61.71	41510.40	13.17	21.34	35285.20	4.48	7.26	337134.60	17.09	27.69
75	83124.80	72.52	49338.00	15.62	21.54	26619.10	3.58	4.94	429164.30	21.83	30.11
90	59075.50	80.44	55962.60	17.70	22.00	27966.90	3.72	4.63	492421.90	25.10	31.20
105	37107.90	87.67	60455.90	19.10	21.79	20543.00	2.96	3.37	585672.40	29.90	34.11
120	15675.80	94.73	61054.30	19.29	20.37	14552.80	2.34	2.47	632519.20	32.32	34.12

Table E9 Results obtained for photocatalytic reaction of glucose with 10wt.% Ag-TiO₂ (synthesized by sol-microwave method, calcined at 500 °C for 5 h and wet impregnation for Ag doping) catalyst in terms of glucose conversion, yield and selectivity to organic compounds: xylitol, gluconic acid and formic acid.

Time (min)	Glucose		Xylitol			Gluconic acid			Formic acid		
	Peak area	Conversion (%)	Peak area	Yield (%)	Selectivity (%)	Peak area	Yield (%)	Selectivity (%)	Peak area	Yield (%)	Selectivity (%)
0	300945.30	0.00	0.00	0.00	0.00	0.00	0.00	0.00	0.00	0.00	0.00
5	296817.20	1.37	0.00	0.00	0.00	4561.90	1.32	96.36	0.00	0.00	0.00
10	2945240	2.13	0.00	0.00	0.00	9677.30	1.85	86.90	10286.20	0.24	11.06
15	287598.80	4.43	0.00	0.00	0.00	11132.90	2.00	45.22	18394.90	0.66	14.83
30	272616.50	9.40	0.00	0.00	0.00	11854.80	2.08	22.10	31134.40	1.32	14.03
45	256572.50	14.73	7071.60	2.39	16.26	13975.20	2.30	15.61	44484.90	2.01	13.67
60	241976.80	19.57	11637.10	3.84	19.60	16037.30	2.51	12.84	63055.60	2.98	15.22
75	220797.00	26.60	13302.70	4.36	16.40	25612.50	3.51	13.19	120092.50	5.94	22.34
90	199491.20	33.68	17688.00	5.75	17.07	31722.00	4.14	12.31	179395.50	9.03	26.80
105	186484.50	37.99	21425.90	6.93	18.24	38478.40	4.85	12.76	213451.80	10.80	28.42
120	171278.50	43.04	25503.90	8.22	19.09	51560.10	6.21	14.42	270890.80	13.78	32.02

Table E10 Results obtained for photocatalytic reaction of glucose with 1wt.% Cu-TiO₂ (synthesized by sol-microwave method, calcined at 500 °C for 5 h and wet impregnation for Cu doping) catalyst in terms of glucose conversion, yield and selectivity to organic compounds: xylitol, gluconic acid and formic acid.

Time (min)	Glucose		Xylitol			Gluconic acid			Formic acid		
	Peak area	Conversion (%)	Peak area	Yield (%)	Selectivity (%)	Peak area	Yield (%)	Selectivity (%)	Peak area	Yield (%)	Selectivity (%)
0	311576.90	0.00	0.00	0.00	0.00	0.00	0.00	0.00	0.00	0.00	0.00
5	302937.20	2.77	0.00	0.00	0.00	2506.90	1.07	38.59	9319.30	0.18	6.46
10	291939.80	6.30	0.00	0.00	0.00	7335.80	1.55	24.68	22769.70	0.85	13.57
15	279941.30	10.14	0.00	0.00	0.00	11717.10	1.99	19.66	38570.90	1.65	16.24
30	248408.60	20.25	7051.40	2.31	11.39	22840.50	3.11	15.36	97462.80	4.60	22.73
45	218143.60	29.96	12443.90	3.95	13.19	32028.40	4.03	13.46	176105.20	8.55	28.55
60	196731.60	36.82	16566.50	5.21	14.15	38943.20	4.73	12.84	271296.00	13.33	36.21
75	167892.70	46.07	20055.80	6.27	13.62	40991.20	4.93	10.71	298624.80	14.70	31.92
90	149317.20	52.02	23240.70	7.25	13.93	45037.20	5.34	10.26	410363.20	20.31	39.05
105	128546.20	58.68	25935.70	8.07	13.75	44573.80	5.29	9.02	445281.20	22.07	37.60
120	107891.70	65.30	26796.60	8.33	12.76	43425.40	5.18	7.93	522931.70	25.97	39.76

Table E11 Results obtained for photocatalytic reaction of glucose with 3wt.% Cu-TiO₂ (synthesized by sol-microwave method, calcined at 500 °C for 5 h and wet impregnation for Cu doping) catalyst in terms of glucose conversion, yield and selectivity to organic compounds: xylitol, gluconic acid and formic acid.

Time (min)	Glucose		Xylitol			Gluconic acid			Formic acid		
	Peak area	Conversion (%)	Peak area	Yield (%)	Selectivity (%)	Peak area	Yield (%)	Selectivity (%)	Peak area	Yield (%)	Selectivity (%)
0	305913.20	0.00	0.00	0.00	0.00	0.00	0.00	0.00	0.00	0.00	0.00
5	292343.50	4.43	0.00	0.00	0.00	4859.60	1.33	30.00	22619.20	0.86	19.46
10	277972.20	9.12	0.00	0.00	0.00	9503.10	1.80	19.77	48801.70	2.20	24.13
15	264138.80	13.64	0.00	0.00	0.00	14554.90	2.32	17.01	73215.80	3.45	25.29
30	227816.10	25.50	12069.00	3.91	15.33	26581.70	3.55	13.92	155670.90	7.67	30.06
45	196552.70	35.71	17383.60	5.56	15.57	35273.60	4.44	12.43	227701.20	11.35	31.78
60	169249.10	44.63	22087.30	7.02	15.73	41333.90	5.06	11.34	315718.10	15.85	35.52
75	142761.60	53.28	25999.90	8.24	15.46	44775.80	5.41	10.16	384826.00	19.38	36.38
90	119401.40	60.90	29486.60	9.32	15.30	46447.70	5.58	9.17	455046.20	22.97	37.72
105	98372.20	67.77	32432.70	10.24	15.10	45740.00	5.51	8.13	518381.00	26.21	38.68
120	82753.60	72.87	34076.10	10.75	14.75	42285.90	5.16	7.08	572938.70	29.00	39.80

Table E12 Results obtained for photocatalytic reaction of glucose with 10wt.% Cu-TiO₂ (synthesized by sol-microwave method, calcined at 500 °C for 5 h and wet impregnation for Cu doping) catalyst in terms of glucose conversion, yield and selectivity to organic compounds: xylitol, gluconic acid and formic acid.

Time (min)	Glucose		Xylitol			Gluconic acid			Formic acid		
	Peak area	Conversion (%)	Peak area	Yield (%)	Selectivity (%)	Peak area	Yield (%)	Selectivity (%)	Peak area	Yield (%)	Selectivity (%)
0	300281.30	0.00	0.00	0.00	0.00	0	0.00	0.00	0.00	0.00	0.00
5	296565.30	1.24	0.00	0.00	0.00	3197.00	1.18	95.54	5874.70	0.01	0.51
10	287582.60	4.22	0.00	0.00	0.00	7399.50	1.62	38.32	17359.20	0.60	14.31
15	276259.80	7.99	2894.20	1.08	13.48	11956.10	2.09	26.20	31813.90	1.36	16.99
30	239645.00	20.17	6319.40	2.16	10.72	23234.30	3.27	16.20	132033.40	6.58	32.61
45	206103.80	31.33	12429.30	4.10	13.07	33780.70	4.37	13.94	211067.80	10.70	34.14
60	168226.90	43.93	17862.50	5.82	13.24	43713.70	5.40	12.30	296588.10	15.15	34.49
75	133338.20	55.54	23393.80	7.57	13.62	49173.80	5.97	10.75	373683.90	19.17	34.51
90	110361.30	63.18	24564.40	7.94	12.56	49892.20	6.05	9.57	469495.80	24.16	38.24
105	82735.80	72.37	27333.70	8.81	12.18	47357.90	5.78	7.99	539033.00	27.78	38.39
120	53165.10	82.21	26883.00	8.67	10.55	41572.00	5.18	6.30	632434.60	32.65	39.71

Table E13 Results obtained for photocatalytic reaction of glucose with 1wt.% Ag-3wt.% Cu-TiO₂ (synthesized by sol-microwave method, calcined at 500 °C for 5 h and wet impregnation for Ag-Cu co-doping) catalyst in terms of glucose conversion, yield and selectivity to organic compounds: xylitol, gluconic acid and formic acid.

Time (min)	Glucose		Xylitol			Gluconic acid			Formic acid		
	Peak area	Conversion (%)	Peak area	Yield (%)	Selectivity (%)	Peak area	Yield (%)	Selectivity (%)	Peak area	Yield (%)	Selectivity (%)
0	309152.70	0.00	0.00	0.00	0.00	0.00	0.00	0.00	0.00	0.00	0.00
5	301370.50	2.51	0.00	0.00	0.00	1961.70	1.02	40.65	6147.60	0.02	0.79
10	292764.20	5.30	0.00	0.00	0.00	7006.60	1.53	28.94	19331.80	0.69	12.98
15	282981.50	8.46	0.00	0.00	0.00	9833.30	1.82	21.51	32504.80	1.35	16.01
30	257381.80	16.73	5024.30	1.70	10.17	23219.00	3.17	18.97	74471.10	3.48	20.79
45	233195.00	24.54	10696.20	3.45	14.04	45866.90	5.47	22.27	132384.30	6.41	26.11
60	207168.10	32.95	14904.90	4.74	14.38	49332.30	5.82	17.65	214053.00	10.54	31.98
75	179014.90	42.05	17869.90	5.65	13.44	59459.60	6.84	16.27	271140.40	13.43	31.93
90	157210.20	49.10	20870.60	6.57	13.39	66590.80	7.56	15.40	340042.20	16.91	34.45
105	136816.60	55.69	24634.10	7.73	13.88	75837.90	8.50	15.26	375724.70	18.72	33.62
120	117745.40	61.85	26583.80	8.33	13.47	90742.90	10.00	16.18	441276.80	22.04	35.63

Table E14 Results obtained for photocatalytic reaction of glucose with 1wt.% Ag-TiO₂ (synthesized by sol-microwave method, calcined at 500 °C for 5 h and microwave assisted wet impregnation for Ag doping) catalyst in terms of glucose conversion, yield and selectivity to organic compounds: xylitol, gluconic acid and formic acid.

Time (min)	Glucose		Xylitol			Gluconic acid			Formic acid		
	Peak area	Conversion (%)	Peak area	Yield (%)	Selectivity (%)	Peak area	Yield (%)	Selectivity (%)	Peak area	Yield (%)	Selectivity (%)
0	307596.50	0.00	0.00	0.00	0.00	0.00	0.00	0.00	0.00	0.00	0.00
5	273239.20	11.16	4958.30	1.69	15.14	10468.90	1.89	16.96	26914.50	1.08	9.65
10	241219.50	21.56	12471.80	4.01	18.61	18146.80	2.67	12.40	124976.80	6.06	28.13
15	217963.70	29.11	19986.20	6.33	21.76	19199.70	2.78	9.55	175973.80	8.66	29.74
30	158255.10	48.50	34166.20	10.72	22.10	46011.50	5.51	11.36	259245.40	12.89	26.58
45	116788.40	61.97	43591.70	13.63	21.99	52222.30	6.14	9.91	344029.20	17.20	27.76
60	87468.10	71.49	49493.20	15.45	21.62	53931.20	6.31	8.83	470519.90	23.64	33.06
75	63828.30	79.17	54085.50	16.87	21.31	47398.60	5.65	7.14	546295.50	27.49	34.72
90	47651.50	84.42	57638.90	17.97	21.29	38789.50	4.77	5.65	618461.80	31.16	36.91
105	21875.90	92.79	44236.90	13.83	14.90	29260.00	3.80	4.10	692247.30	34.91	37.62
120	14848.60	95.07	42555.00	13.31	14.00	23822.00	3.25	3.42	750692.10	37.88	39.85

Table E15 Results obtained for photocatalytic reaction of glucose with P25 (commercial grade TiO₂) catalyst in terms of glucose conversion, yield and selectivity to organic compounds: xylitol, gluconic acid and formic acid.

Time (min)	Glucose		Xylitol			Gluconic acid			Formic acid		
	Peak area	Conversion (%)	Peak area	Yield (%)	Selectivity (%)	Peak area	Yield (%)	Selectivity (%)	Peak area	Yield (%)	Selectivity (%)
0	271951.50	0.00	0.00	0.00	0.00	0.00	0.00	0.00	0.00	0.00	0.00
5	231360.00	14.91	0.00	0.00	0.00	12853.40	2.41	16.20	31451.00	1.48	9.91
10	222897.10	18.02	3828.30	1.52	8.41	23276.30	3.61	20.06	70521.00	3.73	20.68
15	207557.90	23.65	7777.10	2.90	12.24	29773.60	4.36	18.44	131684.00	7.24	30.62
30	162670.40	40.14	14791.00	5.35	13.32	38006.20	5.31	13.22	213942.00	11.97	29.83
45	123741.50	54.43	21072.70	7.54	13.86	39616.60	5.49	10.09	322828.00	18.24	33.50
60	92774.10	65.81	26395.60	9.40	14.29	37267.70	5.22	7.94	384668.00	21.79	33.12
75	67707.90	75.01	29907.10	10.63	14.17	30010.80	4.39	5.85	468166.00	26.59	35.45
90	47918.60	82.28	31490.60	11.18	13.59	22819.20	3.56	4.33	544551.00	30.99	37.66
105	33610.80	87.54	32032.90	11.37	12.99	15815.90	2.76	3.15	616359.00	35.12	40.12
120	24948.70	90.72	32289.30	11.46	12.64	10285.90	2.12	2.34	695370.00	39.66	43.72

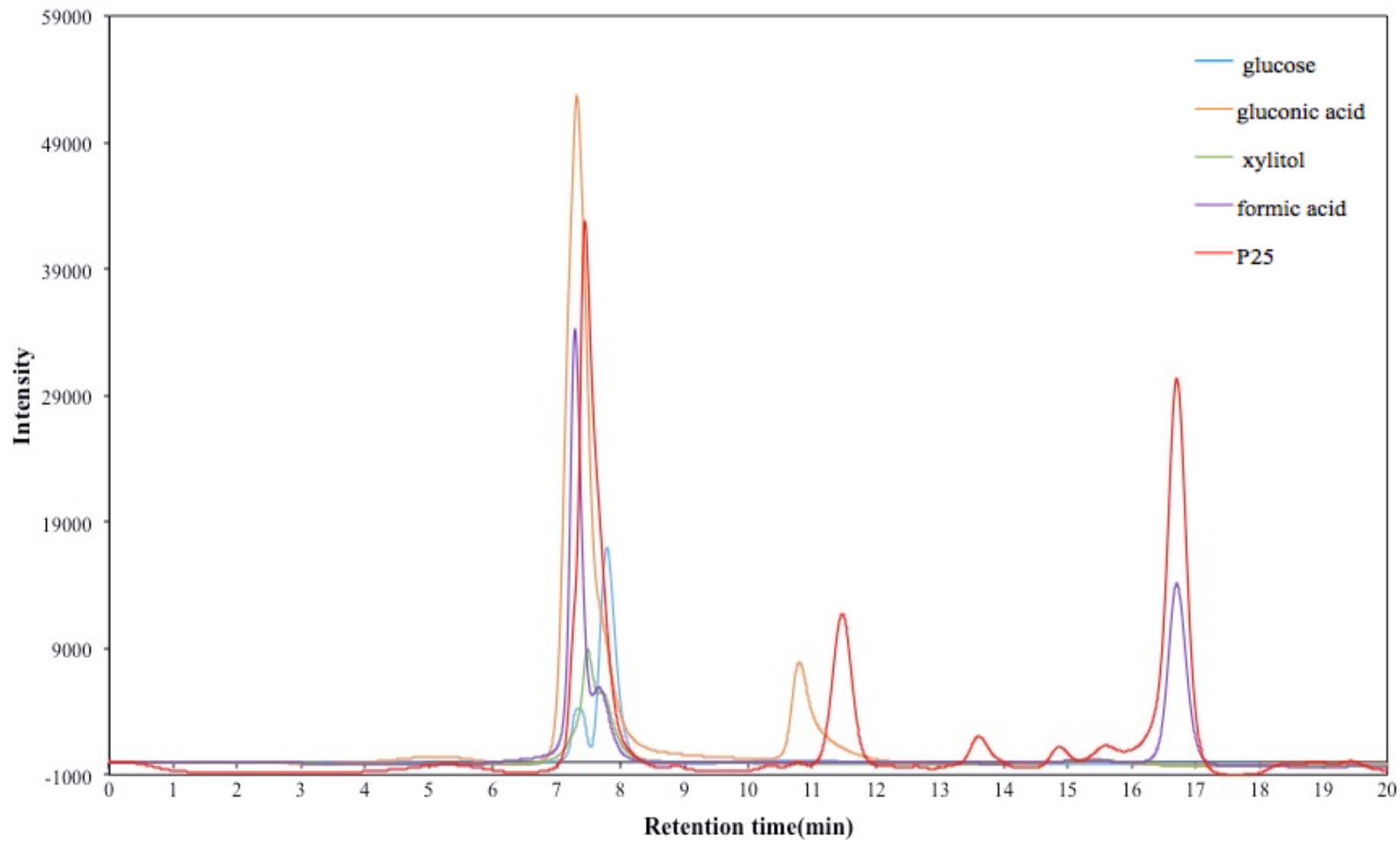


Fig. E1 Results of HPLC with UV detector

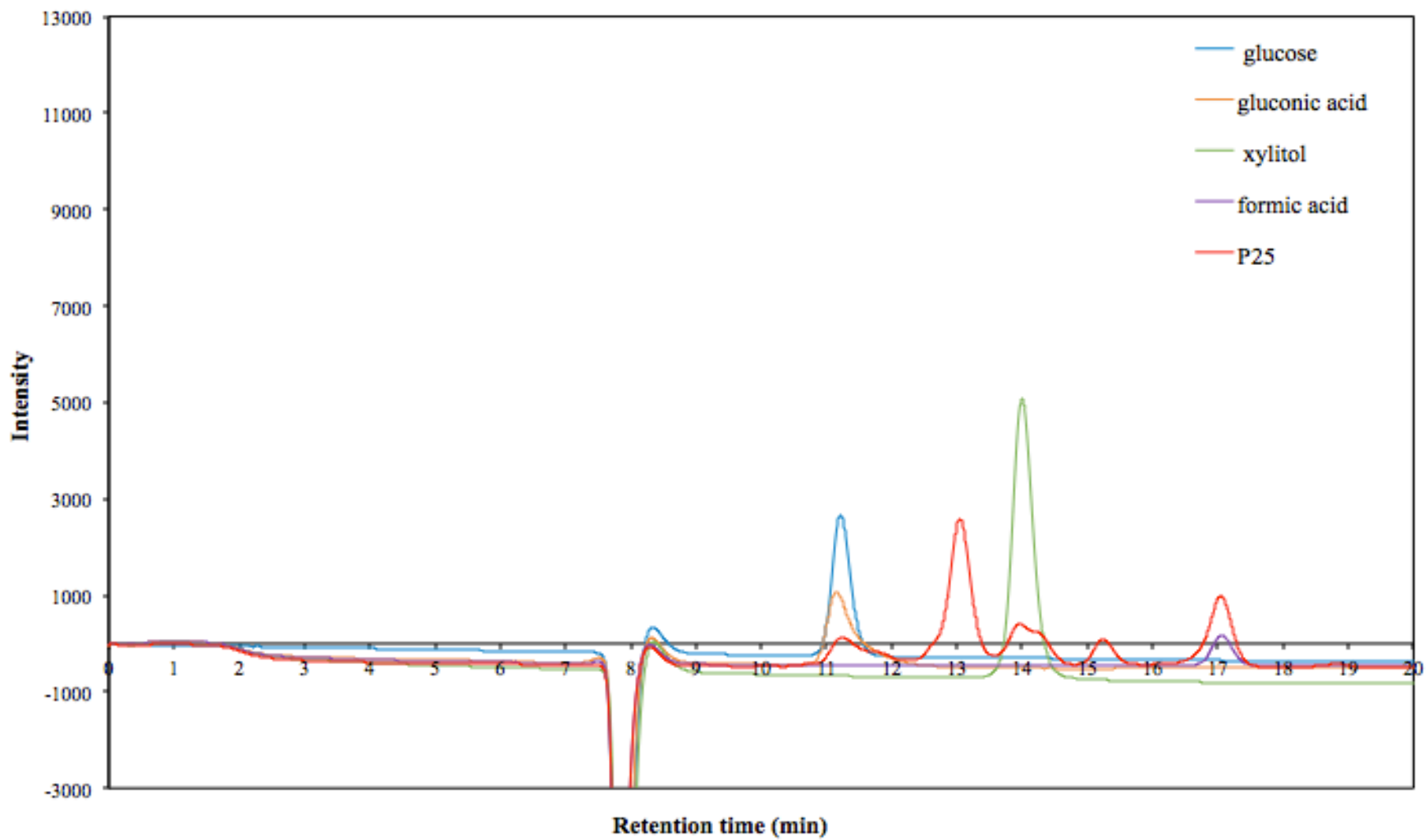


Fig. E2 Results of HPLC with RI detector.